Synthesis and Characterization of Composite Textured Surfaces with Enhanced Tribological Responses on Icy Surfaces

Sara Zahmatkesh

A DISSERTATION SUBMITTED TO

THE FACULTY OF GRADUATE STUDIES

IN PARTIAL FULFILLMENT OF THE REQUIREMENTS

FOR THE DEGREE OF

DOCTOR OF PHILOSOPHY

GRADUATE PROGRAM IN MECHANICAL ENGINEERING

YORK UNIVERSITY

TORONTO, ONTARIO

October 2026

© Sara Zahmatkesh, 2026

Abstract

Slips and falls on icy surfaces remain a major safety concern in cold-climate regions, creating a need for footwear materials that provide both high traction and long-term durability. Although elastomers are widely used in outsoles due to their flexibility and deformation capability, their performance on ice is limited by the presence of a thin liquid-like interfacial layer. In addition, abrasion can remove traction-enhancing surface features and reduce service performance. This dissertation addresses these challenges through the development, characterization, tribological testing, and data-driven prediction of textured elastomeric composite surfaces for improved ice traction and abrasion resistance.

First, a lab-scale high-velocity ice tribotesting method was developed using a modified Bruker UMT Tribolab. Custom sample holders, ice trays, and testing scripts enabled controlled testing of small rubber and composite specimens under walking-relevant load and sliding speed conditions. The effects of load tuning, dwell time, sampling rate, and sliding mode were evaluated. Rotational sliding provided a more reliable representation of rubber-ice friction than reciprocating motion, which introduced ploughing effects and artificially high kinetic friction values. The developed method provides a practical high-throughput platform for screening ice-traction materials without requiring full-size footwear samples.

Second, thermoplastic polyurethane/graphene nanoplatelet (TPU/GNP) nanocomposites were developed as durable ice-traction materials. Pristine and acid-functionalized GNPs were incorporated into TPU to evaluate the effects of filler dispersion, interfacial bonding, and wear-induced surface evolution. Functionalization improved filler-matrix adhesion, dispersion, tensile reinforcement, and thermal stability. Wire-brushed surface texturing enhanced ice traction by creating micro-asperities and exposed rigid features. Post-abrasion analysis showed that wear could generate new functional asperities and microchannels, allowing the surface to retain traction after abrasion. Among the investigated formulations, TPU-20 f/GNP showed the best overall balance, with the lowest abrasion volume loss, highest abrasion resistance index, and strong post-abrasion ice traction.

Third, machine learning models were developed to predict TPU abrasion resistance from mechanical and viscoelastic properties. Nonlinear regression models, particularly support vector regression and gradient boosting regression, showed the strongest predictive performance, demonstrating the potential of machine learning as an early-stage screening tool for durable TPU materials.

An additional industrial case study extended the data-driven approach to automotive polymer composites through experimental data generation, predictive model development, and graphical user interface implementation for service-condition-based performance prediction. Overall, this dissertation establishes an integrated experimental and computational framework for designing durable, wear-adaptive, and ice-traction-enhanced elastomeric composite surfaces.

Acknowledgements

I would like to express my sincere gratitude to my supervisor, Dr. Reza Rizvi, for his guidance, support, and encouragement throughout my PhD journey. His mentorship has played an important role in shaping my professional development as a researcher, and I am truly grateful for the knowledge, opportunities, and confidence he has provided along the way.

I would also like to thank my supervisory committee members, Dr. Aleksander Czekanski and Dr. Paul G. O'Brien, for their valuable feedback, thoughtful suggestions, and constructive guidance. Their insights have helped strengthen this dissertation and broaden my perspective on the research.

I am grateful to my lab mates at the Polymer and Inorganic Composites, Structures and Surfaces Lab (PICSSL), as well as my colleagues, fellow researchers, and friends at the Lassonde School of Engineering. Their support, collaboration, and encouragement made this journey more meaningful and memorable.

My deepest appreciation goes to my husband, Farhad, for his constant love, patience, and support. His belief in me, especially during the most challenging moments, gave me strength and motivation to continue. I am also deeply thankful to my parents for their unconditional love, sacrifices, and unwavering support throughout my life and education. Their encouragement has always been one of my greatest sources of strength.

Finally, I would like to thank everyone who, in different ways, supported me during this journey. This dissertation would not have been possible without the guidance, kindness, and encouragement of the people who stood beside me.

Table of Contents

Abstract……..……..……..…….ii

Acknowledgments……...……..…….iv

Table of Contents…….……..……..v

List of Tables……..……ix

List of Figures……...……...x

Chapter 1: Introduction 1

1-1- Problem Statement 1

1-2- Knowledge Gaps 3

1-3- Research Hypothesis 6

1-4- Research Objectives 7

1-5- Dissertation Structure 11

1-6- List of Publications and Presentations 13

Journal Publications 13

Conference Presentations 13

1-7- References 14

Chapter 2: Background and Fundamentals 16

2-1- Ice Tribology and Slip Resistance 16

2-2- Rubber and Elastomeric Friction 18

2-3- Surface Texturing and Bioinspired Anti-Slip Design 22

2-4- Thermoplastic Polyurethane for Anti-Slip and Durable Surfaces 26

2-5- Graphene Nanoplatelet-Reinforced Elastomeric Composites 29

2-6- Abrasion Resistance and Wear Mechanisms in TPU/Rubber Systems 31

2-7- Machine Learning and Triboinformatics for Materials Design 34

2-8- References 38

Chapter 3: Evaluating Surface Texturing Technologies of Rubber Composites on Ice Using a Novel High-Velocity Tribotest Method 45
3-1- Chapter Preface 45
3-2- Abstract 45
3-3- Literature Review and Research Gaps 46
3-4- Development of Lab-Scale Ice Friction Tester 49
3-4-1- Mold Designing and Installation 49
3-4-2- Sample Preparations 50
3-4-3- Surface Characterization of Samples 51
3-4-4- Ice Surface Preparation 51
3-4-5- Definition of Ice Friction Testing Parameters 52
3-5- Results and Discussion 53
3-5-1- SEM/EDS Morphological Analysis of Sample Surfaces 53
3-5-2- Influence of Testing Parameters on Ice Tribology 55
3-5-3- Comparison of Reciprocating and Rotational Sliding Modes on Ice 59
3-5-4- Reliability Assessment of the Testing Protocol 65
3-5-5- Ice Frictional Response of Rubber Composites 66
3-6- Conclusions 69
3-7- References 70
Chapter 4: Wear-Activated Surface Engineering of TPU/Graphene Nanoplatelet Nanocomposites for Ice Friction Control 73
4-1- Chapter Preface 73
4-2- Abstract 73
4-3- Literature Review and Research Hypothesis 74
4-4- Fabrication of Composites with Enhanced Tribological Behavior 77
4-4-1- Surface functionalization of Graphene nanoplatelets (GNPs) and Characterization 77

4-4-2- Composites Synthesis 79
4-4-3- Composites Characterizations 79
4-4-4- Surface Texturing and Tribology Investigations 80
4-5- Results and Discussion 83
4-5-1- FTIR Characterization of GNPs vs. *f*/GNPs 83
4-5-2- Effect of Graphene Functionalization on TPU Nanocomposites 85
4-6- Conclusions 100
4-7- References 101
Chapter 5: Predicting Abrasion Resistance in Thermoplastic Polyurethanes Using Machine Learning 105
5-1- Chapter Preface 105
5-2- Abstract 105
5-3- Introduction and Literature Review 106
5-4- Mechanical and Structural Properties Influencing TPU Abrasion Resistance 109
5-5- Machine Learning Model Development 113
5-5-5- Parameters Optimization and Hyperparameters Search Space 121
5-6- Results and Discussion 122
5-7- Conclusions 128
5-8- References 129
Chapter 6: Case Study [Industrial Contribution] Machine Learning-Aided Accelerated Design and Characterization of Automotive Composites 134
6-1- Chapter Preface 134
6-2- Background: Automotive Composite Materials 134
6-3- Project Motivation and Industrial Relevance 137
6-4- Materials and Methods: Industrial Contribution Workflow 138
6-4-1- Materials Selection and Formulation Review 138
6-4-2- Mechanical Testing and Characterization 138

6-4-3- Data Organization and Preprocessing 139
6-4-4- Data Analysis and Model Development 139
6-4-5- Comparison Against Baseline Materials 140
6-5- Results and Technical Contribution [Non-Confidential Results and Technical Contributions] 140
6-6- Relevance to Dissertation Theme 141
6-7- References 142
Chapter 7: Conclusions and Future Work 143
7-1- Summary of Key Findings 143
7-2- Main Contributions 145
7-3- Future Research Directions 148
7-4- Closing Remarks 150

List of Tables

Chapter 3

Table 3- 1- Friction script definition 53
Table 3- 2- Ice-rubber contact dynamic parameters optimization 56

Chapter 4

Table 4- 1- Abrasion Resistance Index (ARI) of composites 96

Chapter 5

Table 5- 1- TPU grades selected from the database 113
Table 5- 2- Hyperparameters optimization and their search space for ML models 121
Table 5- 3- Evaluation metrics performed on ML models and their statistical description 123
Table 5- 4– ML models' performances on abrasion volume loss prediction of TPU elastomers 124

List of Figures

Chapter 2

Fig. 2- 1- (a) Fundamentals of tribology and friction force responses on ice: (b) smooth sliding and (c) stick-slip behavior [5]. 17

Fig. 2- 2- Surface texturing and outsole design factors contributing to the frictional response of shoe soles on ice. 20

Fig. 2- 3- Bioinspired mechanisms for enhanced traction: a) Polar bear feet with papillae structures that increase adhesion through surface depression, combined with hard claws for mechanical interlocking; b) arctic seal with rotated flippers and sharp hairy body that enhance frictional grip; c) Snake scales that improve mechanical interlocking and shear resistance upon activation; d) Penguin feet with microchannels that dissipate surface fluids, promoting dry contact, supplemented by strong claws for increased traction. 22

Fig. 2- 4- Damage Induced Surface Textured (DIST) composites: the schematic of fabrication practice and the obtained textured surface [49] 25

Fig. 2- 5- Schematic illustration of chain structure of Thermoplastic Polyurethane (TPU) composed of sequentially hard and soft segments [57] 27

Fig. 2- 6- Schematic representation of the layered graphite structure and the exfoliation process into few-layer graphene nanoplatelets and single-/few-layer graphene sheets. 29

Fig. 2- 7- Machine learning workflow for mechanical materials prediction, design, and computational modeling [100]. 36

Chapter 3

Fig. 3- 1- a) rubbers' dry interaction with roadbeds, vs. b) rubbers' wet interaction with roadbeds, and c) presence of a liquid-like-layer on the surface of ice 46

Fig. 3- 2- Testing setup featuring two-part ice molds mounted on separate rotary drives, with rubber samples secured in a 3D-printed holder, which is mounted on the load cell. Configurations are shown for: a) rotary motion and b) reciprocating motion. 50

Fig. 3- 3- Sample preparation of commercial slip-resistant footwear: a) Selection based on the maximum achievable angle for walking on an icy surface, as tested by an individual wearing the boots [21], b) IceFX, including slip resistance scores and an outsole sample, and c) Arctic Grip, with reported slip resistance scores and an outsole sample. 51

Fig. 3- 4- SEM morphology analyses of textured surfaces of specimens; a) IceFX, b) Arctic-Grip, and c) TPU-GFs[19] composites 54
Fig. 3- 5- EDS analytical studies on the textured surfaces of a) Arctic Grip composite, and b) IceFX composite 55
Fig. 3- 6- Optimized dynamic of contact variables for script definition 57
Fig. 3- 7- Influence of Contact Timing on Normal Force Stability. Blue plot represents a 60-second duration of ice-rubber initial contact before movement initiation, while the red plot illustrates a 10-second duration. 58
Fig. 3- 8- Effect of data sampling rate on static frictional force recognition on ice in a) rotation, and b) reciprocation test setups 59
Fig. 3- 9- Static and Kinetic friction behavior of Arctic Grip composite on ice at room temperature, a) reciprocation, b) rotation, and c) comparison of static friction in rotation vs. reciprocation ... 60
Fig. 3- 10- Kinetic friction of rubber on ice in rotational mode: a) four sequential cycles in kinetic region, b) friction and normal force signals in revolution 2 in the kinetic region, and c) schematic of the process and the contact dynamic of the machine 61
Fig. 3- 11- Kinetic friction of rubber on ice in reciprocation mode: a) four sequential cycles (forward and backward) in kinetic region, b) friction and normal force signals in cycle 2 in the kinetic region, and c) the schematic of process and physical phenomena 63
Fig. 3- 12- Friction testing protocols and obtained responses of pristine TPU and TPU-10%wt.GF obtained by: a) SATRA setup [19], and b) Newly developed rotational protocol 66
Fig. 3- 13- Specimens' friction and normal force on ice on the left, and their corresponded CoF on the right, evaluated by rotational sliding testing protocol, a) TPU and its glass-fiber composites, b) Midsole and IceFX rubber composites, and c) Midsole and Arctic-Grip composites. 67

Chapter 4

Fig. 4- 1- Transmission electron microscopy (TEM) images of graphene nanoplatelets (GNPs): (A) lateral flake morphology and size distribution; (B) stacked multilayer graphene sheets showing nanoscale thickness. The copyrighted image is used by permission of ACS Material LLC [16]. 78
Fig. 4- 2- Schematics illustrating A) hierarchical surface texture formation induced by micro-wire brushing, the exposed and anchored functionalized GNPs, and B) the lab-scale ice traction testing method 81

Fig. 4- 3- Schematic illustration of the fabrication, wear-activated surface texturing, and tribology testing workflow of f/GNP-reinforced TPU nanocomposites 83
Fig. 4- 4- Surface functionalization of graphene nanoplatelets (GNPs):(A) Schematic illustration of functional group formation at GNP edges and their potential to form covalent bonds with TPU chains; (B) FTIR spectra comparing pristine GNPs and functionalized GNPs (f-GNPs), and c) TGA curves of GNPs and f-GNPs. 84
Fig. 4- 5- SEM micrographs of cryogenically fractured surfaces prepared using liquid nitrogen. (A, B) TPU–20GNP composites exhibit coarser graphene nanoplatelets and weak interfacial bonding with the TPU matrix. (C, D) TPU–20 f/GNP composites show a more uniform platelet distribution, finer particle dispersion, and improved interfacial adhesion..... 86
Fig. 4- 6- Engineering stress–strain curves of neat TPU and TPU–GNPs nanocomposites with non-functionalized and functionalized graphene nanoplatelets at 20phr and 40phr loadings. 88
Fig. 4- 7- Thermogravimetric analysis (TGA) of fabricated nanocomposites compared with neat TPU. 89
Fig. 4- 8- SEM micrographs of wire-brushed (WB) textured surfaces. (A1) Low-magnification image of wire-brushed pristine TPU, illustrating the formation of continuous, wavy surface features. (A2) Higher-magnification view of the same wire-brushed pristine TPU surface, revealing localized roughening and micro-scale asperities along the brushing direction. (B) Wire-brushed TPU–20 f/GNP nanocomposite, showing exposed 2D graphene nanoplatelets anchors within the textured surface. (C) Wire-brushed TPU–40 f/GNP nanocomposite, exhibiting a denser hierarchical texture with increased graphene-rich feature. 91
Fig. 4- 9- Static Coefficient of friction (SCOF) response of molded pure TPU, as a representative composition and surface texture, sliding on ice over repeated runs. Solid lines denote CoF, while dotted and dashed curves correspond to the normal force (Fz) and tangential friction force (Ff), respectively. 94
Fig. 4- 10- Static coefficient of friction of TPU–GNP composites with different surface conditions: as-molded (MO), wire-brushed (WB), and post-abrasion (DA) 94
Fig. 4- 11- (A) Abrasion volume loss of TPU–GNP nanocomposites measured using the drum abrasion test in accordance with ISO 4649. (B) Ice-traction performance of the composites evaluated after abrasion, corresponding to the abraded surface state presented in Fig. 4-10. 97
Fig. 4- 12- low magnification SEM images of TPU-GNP composites, (A) is the molded surface (MO) of the TPU- 40 GNP as a representative; and post abrasion surfaces of (B) TPU- 20GNP, (C) TPU-40GNP, (D) TPU- 20 f/GNP, and (E) TPU- 40 f/GNP 98

Fig. 4- 13- High magnification SEM images of post-abrasion surfaces of composites; (A) TPU- 20GNP, (B) TPU- 40GNP, (C) TPU- 20 f/GNP, (D) TPU- 40 f/GNP 99

Chapter 5

Fig. 5- 1- a) Materials properties, and TEM images of b) ether-based TPU, c) ester-based TPU, and d) carbonate-based TPU (reprinted with permission from eXPRESS Polymer Letters [28]) 110

Fig. 5- 2- a) Abrasion mass loss during Abrasion test on 500 mm of P180 abrasive paper, b) master curves of E'' (loss or viscous modulus for the various TPUs, SEM images of abraded surface of c) ether-based TPU, and d) ester-based TPU (reprinted with permission from eXPRESS Polymer Letters [28]). 110

Fig. 5- 3– a) Schematic of polyol (soft) and isocyanate (hard) segments in TPU, b) how variations in ratios of soft and hard segments influence TPU stress-strain curve, c) chemical structure of TPU, comprising soft(ether or ester) and hard segments, and d) tensile moduli of soft-chained TPU and hard-chained TPU [31]. 111

Fig. 5- 4- Abrasion weight loss as a function of shore hardness for TPU [40]. 113

Fig. 5- 5- Selected features as most correlated inputs to the abrasion resistivity performance of TPUs 116

Fig. 5- 6- linear correlation between the target feature and two most correlated mechanical properties: a) stress at break, and b) tear strength. 116

Fig. 5- 7- Flowchart outlining the approach for ML-based TPUs abrasion resistivity prediction 122

Fig. 5- 8- Regression model performance in prediction of abrasion resistivity, a) linear regression, and b) polynomial regression 124

Fig. 5- 9- Evaluating ML models on training and testing performance based on: a) R^2 score and b) root mean square error 126

Fig. 5- 10- Evaluation analysis on Decision Tree and Gradient Boosting regressors in abrasion resistance prediction 127

Chapter 6

Fig. 6- 1- Strength versus density of engineering materials. Composites demonstrate strength comparable to metals while exhibiting lower density [5]. 135

Fig. 6- 2- Diverse applications of polymer composites in the automotive industry [7]. 136

Chapter 1:
Introduction

1-1- Problem Statement

Slips and falls on icy surfaces represent a major public safety concern, particularly in cold-climate countries such as Canada, Russia, the United Kingdom, the United States, and Nordic regions, where winter conditions significantly increase the risk of injury. According to recent statistics from the Canadian Institute for Health Information, slipping on ice is one of the leading causes of winter-related injuries, highlighting the need to develop effective strategies for reducing ice-slip incidents [1]. In Canada, injuries associated with snow and ice are among the most frequent winter-related hazards [2], [3]. Similar concerns are reported internationally, with approximately 1 million fall-related cases and 20,000 deaths occurring annually in the United States alone during winter conditions. The economic burden of these incidents exceeds $100 billion, affecting healthcare systems, social security, insurance, and employment through medical costs, job losses, and workforce shortages [4].

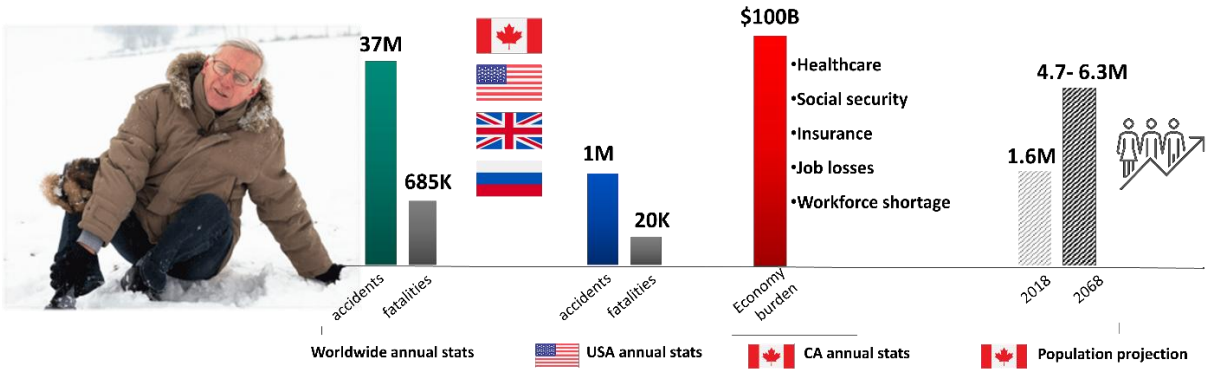


Fig. 1- 1- Overview of winter slip-and-fall injuries, associated economic burden, and projected growth of vulnerable aging populations in cold-climate regions

The consequences of ice-related slips and falls are especially severe for vulnerable populations, including older adults and individuals with limited mobility. For these groups, hazardous winter surfaces can restrict Activities of Daily Living (ADL), reduce independence, and negatively affect physical and mental well-being. This issue is expected to become increasingly important as

Canada's population continues to age. Population projections indicate that the number of seniors aged 80 years and older may increase from 1.6 million in 2018 to between 4.7 and 6.3 million by 2068 [5]. In addition to ice-specific hazards, slips and falls on walking surfaces more broadly represent a major source of injury. Canadian statistics show that approximately 1.7 million falls occur annually among adults and older individuals, with slips and falls accounting for a substantial portion of all injuries [6].

Current winter safety strategies include public-level interventions such as salting, snow removal, surface maintenance, and hazard awareness. At the individual level, traction-enhancing footwear accessories, including crampons, chains, and metal cleats, are commonly used to improve grip on icy surfaces [7]. However, these approaches are not always practical for daily use, as they may increase weight, reduce comfort, alter walking biomechanics, damage indoor flooring, or create inconvenience when transitioning between outdoor and indoor environments [8]. Therefore, there is a need for integrated material-based solutions that can improve ice traction directly through the design of footwear outsole materials and surface structures.

Ice becomes particularly slippery near its melting temperature due to the formation of a thin liquid-like water layer at the surface, which acts as a lubricant and reduces friction at the contact interface [9]. This phenomenon contributes to a wide range of winter-related accidents, including pedestrian falls and vehicle incidents, which are reported annually in cold-weather conditions. Although ice is a crystalline solid, a quasi-liquid film can exist on its surface even below the melting point. As the temperature approaches 0 °C, this film becomes more pronounced and further reduces friction by acting as a lubricating medium at the ice-material interface [10].

Elastomers and rubbers are widely used in footwear outsoles and automobile tires because of their hyperelastic behavior, which allows them to deform and recover when pressed against rough surfaces such as asphalt or concrete [11]. This deformation can increase the real contact area and support friction generation on many dry or rough substrates. However, these materials often exhibit poor traction on wet or icy surfaces, where the lubricating interfacial layer reduces adhesion and shear resistance [9]. As a result, conventional elastomeric outsole materials may be insufficient for preventing slips under winter conditions.

Another important limitation of rubber-based outsole materials is their susceptibility to abrasion and wear. During repeated contact with roads, sidewalks, and trails, footwear outsoles can lose

material, which not only shortens their service life but also contributes to the release of microplastic particles into the environment. Microplastics consist of heterogeneous plastic particles ranging from micrometre to millimetre scales and vary in shape, size, and chemical composition [12]. These particles can negatively affect ecosystems by altering plant growth, affecting organisms, and modifying soil physical properties, microbiology, and overall soil function [13]. Since shoe outsoles experience continuous abrasion during walking, they are considered a notable contributor to microplastic pollution [14][15]. Therefore, outsole materials must not only provide high traction on ice but also maintain durability under abrasive service conditions.

The central challenge is the trade-off between ice traction and abrasion resistance in elastomeric materials. Strategies that increase surface roughness, softness, or interfacial adaptability may enhance grip on ice, but they can also accelerate wear and reduce long-term durability [16]. Conversely, highly wear-resistant materials may lack the surface compliance, texture, or interfacial behavior required for reliable ice traction. Composite materials offer a promising route to address this challenge because they can combine a soft elastomeric matrix with reinforcing phases that improve mechanical strength, abrasion resistance, and tribological performance [17]. Microscopic or nanoscale composites consisting of a hard phase dispersed within a soft polymer matrix may provide an opportunity to engineer outsole materials with an improved balance between friction and durability.

Despite progress in polymer composites and tribological surface design, there remains a need to develop multifunctional elastomeric composite surfaces that can simultaneously improve traction on ice, resist abrasion, and maintain functional surface characteristics during wear. This dissertation addresses this problem by investigating TPU-based graphene nanoplatelet composites, interfacial engineering through filler functionalization, and bioinspired textured surfaces as integrated strategies for improving ice friction and abrasion durability in elastomeric outsole materials.

1-2- Knowledge Gaps

Although advances have been made in polymer composites and tribological surface design, key gaps remain in elastomeric materials for ice traction. The primary challenge is balancing high ice friction with abrasion resistance. Surface roughness, softness, and interfacial adaptability may

improve grip but can accelerate wear, while highly abrasion-resistant materials may lack the compliance or surface response required for effective ice traction.

Micro- and nanoscale fillers can tailor the structural and tribological response of elastomeric composites by modifying stiffness, deformation behavior, surface morphology, and interfacial interactions. Their microstructural arrangement is particularly important for promoting mechanical interlocking with ice [18]. Additives such as abrasives, binders, friction modifiers, and fillers have also been used to enhance polymer-based friction performance [19]. In addition, smaller and more irregular fillers have been reported to improve sliding friction behavior [20]. However, the combined effects of filler morphology, dispersion, interfacial bonding, abrasion resistance, and ice traction remain insufficiently understood.

Therefore, multifunctional elastomeric composites are needed to provide both reliable ice traction and durability under abrasive conditions. These materials must simultaneously maximize frictional performance and resist wear, material loss, and environmental degradation. In parallel, AI/ML-based approaches offer a promising route to predict abrasion resistance and identify the key material and structural descriptors governing wear performance.

Based on these challenges, the following knowledge gaps are identified.

***Gap 1*: Limited understanding of the role of 2D filler exfoliation and dispersion in ice traction**

Two-dimensional materials, such as graphene-based nanoplatelets, have strong potential to improve the tribological and mechanical performance of elastomeric composites [7]. However, their effectiveness depends strongly on their degree of exfoliation, dispersion, and orientation within the polymer matrix. Agglomeration of 2D nanoplatelets can reduce available filler surface area, create stress concentration sites, and limit the contribution of the filler to frictional performance. Therefore, the effect of 2D filler exfoliation and dispersion on the ice-traction response of elastomeric composites remains an important knowledge gap.

***Gap 2*: Insufficient understanding of filler-matrix interfacial effects on wear resistance and durability**

The durability of ice-traction composites is strongly influenced by the quality of adhesion between the reinforcing filler and the elastomeric matrix [21]. Poor interfacial bonding can lead to filler

pull-out, particle debonding, crack initiation, and accelerated material loss during abrasion, which yields to weak wear performance [22]. In addition to particle fracture, debonding from the matrix is an important wear mechanism in composite materials designed for ice-traction applications. However, the effect of interfacial improvement between 2D fillers and elastomeric matrices on abrasion resistance, wear mechanisms, and long-term durability has not been fully established.

***Gap 3*: Lack of integrated strategies for balancing ice traction and abrasion resistance**

Many studies focus primarily on improving either frictional performance or mechanical durability, while fewer studies consider the coupled relationship between ice traction and abrasion resistance. For practical outsole-related applications, a material must not only provide high friction under icy conditions but also retain its performance after repeated sliding and material loss. Therefore, integrated material and surface design strategies are needed to address ice traction and abrasion resistance simultaneously.

***Gap 4*: Limited use of AI/ML approaches for predicting TPU abrasion resistance from mechanical and viscoelastic properties**

The abrasion resistance of TPU is strongly influenced by its mechanical and viscoelastic behavior, including properties such as hardness, tensile strength, elongation, modulus, resilience, and energy dissipation [23]. However, the relationships between these properties and abrasion performance are often nonlinear and difficult to interpret using conventional experimental analysis alone. Traditional approaches typically evaluate abrasion resistance through direct testing, which can be time-consuming and may not reveal the relative importance of underlying material descriptors. Artificial intelligence and machine learning provide a data-driven framework for linking mechanical and viscoelastic properties to abrasion resistance. By capturing nonlinear correlations among material descriptors, these models can predict abrasion performance, identify dominant property–wear relationships, and support a deeper understanding of abrasion mechanisms in TPU systems. However, the application of AI/ML specifically for predicting TPU abrasion resistance from mechanical and viscoelastic property correlations remains limited.

Together, these gaps demonstrate the need for a systematic investigation of TPU-based graphene nanoplatelet composites, interfacial engineering through filler functionalization, bioinspired surface design, and AI/ML-assisted abrasion resistance prediction. Addressing these gaps can

support the development of multifunctional elastomeric surfaces with improved ice traction and enhanced durability under abrasive conditions.

1-3- Research Hypothesis

Based on the problem statement and identified knowledge gaps, this dissertation is guided by the following research hypotheses. These hypotheses link the development of a controlled ice tribological testing method with surface texturing, TPU/graphene nanoplatelet composite design, interfacial engineering, wear-activated surface functionality, and AI/ML-assisted abrasion resistance prediction.

***Hypothesis 1*: A lab-scale high-velocity ice tribotesting method can be developed to evaluate ice friction performance**

A controlled lab-scale tribological testing method can be developed to measure the ice friction behavior of elastomeric materials under high-velocity sliding conditions. Because ice friction is highly sensitive to sliding speed, normal load, temperature, contact pressure, and ice surface condition, a controlled laboratory-scale method is needed to evaluate material and surface effects under defined testing conditions. It is hypothesized that a lab-scale method can generate systematic friction data aligned with established large-scale testing approaches, enabling assessment of the influence of surface texture, composite formulation, and wear on ice traction performance.

***Hypothesis 2*: Surface texturing can improve the ice traction response of rubber composite surfaces**

Surface morphology plays a critical role in the frictional response of elastomeric materials on ice. It is hypothesized that engineered surface texturing can enhance ice traction by increasing effective contact interactions and promoting mechanical interlocking with the ice surface. Therefore, textured rubber composite surfaces are expected to show improved ice friction compared with untextured or less-optimized surfaces under high-velocity sliding conditions.

***Hypothesis 3*: Graphene nanoplatelet dispersion and interfacial adhesion can enhance TPU composite durability**

The incorporation of two-dimensional fillers, such as graphene nanoplatelets, into TPU can modify the composite microstructure, mechanical response, and friction behavior. However, their

effectiveness depends strongly on dispersion quality and filler–matrix interfacial adhesion. It is hypothesized that improved graphene nanoplatelet dispersion and stronger interaction with the TPU matrix can reduce agglomeration, filler pull-out, particle debonding, and crack initiation during abrasion, leading to improved durability and wear resistance.

***Hypothesis 4*: Wear-activated surface engineering can improve ice friction control in TPU/GNP nanocomposites**

Abrasion-induced surface evolution can alter the frictional response of TPU/GNP nanocomposites on ice. It is hypothesized that controlled wear-activated surface features can contribute to ice friction control by generating or maintaining functional microstructures during progressive abrasion. These surface features are expected to support mechanical interaction with ice and help retain traction performance as the material undergoes wear.

***Hypothesis 5*: AI/ML models can predict TPU abrasion resistance from mechanical and viscoelastic properties**

The abrasion resistance of TPU is influenced by mechanical and viscoelastic properties such as hardness, tensile modulus, resilience, and energy dissipation. It is hypothesized that artificial intelligence and machine learning models can identify correlations between mechanical/viscoelastic descriptors and abrasion resistance, enabling prediction of TPU wear performance and supporting a deeper understanding of property-wear relationships.

1-4- Research Objectives

The overall objective of this dissertation is to develop, evaluate, and predict the performance of elastomeric and composite materials for improved ice traction and abrasion resistance. This research addresses the scientific and engineering challenge of designing durable anti-slip materials that can provide reliable frictional performance on ice while resisting material loss under abrasive conditions. To achieve this goal, the dissertation is organized around three main research objectives, followed by an industry-focused case study that extends the application of data-driven materials design to automotive composites.

***Objective 1*: Evaluation of the influence of surface texturing on the ice friction performance of rubber composites under lab-scale high-velocity sliding conditions**

The first objective of this dissertation is to develop and apply a controlled lab-scale tribological testing method for evaluating the ice friction performance of rubber composite surfaces under high-velocity sliding conditions. Ice friction is strongly influenced by testing parameters such as sliding speed, normal load, temperature, contact configuration, and ice surface condition. Therefore, a systematic laboratory-scale testing method is required to compare the traction performance of different surface texturing technologies under controlled conditions.

This objective is addressed in **Chapter 3**, which focuses on evaluating surface texturing technologies of rubber composites on ice using a novel high-velocity tribotest method. The purpose of this chapter is to establish an experimental framework for measuring ice friction and to assess how different surface textures influence the coefficient of friction under dynamic sliding conditions. This objective provides the testing foundation for understanding the role of surface design in ice traction performance.

Specifically, this objective aims to:

- develop a lab-scale high-velocity tribotest method for measuring friction on ice;
- define key testing parameters, including sliding speed, normal load, and contact conditions;
- evaluate the repeatability and applicability of the method for comparing rubber composite surfaces;
- investigate the effect of surface texturing technologies on ice friction performance;
- establish a controlled experimental approach for evaluating anti-slip elastomeric materials.

***Objective 2*: Role of graphene nanoplatelet reinforcement and wear-activated surface evolution in TPU nanocomposite ice friction**

The second objective is to develop TPU/graphene nanoplatelet nanocomposites and investigate how composition, filler dispersion, interfacial interactions, and wear-activated surface morphology influence ice friction and abrasion resistance. TPU is selected because of its flexibility, processability, and abrasion resistance, while graphene nanoplatelets are used as reinforcing two-dimensional fillers with the potential to improve mechanical and tribological performance.

This objective is addressed in **Chapter 4**, which focuses on wear-activated surface engineering of TPU/GNP nanocomposites for ice friction control. The chapter investigates how graphene nanoplatelet incorporation and surface evolution during abrasion can contribute to friction control on ice. The objective also examines the role of filler-matrix interactions in supporting durability and maintaining functional surface characteristics during wear.

Specifically, this objective aims to:

- fabricate TPU/GNP nanocomposites with controlled filler composition;
- investigate the influence of graphene nanoplatelets on morphology, mechanical response, thermal stability, abrasion resistance, and ice friction;
- examine the role of filler dispersion and filler-matrix interaction in composite performance;
- evaluate how wear-activated surface features contribute to ice friction control;
- determine the relationship between composite structure, abrasion behavior, and ice traction performance.

***Objective 3*: Prediction of TPU abrasion resistance using machine learning models**

The third objective is to apply machine learning approaches to predict abrasion resistance in thermoplastic polyurethanes. Abrasion behavior in TPU-based materials is governed by multiple interacting variables, including chemical structure, hardness, modulus, elongation, filler characteristics, morphology, and testing conditions. These relationships can be complex and nonlinear, making abrasion performance difficult to predict using conventional experimental interpretation alone.

This objective is addressed in **Chapter 5**, which focuses on predicting abrasion resistance in thermoplastic polyurethanes using machine learning. The chapter develops a data-driven framework to identify important mechanical and structural descriptors influencing TPU abrasion resistance and to evaluate the predictive capability of machine learning models.

Specifically, this objective aims to:

- compile and structure a dataset containing TPU properties and abrasion resistance data;

- identify mechanical and structural properties that influence TPU abrasion behavior;
- develop machine learning models to predict abrasion volume loss;
- evaluate model accuracy and limitations;
- identify key descriptors that control abrasion performance;
- demonstrate the potential of machine learning as a predictive tool for designing durable TPU-based materials.

***Industry case study*: Machine learning-aided accelerated design and characterization of automotive composites**

In addition to the three main research objectives, this dissertation includes an industry-focused case study based on work conducted with a Tier-1 automotive company during the doctoral program, presented in **Chapter 6**. This chapter is not framed as a core research objective and is not directly integrated with the main dissertation theme. Rather, it is included as an additional scholarly and technical contribution completed during the PhD period, demonstrating the broader application of machine learning-aided materials design in an industrial context.

The case study focuses on the accelerated design and characterization of automotive composites using machine learning-supported approaches. It highlights the use of materials selection, formulation review, mechanical testing or characterization, data analysis, model development, and comparison against baseline materials within an industrial context. Due to confidentiality requirements, only disclosable results and technical contributions are included. This chapter supports the broader dissertation theme by showing how experimental characterization and data-driven modeling can be integrated to guide composite material development.

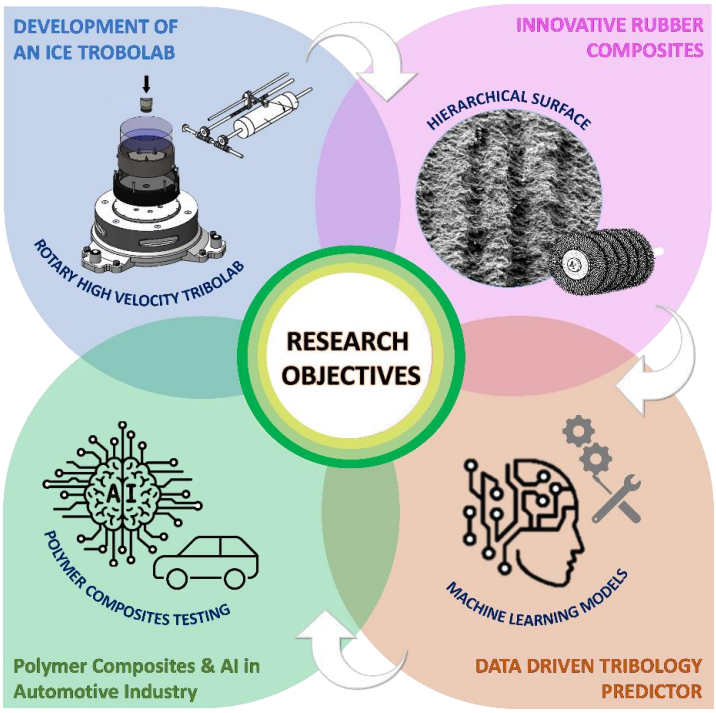


Fig. 1- 2- Schematic overview of the dissertation research objectives

1-5- Dissertation Structure

This dissertation is organized into seven chapters and follows a manuscript-based structure. The dissertation begins with the research motivation and fundamental background, followed by three main research chapters, an industry-focused case study, and a final conclusions chapter.

Chapter 1 introduces the overall research problem, knowledge gaps, research hypotheses, and research objectives. It outlines the motivation for developing durable elastomeric and composite materials for ice-traction applications and presents the structure of the dissertation. This chapter also includes the list of publications and presentations associated with the research.

Chapter 2 provides the background and fundamental concepts required to understand the dissertation. It reviews ice tribology and slips resistance, rubber and elastomeric friction, thermoplastic polyurethane for anti-slip and durable surfaces, graphene nanoplatelet-reinforced elastomeric composites, surface texturing and bioinspired anti-slip design, abrasion resistance and wear mechanisms in TPU/rubber systems, and machine learning and triboinformatics for materials design. This chapter establishes the scientific foundation for the experimental and data-driven studies presented in the following chapters.

Chapter 3, titled *Evaluating Surface Texturing Technologies of Rubber Composites on Ice Using a Novel High-Velocity Tribotest Method*, addresses the first research objective. This chapter develops and applies a lab-scale high-velocity tribotest method to evaluate the ice friction performance of textured rubber composite surfaces. It includes the chapter preface, abstract, literature review and research gaps, development of the lab-scale ice friction tester, results and discussion, conclusions, and references. This chapter establishes the experimental framework used to investigate how surface texturing influences ice traction under controlled sliding conditions.

Chapter 4, titled *Wear-Activated Surface Engineering of TPU/Graphene Nanoplatelet Nanocomposites for Ice Friction Control*, addresses the second research objective. This chapter focuses on the fabrication and characterization of TPU/GNP nanocomposites with enhanced tribological behavior and examines how graphene functionalization, filler-matrix interaction, surface texturing, abrasion resistance, and wear-activated surface evolution influence ice friction performance. It includes the chapter preface, abstract, literature review and research hypothesis, composite fabrication and characterization, results and discussion, conclusions, and references.

Chapter 5, titled *Predicting Abrasion Resistance in Thermoplastic Polyurethanes Using Machine Learning*, addresses the third research objective. This chapter develops a machine learning-based framework for predicting TPU abrasion resistance from mechanical and viscoelastic material properties. It includes the chapter preface, abstract, introduction and literature review, mechanical and structural properties influencing TPU abrasion resistance, machine learning model development, parameter optimization and hyperparameter search, results and discussion, conclusions, and references.

Chapter 6, titled *Case Study [Industrial Collaboration]: Machine Learning-Aided Accelerated Design and Characterization of Automotive Composites*, presents an industry-focused contribution completed during the doctoral program. This chapter discusses the background of automotive composite materials, the project motivation and industrial relevance, the industrial contribution workflow, data organization and preprocessing, model development, comparison against baseline materials, disclosable technical contributions, and the relevance of the case study to the broader dissertation theme. Due to confidentiality requirements, proprietary materials, datasets, processing details, and quantitative results are not disclosed.

Chapter 7 summarizes the main findings and contributions of the dissertation. It presents the key conclusions from the research chapters, highlights the original contributions of the work, discusses future research directions, and provides closing remarks.

1-6- List of Publications and Presentations

The findings of this dissertation have been shared through peer-reviewed journal publications and conference presentations, as listed below.

Journal Publications

1. S. Zahmatkesh and R. Rizvi," Evaluating Surface Texturing Technologies of Rubber Composites on Ice Using a Novel High-Velocity Tribotest Method" Tribology International, vol. 206, p. 110538, June 2025.
2. S. Zahmatkesh, H. Esmaeili, A.T. Valerio, R. Rizvi," Predicting Abrasion Resistance in Thermoplastic Polyurethanes Using Machine Learning" Journal of Applied Polymer Science, Volume 142, Issue 42, e57619, July 2025.
3. S. Zahmatkesh, SN. Leung, R. Rizvi," Wear-Activated Surface Engineering of TPU/Graphene Nanoplatelet Nanocomposites for Ice Friction Control" Journal of Polymer Composites, accepted and published online.

Conference Presentations

1. S. Zahmatkesh and R. Rizvi," Bioinspired rubber composites for superior ice traction: enhancing winter safety through innovative laboratory testing in tribology", SPIE Smart Structures + Non-Destructive Evaluations, Biologically Inspired Materials, Processes, and Systems (BIMPS) 2025; Proceedings Volume 13430, Vancouver, March 2025.
2. S. Zahmatkesh and R. Rizvi," Effect of sliding speed on tribological responses of ice traction in surface-damaged elastomeric composites", Progress in Canadian Mechanical Engineering, CSME Conference, Université de Sherbrooke, May 2023.
3. S. Zahmatkesh and R. Rizvi," Data-Driven Prediction of Abrasion Resistance in Thermoplastic Polyurethane Elastomers Using Machine Learning Approach", 25th International Conference on Wear of Materials (WOM), Sitges, Spain, April 2025.

1-7- References

[1] CIHI, “Canadian Institute for Health Information / economic burden of falls in Canada.” [Online]. Available: https://www.cihi.ca/en/quick-stats

[2] R. S. Kakara, B. L. Moreland, Y. K. Haddad, I. Shakya, and G. Bergen, “Seasonal variation in fall-related emergency department visits by location of fall – United States, 2015,” *J. Safety Res.*, vol. 79, pp. 38–44, 2021, doi: 10.1016/j.jsr.2021.08.002.

[3] C. Aschan, M. Hirvonen, E. Rajamäki, T. Mannelin, J. Ruotsalainen, and R. Ruuhela, “Performance of slippery and slip-resistant footwear in different wintry weather conditions measured in situ,” *Saf. Sci.*, vol. 47, no. 8, pp. 1195–1200, 2009, doi: 10.1016/j.ssci.2009.01.006.

[4] Z. S. Bagheri *et al.*, “Selecting slip resistant winter footwear for personal support workers,” *Work*, vol. 64, no. 1, pp. 135–151, 2019, doi: 10.3233/WOR-192947.

[5] S. Canada, “Population Projections for Canada (2018 to 2068), Provinces and Territories (2018 to 2043),” 2019.

[6] HG.org, “Slip and Fall Accident Facts,” *Legal Resources*.

[7] N. Namdari, G. J. Otto, G. Guo, H. Sojoudi, and R. Rizvi, “Nanotextured surfaces with enhanced ice-traction and wear-resistance,” *Compos. Part B Eng.*, vol. 238, p. 109916, 2022, doi: 10.1016/j.compositesb.2022.109916.

[8] R. C. Browning, R. N. Kurtz, and H. Kerherve, “Biomechanics of walking with snowshoes,” *Sport. Biomech.*, vol. 11, no. 1, pp. 73–84, 2012, doi: 10.1080/14763141.2011.637129.

[9] X. Zhang *et al.*, “A common supersolid skin covering both water and ice,” *Phys. Chem. Chem. Phys.*, vol. 16, no. 42, pp. 22987–22994, 2014, doi: 10.1039/c4cp02516d.

[10] A. M. Kietzig, S. G. Hatzikiriakos, and P. Englezos, “Physics of ice friction,” *J. Appl. Phys.*, vol. 107, no. 8, 2010, doi: 10.1063/1.3340792.

[11] C. H. Kang, W. Bin Jung, H. J. Kim, and H. T. Jung, “Highly enhanced tire performance achieved by using combined carbon nanotubes and soybean oil,” *J. Appl. Polym. Sci.*, vol. 138, no. 10, pp. 1–13, 2021, doi: 10.1002/app.49945.

[12] N. A. Forster, S. C. Wilson, and M. K. Tighe, “Examining sampling protocols for microplastics on recreational trails,” *Sci. Total Environ.*, vol. 818, p. 151813, 2022, doi: 10.1016/j.scitotenv.2021.151813.

[13] K. Yin *et al.*, “A comparative review of microplastics and nanoplastics: Toxicity hazards on digestive, reproductive and nervous system,” *Sci. Total Environ.*, vol. 774, p. 145758, 2021, doi: 10.1016/j.scitotenv.2021.145758.

[14] N. A. Forster, M. K. Tighe, and S. C. Wilson, “Microplastics in soils of wilderness areas: What is the significance of outdoor clothing and footwear?,” *Geoderma*, vol. 378, no. August, 2020, doi: 10.1016/j.geoderma.2020.114612.

[15] T. Y. Lee, L. Kim, D. Kim, S. An, and Y. J. An, “Microplastics from shoe sole fragments cause oxidative stress in a plant (Vigna radiata) and impair soil environment,” *J. Hazard. Mater.*, vol. 429, no. January, p. 128306, 2022, doi: 10.1016/j.jhazmat.2022.128306.

[16] Z. S. Bagheri, J. D. Beltran, P. Holyoke, and T. Dutta, “Reducing fall risk for home care workers with slip resistant winter footwear,” *Appl. Ergon.*, vol. 90, no. July 2020, p. 103230, 2021, doi: 10.1016/j.apergo.2020.103230.

[17] S. Zahmatkesh and R. Rizvi, “Evaluating surface texturing technologies of rubber composites on ice using a novel high-velocity tribotest method,” *Tribol. Int.*, vol. 206, no. October 2024, 2025, doi: 10.1016/j.triboint.2025.110538.

[18] J. Zhang and L. Zhao, "(12) United States Patent," vol. 2, 2021.

[19] R. Arsada, E. Surojo, D. Ariawan, N. Muhayat, and W. W. Raharjo, "Effect of NBR (Nitrile Butadiene Rubber) on flexural strength of composite friction brake," *IOP Conf. Ser. Mater. Sci. Eng.*, vol. 420, no. 1, 2018, doi: 10.1088/1757-899X/420/1/012057.

[20] V. Ahlawat, S. Kajal, and A. Parinam, "Exploring the suitability of milled fly ash for brake friction composites: characterization and tribo-performance," *Mater. Res. Express*, vol. 6, 2019, doi: https://doi.org/10.1088/2053-1591/aafc00.

[21] R. Rizvi, H. Naguib, G. Fernie, and T. Dutta, "High friction on ice provided by elastomeric fiber composites with textured surfaces," *Appl. Phys. Lett.*, vol. 106, no. 11, 2015, doi: 10.1063/1.4913676.

[22] Z. S. Bagheri, Y. Li, A. R. Fekr, and T. Dutta, "The effect of wear on slip-resistance of winter footwear with composite outsoles: A pilot study," *Appl. Ergon.*, vol. 99, p. 103611, 2022, doi: 10.1016/j.apergo.2021.103611.

[23] M. S. Hasan, A. Kordijazi, P. K. Rohatgi, and M. Nosonovsky, "Triboinformatics approach for friction and wear prediction of Al-graphite composites using machine learning methods," *J. Tribol.*, vol. 144, no. 1, pp. 1–13, 2022, doi: 10.1115/1.4050525.

Chapter 2:
Background and Fundamentals

2-1- Ice Tribology and Slip Resistance

Tribology is the science and engineering of interacting surfaces in relative motion, with emphasis on friction, wear, and lubrication [1]. It provides the fundamental framework for understanding how materials interact under contact, how resistance to motion is generated, and how surfaces degrade during repeated sliding [2]. In practical applications such as footwear, tires, seals, and mechanical components, tribological performance is strongly influenced by material properties, surface morphology, contact pressure, sliding speed, and the presence of lubricating layers [3].

Ice tribology is a specialized branch of tribology that focuses on friction, lubrication, and wear at ice-contacting interfaces. In the context of this dissertation, ice tribology is particularly important because slip resistance on ice depends on the ability of an elastomeric surface to generate sufficient friction while maintaining durability during repeated sliding [4]. Improving ice traction requires increasing effective solid-solid interactions at the ice-material interface, while limiting excessive wear of the composite surface under contact with hard substrates [5].

Although ice is a crystalline solid, its surface is typically covered by a thin quasi-liquid film (QLF), even at subzero temperatures. This liquid-like layer becomes more pronounced as the temperature approaches the melting point, leading to reduced friction and increased slipperiness [6]. The formation of this layer is associated with weakened hydrogen bonding within O–H groups, which results in partial molecular mobility at the ice surface [7]. In ice tribology, this interfacial water layer acts as the primary lubricating medium and strongly influences the frictional response [8]. Ice can therefore behave as a hard solid with a lubricated surface. The low friction of ice is commonly attributed to the presence of this thin water film, which may form or thicken due to pressure melting and frictional heating during sliding contact [8]. As the contact pressure or frictional force increases, a thicker liquid-like layer may develop at the interface [9]. This can reduce direct solid-solid contact and significantly decrease friction through hydrodynamic lubrication effects [10]. Consequently, the thickness and stability of the liquid-like layer are critical factors controlling the interaction between rubber or elastomeric materials and ice.

Frictional behavior on ice is generally observed in two main modes: smooth sliding and stick-slip motion [5]. As schematically shown in Fig. 2-1, smooth sliding is characterized by an initial peak in friction force, corresponding to the static friction force, F_s, followed by a relatively stable plateau associated with the kinetic friction force, F_k. In contrast, stick-slip behavior involves periodic fluctuations in friction force between maximum and minimum values, representing repeated sticking and slipping events at the interface [11]. These frictional modes are important for understanding the performance of anti-slip materials, as they reflect contact stability and the ability of the surface to maintain traction during sliding.

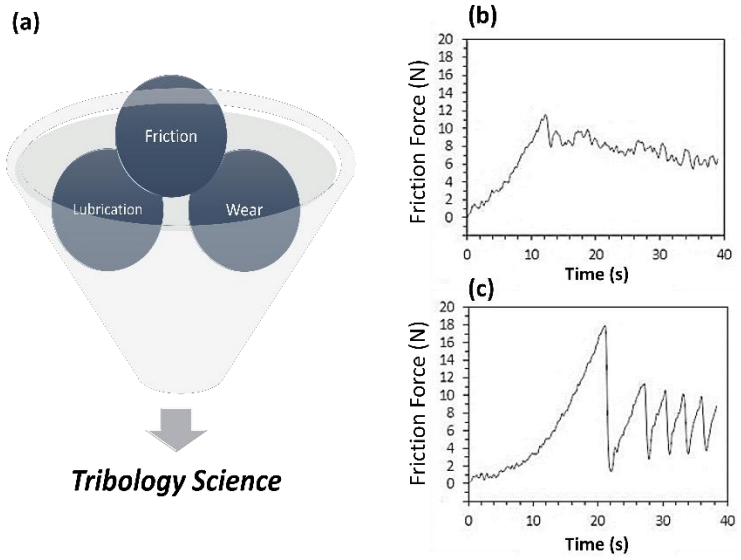


Fig. 2- 1- (a) Fundamentals of tribology and friction force responses on ice: (b) smooth sliding and (c) stick-slip behavior [5].

The thickness of the liquid-like layer directly affects the degree of solid-solid interaction between the elastomer and the ice surface. A thicker interfacial water layer reduces mechanical interaction between the material and the underlying ice, leading to lower friction [12]. Therefore, effective anti-slip surface design should aim to disrupt or manage this lubricating layer while promoting mechanical interlocking, localized contact, or drainage pathways that improve traction [13].

Several standardized methods have been developed to evaluate the slip resistance of footwear and outsole materials. ISO 13287:2019 [14] is one of the commonly used standards for assessing footwear slip resistance. ASTM F2913-11 [15] provides guidance for measuring the dynamic coefficient of friction under laboratory conditions, which is particularly relevant for evaluating the interaction between footwear and flooring materials including ice.

SATRA [16], a UK-based research and testing organization, is widely recognized for footwear testing and the development of slip-resistance evaluation equipment. SATRA TM144 is a test method used to determine the dynamic coefficient of friction between footwear and flooring surfaces [17]. The SATRA STM 603 slip-resistance testing machine is designed to perform such tests under controlled conditions [18]. Its testing protocols are based on biomechanical studies of slip occurrence and can be configured according to SATRA TM144, EN 13287, or other procedures. The system measures the coefficient of friction between the footwear sample and the underlying test surface, including ice trays, and can perform tests at different sliding speeds.

In addition to slip resistance, abrasion resistance is a critical performance requirement for footwear materials. SATRA also provides equipment and test methods, such as the Martindale abrasion test [19], to evaluate the wear resistance of footwear components, excluding the outsole. This test assesses material durability under controlled conditions, defined test speeds, and specified numbers of abrasion cycles. The principle of the Martindale abrasion test is based on the relative motion between the specimen and an abradant, allowing comparative evaluation of material resistance to surface wear.

Overall, ice tribology involves the interaction of friction, lubrication, surface deformation, and wear at the ice-material interface. The presence of a quasi-liquid film makes ice friction fundamentally different from dry friction on rough solids. Therefore, the development of ice-traction materials requires an understanding of both interfacial lubrication mechanisms and the material properties that control contact, deformation, surface texture, and durability.

2-2- Rubber and Elastomeric Friction

Rubber friction is controlled by the coupled effects of material deformation, surface geometry, interfacial adhesion, and contact mechanics [4]. In contrast to rigid solids, rubbers can undergo large recoverable deformation when loaded against a counter surface [20]. This deformation enables the rubber to conform to surface asperities and generate friction through two main mechanisms: viscoelastic energy dissipation within the bulk material and interfacial shear at the real contact area [21]. Therefore, in applications such as footwear outsoles and tires, friction is not governed by a single factor, but by the combined influence of elastomer properties, outsole geometry, and surface texture [22].

The total friction force of a rubber outsole can be described as the sum of the viscoelastic contribution and the interfacial shear contribution at the real contact area [23]. In this framework, the friction force, F_f, can be expressed as:

$$F_f = F_{visc} + \tau_f \, \mathrm{A} \qquad \text{Equation (2-1)}$$

where $F_{visc.}$ represents the viscoelastic contribution, τ_f is the shear stress at the contact interface, and A is the real contact area. The viscoelastic component can be represented using a simplified Kelvin–Voigt model [24], as shown in Equation (2-2):

$$F_{visc.} = \left(E\varepsilon + \mathrm{h}\frac{d\varepsilon}{dt} \right) \times A \qquad \text{Equation (2-2)}$$

where E is the elastic modulus of the rubber, η is the viscosity, ε is the strain, and $\frac{d\varepsilon}{dt}$ is the strain rate. This relationship indicates that the deformation response depends on both the elastic resistance of the material and its time-dependent viscous dissipation.

Surface geometry also plays a central role in elastomeric friction. Surface texturing should be considered across multiple length scales rather than only at the macroscopic level [25]. Surface texture is commonly divided into three main categories: macro-geometrical form, waviness, and roughness [26]. These components collectively determine how an elastomeric surface contacts and interacts with an opposing surface. Macro-geometrical form describes the overall shape and tread design, waviness represents intermediate-scale surface undulations, and roughness refers to fine-scale asperities and micro textures. Together, these scales control contact area, pressure distribution, deformation behavior, and the ability of the surface to interact mechanically with ice or other substrates, as schematically illustrated in Fig.2-2.

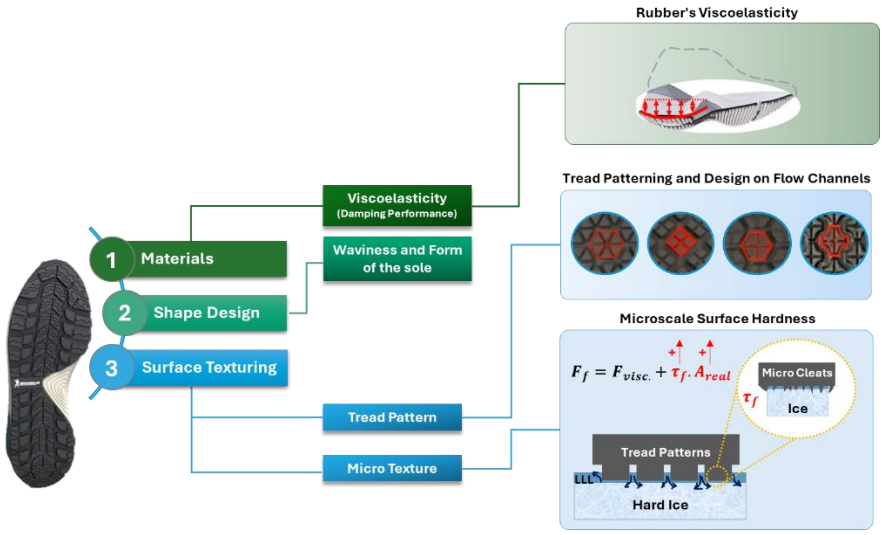


Fig. 2- 2- Surface texturing and outsole design factors contributing to the frictional response of shoe soles on ice.

In ice-traction applications, all three surface-texture scales are important. Increased surface roughness can improve ice gripping by promoting local mechanical interaction, provided that the macro-scale form and waviness also support effective contact. Macro-geometrical design is particularly important in footwear and tire applications because it is controlled by tread patterns [27].

In rubber industries, including automobile tires and footwear outsoles, tread design is a fundamental factor affecting traction, and extensive research has investigated the influence of tread shape on frictional performance [28]. Tread patterns improve traction through several mechanisms. First, they concentrate load into discrete contact regions, increasing local contact pressure. This localized pressure can enhance mechanical interaction with the counter surface, particularly on ice or wet surfaces. Second, tread grooves and sipes act as flow channels that help remove water, slush, or contaminants from the contact interface. This drainage function is important because a continuous liquid film can reduce direct rubber-surface contact and promote lubrication. By interrupting the formation of a continuous water layer, tread structures help increase dry or semi-dry rubber–surface interaction [29].

The role of tread channels can also be interpreted from a fluid-flow perspective. When water or a quasi-liquid layer is present at the interface, the tread geometry influences pressure distribution and fluid displacement. Bernoulli's principle [30] provides a simplified description of the relationship between pressure, fluid velocity, and elevation in a flowing fluid, as expressed in Equation (2-3):

$$P + \frac{1}{2}\rho n^2 + \rho g h = C \qquad \text{Equation (2-3)}$$

where P is the fluid pressure, ρ is the fluid density, v is the fluid velocity, g is the gravitational acceleration, h is the fluid height, and C is a constant.

For more complex flow conditions, the Navier-Stokes equation [31] describes the momentum balance of a viscous fluid, as shown in Equation (2-4):

$$\rho\left(\frac{\delta n}{\delta t} + n.\nabla n\right) = -\nabla P + \mu\nabla^2 n + F \qquad \text{Equation (2-4)}$$

where v is the velocity field, t is time, ∇P is the pressure gradient, μ is the dynamic viscosity, and F represents external body forces.

These relationships conceptually describe how pressure, velocity, viscosity, and channel geometry can influence fluid removal from the contact zone. Therefore, outsole patterns are not only mechanical features but also fluid-management structures that affect the lubrication state at the interface.

At the microscale, surface hardness and local contact mechanics further affect friction. Microtextures or micro-cleats can increase local stress concentration and promote mechanical interlocking with hard ice as described with Hertzian contact theory [32] (Equation 2-5).

$$P_{max} = \frac{3}{2}\frac{F}{\pi a^2} \qquad \text{Equation (2-5)}$$

Where P_{max} is the contact pressure, F is the applied normal force on the contact surface, and a is the contact radius. Based on contact mechanics concepts, the maximum contact pressure depends on the applied force and contact radius. Smaller asperities or microfeatures can therefore generate higher local pressures, which may help penetrate or disrupt the interfacial liquid-like layer on ice. This mechanism is particularly relevant for bioinspired designs, where microscale features can be used to mimic natural traction systems, such as scale-like structures for mechanical interlocking or channel-like features for water management [33].

Overall, rubber and elastomeric friction results from the interaction of viscoelastic material behavior, tread geometry, surface roughness, local contact pressure, and interfacial lubrication. For ice-traction applications, effective outsole or composite surface design must therefore combine appropriate bulk material properties with hierarchical surface features capable of increasing

contact stability, disrupting lubricating films, and enhancing mechanical interaction with the ice surface.

2-3- Surface Texturing and Bioinspired Anti-Slip Design

Surface texture plays a critical role in controlling the interaction between an engineered material and its surrounding environment. In biological systems, the outer surface is often the first point of contact with external conditions, and many natural surfaces have evolved specialized textures to control adhesion, friction, wetting, drag, and locomotion. Examples include the fibrous setae on gecko feet that enable adhesion to vertical surfaces [34], fractal-like papillae on lotus leaves that promote hydrophobicity and self-cleaning behavior [35], and ridged denticles on shark skin that reduce hydrodynamic drag [36]. These natural systems demonstrate how hierarchical surface structures can produce highly functional interfacial properties.

Bioinspired design uses these natural mechanisms as models for developing engineered materials with tailored surface functions, including high friction, low friction, hydrophobicity, self-cleaning behavior, and anti-slip performance. For ice-traction applications, several biological systems are particularly relevant because they have evolved mechanisms for maintaining grip on snow, ice, or wet surfaces. Figure 2.3 illustrates bioinspired approaches based on animals such as polar bears, Arctic seals [37], snakes [38], [39], and penguins [22].

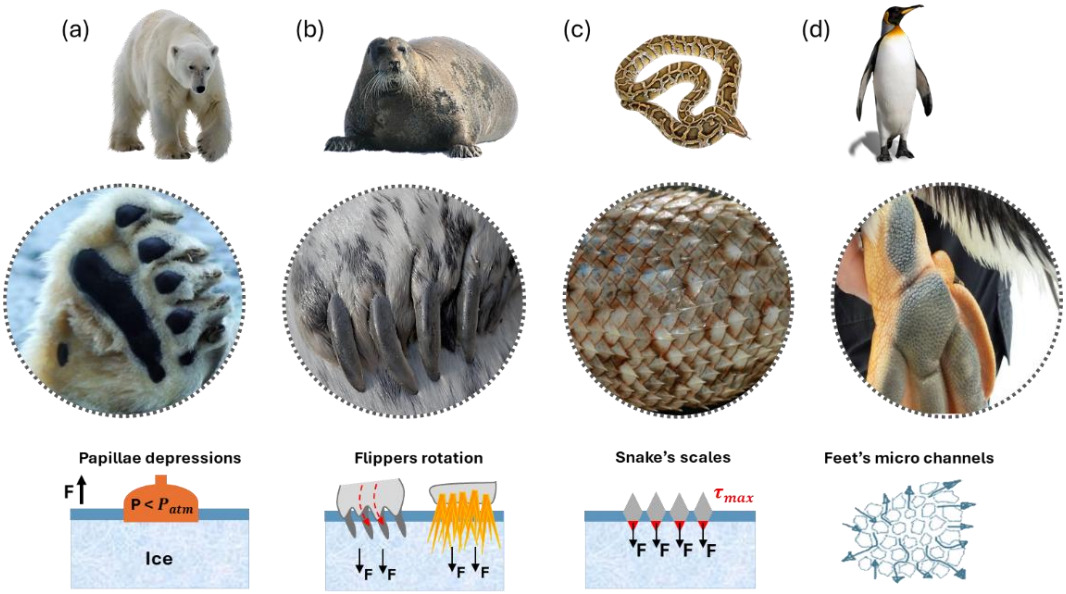


Fig. 2- 3- Bioinspired mechanisms for enhanced traction: a) Polar bear feet with papillae structures that increase adhesion through surface depression, combined with hard claws for mechanical interlocking; b) arctic

seal with rotated flippers and sharp hairy body that enhance frictional grip; c) Snake scales that improve mechanical interlocking and shear resistance upon activation; d) Penguin feet with microchannels that dissipate surface fluids, promoting dry contact, supplemented by strong claws for increased traction.

These species use different surface strategies: papillae-like depressions in polar bear paws [40], rotated clawed flippers and sharp hairy structures in Arctic seals [22], mechanical interlocking in snake scales [41], and microchannel-rich footpads in penguins for fluid dissipation [22]. Together, these examples highlight how surface morphology, stiffness contrast, interlocking features, and fluid-management channels can contribute to enhanced traction.

Among these biological inspirations, polar animal claws and penguin feet are especially relevant to ice traction. The claws of polar animals are composed of keratin, a stiff material that enables penetration and mechanical interlocking with icy surfaces. In contrast, penguin footpads contain microchannels that can assist in dissipating the quasi-liquid film (QLF) present on ice, thereby promoting more effective contact with the underlying surface [22], [42]. These natural strategies suggest that effective anti-slip surfaces should not only increase roughness but also manage interfacial water and generate localized mechanical engagement with ice.

Inspired by these mechanisms, several studies have focused on developing textured elastomeric surfaces for reducing slips and falls on ice. Surface texturing is a widely used strategy for modifying surface roughness at micro- and nanoscales. Common surface texturing methods include imprinting, photolithography, laser ablation, chemical etching, plasma treatment, and mechanical abrasion [43]–[47]. In imprinting, a mold is used to transfer a predefined pattern onto the surface [43]. In photolithography, patterned light exposure is applied to a photoresist layer, followed by chemical development to form the desired texture [44]. Laser ablation produces micro-patterns by selectively removing material from the surface using laser energy [45]. These techniques can generate controlled surface features; however, for ice-traction applications, textures formed from the same soft substrate material may not always provide sufficient hardness or durability for effective mechanical gripping.

This limitation becomes clear when comparing engineered textures with natural ice-traction systems. In polar animals, claws are not formed from the same soft tissue as the footpad; instead, they are made of a harder material that provides strength and mechanical engagement with ice [22]. Therefore, conventional surface texturing approaches that only create asperities from the bulk elastomer may have limited effectiveness for ice traction. This motivates the development of

textured composite surfaces in which harder reinforcing phases can protrude from or interact with the elastomeric matrix to mimic the gripping function of claws [48].

Babaee et al. proposed a bioinspired traction approach using kirigami-based metamaterial surfaces [5]. These structures were designed to protrude out of plane under bending strain and function as sharp ice-gripping features. After evaluating different spike geometries, the optimized kirigami pattern was fabricated as perforated steel sheets and attached to shoe outsoles. During walking, heel-induced bending caused the elements to protrude and improve traction on ice and other flooring surfaces.

Another approach for producing anti-slip elastomeric surfaces is Damage-Induced Surface Texturing (DIST), introduced by Rizvi et al. [49]. In contrast to conventional surface texturing methods such as laser texturing and lithography, DIST intentionally creates roughened composite surfaces through reinforcement debonding and pull-out. This process generates protruding micro-cleats that can mechanically engage with the ice surface. As schematically illustrated in Fig. 2-4, glass fibers are first incorporated into an elastomer matrix, extruded and aligned along the flow direction, and then compression molded into sheets of predefined thickness. The molded composites are subsequently cut transversely, reoriented, and rejoined to create the textured surface. During cutting, debonding of the glass fibers from the elastomer matrix produces hard protruding fibers capable of gripping the ice surface [50]. DIST surfaces have been reported to significantly enhance slip resistance on ice, showing approximately 900% improvement compared with pristine, untextured surfaces [51].

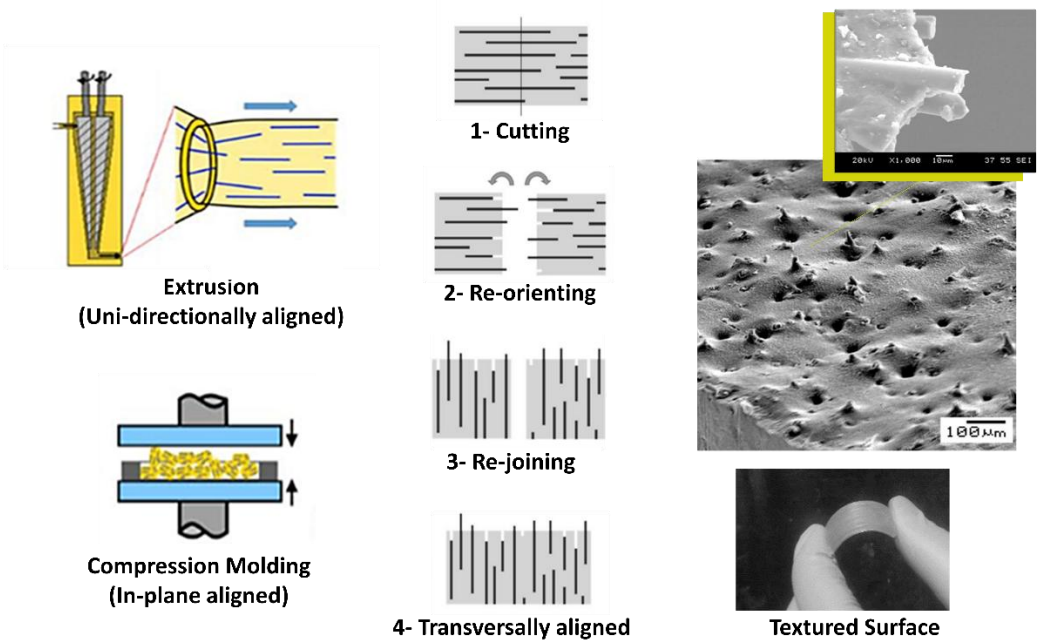


Fig. 2- 4- Damage Induced Surface Textured (DIST) composites: the schematic of fabrication practice and the obtained textured surface [49]

However, DIST surfaces based on one-dimensional hard fibers have an important limitation. The protruding fibers can abrade rapidly when exposed to non-ice surfaces, such as hard pavements, which are unavoidable in footwear applications. As these micro-cleats wear down, the surface may lose its anti-slip functionality, resulting in limited functional lifetime [52]. This limitation underscores the need for surface-engineered materials capable of preserving, regenerating, or re-exposing effective ice-traction features during abrasive wear. In this context, several anti-slip outsole technologies have been developed to enhance friction on icy surfaces, including commercially available systems such as Vibram® Arctic Grip™ [53]. Although these technologies have demonstrated improved ice-traction performance, their long-term durability remains a concern, as repeated exposure to abrasive non-ice substrates can degrade the functional surface features and limit traction performance to a finite walking distance [52].

To address this issue, Namdari and co-workers investigated the use of two-dimensional materials in elastomeric composites [54]. Their approach used solution-based processing followed by compression molding. The composites were then cut transversely to generate damaged textured surfaces, eliminating the need for fiber alignment and reorientation after cutting. This method reduced processing complexity while enabling the formation of functional surface features. Their study compared the ice-traction performance of Styrene-Ethylene/Butylene-Styrene (SEBS)

rubber composites containing both one-dimensional and two-dimensional fillers across micro- and nanoscales. The composites were evaluated before and after abrasion to determine the durability of their traction performance. The results showed that composites containing one-dimensional additives exhibited reduced ice traction after abrasion, whereas composites containing two-dimensional additives showed improved traction after abrasion. Among the investigated fillers, graphene nanoplatelets (GNPs) demonstrated strong ice-traction performance both before and after abrasion, which was attributed to the lower tendency of two-dimensional fillers to buckle compared with one-dimensional fillers [54].

Overall, bioinspired surface design provides a powerful framework for developing anti-slip materials by combining mechanical interlocking, stiffness contrast, surface roughness, and fluid management. For ice-traction applications, effective textured surfaces must not only increase friction initially but also maintain functionality during wear. This requirement is especially important for footwear and tire applications, where materials are exposed to both icy surfaces and abrasive non-ice substrates. Therefore, the integration of bioinspired textures with composite material design offers a promising pathway for developing durable elastomeric surfaces with enhanced ice-traction performance.

2-4- Thermoplastic Polyurethane for Anti-Slip and Durable Surfaces

Thermoplastic polyurethane (TPU) is one of the most widely used elastomers in the footwear outsole industry due to its combination of flexibility, toughness, abrasion resistance, and processability. It is a segmented copolymer composed of alternating soft and hard segments, which together provide the material with rubber-like elasticity and plastic-like mechanical strength [55]. The soft segments, typically based on long-chain polyether or polyester polyols, are responsible for flexibility and low-temperature performance. In contrast, the hard segments are highly polar domains formed through reactions between isocyanates and chain extenders, such as hydroxyl-containing compounds or 1,4-butanediol. These hard domains act as physical crosslinks and contribute to the stiffness, strength, and dimensional stability of TPU [56], [57]. Figure 2-5 schematically illustrates the structure of a TPU chain comprising soft and hard segments.

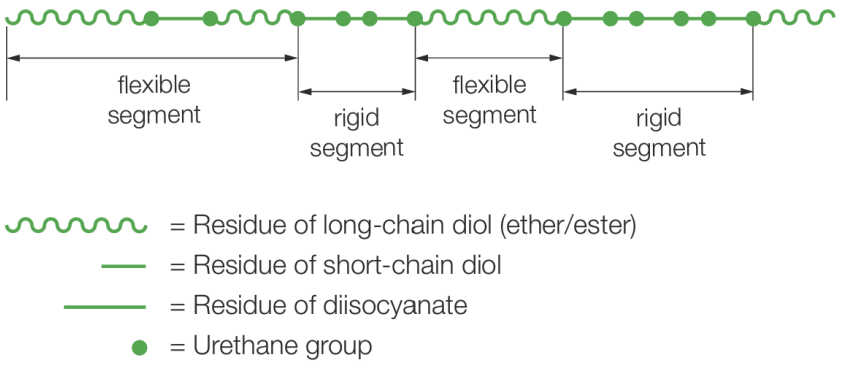


Fig. 2- 5- Schematic illustration of chain structure of Thermoplastic Polyurethane (TPU) composed of sequentially hard and soft segments [57]

The segmented structure of TPU enables a broad range of mechanical and thermal properties. By changing the chemistry, molecular weight, and relative proportion of the soft and hard segments, TPU can be tailored from soft elastomeric grades to hard plastic-like materials [59]. This chemical tunability allows TPU properties such as toughness, flexibility, abrasion resistance, tear strength, and environmental stability to be adjusted for specific applications. Changes in the polyol structure, isocyanate type, chain extender, or stoichiometric ratio can modify TPU phase separation and lead to the formation of distinct hard and soft domains. These morphological changes can influence physical crosslinking, molecular mobility, stiffness, toughness, and abrasion resistance [60]. In particular, the choice of isocyanate plays an important role in controlling the rigidity and mechanical strength of TPU [61]. The hard segments also influence the degree of phase separation between hard and soft domains, which affects morphology, chain mobility, and overall mechanical performance [62]. As a result, TPU occupies a unique position between conventional rubbers and plastics, making it suitable for applications that require both deformation capability and mechanical durability.

TPU has been widely used in several industries, including footwear, automotive, healthcare, electronics, protective equipment, coatings, films, cables, and consumer products [63]. In automotive applications, TPU is used in components that require wear resistance, resilience, and mechanical stability under repeated loading, such as suspension-related components, air bumps, protective covers, and interior or exterior parts exposed to mechanical contact [64], [65]. In footwear, TPU is used in outsoles, midsoles, protective structures, and athletic footwear components because of its lightweight nature, durability, and ability to withstand repeated

deformation [66]. In healthcare, TPU is valued for its biocompatibility and flexibility and is commonly used in medical tubing, and surgical catheters [67], [68].

The application of TPU in footwear, automotive, and biomedical systems often involves exposure to abrasive or sliding contact environments. Therefore, understanding TPU tribological behavior is essential for predicting material performance and service life. Abrasion resistance is particularly important because it determines the durability of TPU-based components such as footwear outsoles, automotive parts, and medical devices exposed to repeated contact or motion [69]. For anti-slip and durable surface applications, TPU must provide not only sufficient frictional response but also resistance to material loss during repeated sliding.

The mechanical performance of TPU is strongly governed by its viscoelastic nature and phase-separated morphology. As an elastomeric material, TPU exhibits both elastic and viscous responses during deformation, which arise from the interaction between flexible soft segments and rigid hard segments [70]. The soft domains provide chain mobility and recoverable deformation, while the hard domains act as physical crosslinking points that reinforce the polymer network. This combination enables TPU to dissipate energy under dynamic loading while maintaining structural integrity.

Beyond elasticity, TPUs exhibit high mechanical strength, tear resistance, toughness, and abrasion resistance. These properties are strongly affected by the organization and distribution of hard and soft segments within the polymer structure. The hard segments occupy a significant volume fraction and act as reinforcing domains, improving load transfer and resistance to mechanical damage. Variations in hard-segment content, soft-segment chemistry, and molecular architecture can therefore substantially influence the morphology and mechanical response of TPU [71].

For ice-traction and anti-slip applications, TPU is attractive because it combines flexibility, surface adaptability, and strong abrasion resistance. Its ability to wet and interact with additives further supports its use as a matrix for composite development. In addition, TPU can exhibit favorable frictional behavior due to its traction-related properties. These characteristics make TPU a promising candidate for the development of durable elastomeric surfaces where both ice friction and wear resistance are required.

2-5- Graphene Nanoplatelet-Reinforced Elastomeric Composites

Graphene nanoplatelets (GNPs) have attracted significant interest as reinforcing fillers in elastomeric composites because of their two-dimensional geometry, high aspect ratio, high surface area, and outstanding mechanical properties. Graphene is among the stiffest two-dimensional materials, with an in-plane Young's modulus in the terapascal range, making it a promising reinforcement for high-performance polymer composites [72], [73]. In elastomeric systems, GNPs can potentially improve stiffness, strength, abrasion resistance, thermal stability, and tribological performance when they are effectively dispersed and strongly bonded to the surrounding matrix [74]. For ice-traction applications, the platelet geometry of GNPs is particularly relevant because two-dimensional fillers can contribute to surface texture formation, load transfer, and wear-induced surface evolution [75].

Large-scale production of GNPs generally relies on graphite as the precursor material. As a result, complete exfoliation into monolayer graphene is not always achieved, and the final material often contains multilayer graphitic platelets [76], [77]. This incomplete exfoliation is important in surface-textured elastomeric composites because poorly exfoliated graphite-like stacks may not function effectively as micro-scale gripping features. Instead, stacked layers may promote debonding, delamination, or self-lubricating behavior within the composite, which can reduce frictional performance and negatively affect durability. Therefore, controlling the exfoliation state of GNPs is a critical factor in designing graphene-reinforced elastomeric composites for tribological applications. Figure 2.6 schematically illustrates the layered structure of GNPs and the possible states of dispersion, including stacked, intercalated, and exfoliated configurations.

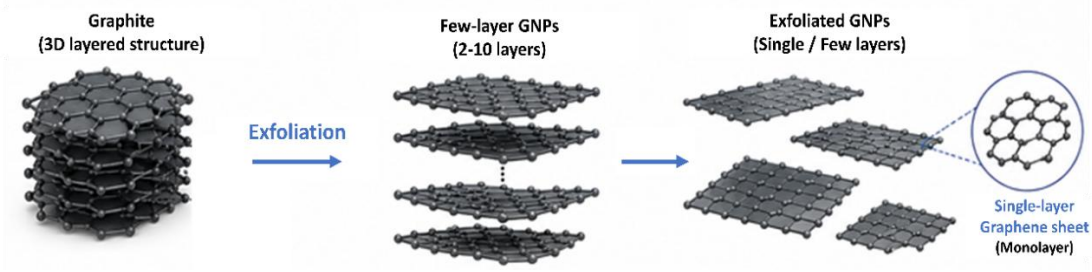


Fig. 2- 6- Schematic representation of the layered graphite structure and the exfoliation process into few-layer graphene nanoplatelets and single-/few-layer graphene sheets.

The performance of GNP-reinforced composites is strongly dependent on the dispersion of GNPs within the polymer matrix. Because graphene sheets have a high surface-to-volume ratio, they are

prone to agglomeration, especially in polymer matrices with weak interfacial compatibility, such as SEBS [78]. Agglomeration can reduce the effective filler surface area, create stress concentration sites, limit load transfer, and reduce the ability of the filler to improve frictional or mechanical behavior. Poor dispersion may also lead to restacking of graphene layers due to strong van der Waals forces and π–π interactions, which is essentially the reverse of exfoliation [72]. Therefore, both exfoliation and dispersion must be controlled to achieve effective reinforcement and stable tribological performance.

Solution mixing is commonly used to synthesize GNP-polymer composites because it enables relatively uniform filler distribution during processing. However, solvent evaporation during this process can promote re-agglomeration of the reinforcing phase [79]. This issue is particularly important for ice-traction composites, where filler distribution can influence surface morphology, micro-cleat formation, and ice-gripping performance. Inadequate dispersion may result in nonuniform surface features and inconsistent frictional response. Therefore, optimizing both processing conditions and filler-matrix interactions is essential for improving the mechanical and tribological performance of GNP-reinforced elastomeric composites.

Graphene-polymer nanocomposites can be prepared through non-covalent and covalent approaches. Non-covalent methods include solution mixing, melt mixing, and in situ polymerization, in which GNPs are dispersed in a monomer solution followed by polymerization. These methods preserve the graphitic structure of the filler but may provide limited interfacial bonding with the matrix. In contrast, covalent approaches introduce functional groups onto the graphene surface, enabling chemical interaction or bonding with the polymer matrix. Covalent modification can be achieved through grafting-from or grafting-to strategies, depending on the polymer chemistry and intended interfacial reaction [80]. In these methods, the carbon surface is chemically modified and subsequently linked to polymer chains, improving compatibility and interfacial adhesion. However, covalent functionalization routes can involve complex chemical procedures, specialized equipment, and large quantities of reagents [81]–[83].

A practical approach for modifying GNP surfaces is acid treatment, which can introduce oxygen-containing functional groups, particularly carboxylic acid moieties, at the edges of carbon nanosheets [72]. These functional groups can provide active sites for improved adhesion between GNPs and the polymer matrix [84]. For TPU-based composites, such functionalization is expected

to improve filler-matrix compatibility by increasing interfacial interaction between the polar functional groups on GNPs and the segmented polyurethane structure.

The interfacial interaction between GNPs and the elastomeric matrix is a key factor governing composite durability. Under abrasive conditions, material loss can occur through particle fracture, filler pull-out, matrix tearing, or debonding at the filler–matrix interface [85]. Although mechanically robust fillers can delay fracture, their reinforcing efficiency depends strongly on the quality of interfacial bonding with the rubber or TPU matrix. Surface modification of graphene sheets can improve both filler dispersion and matrix compatibility, thereby reducing filler detachment and enhancing load transfer during deformation and wear [86], [87]. As a result, functionalized GNPs can contribute to improved abrasion resistance and long-term durability in elastomeric composites.

The dispersion quality of GNPs also influences the formation of a reinforcing filler network within the polymer matrix. When GNPs are well dispersed, they can form interconnected or semi-interconnected structures that substantially affect the macroscopic properties of the composite [87].

For ice-traction applications, GNP-reinforced elastomeric composites are promising because they combine the flexibility of an elastomeric matrix with the stiffness, high aspect ratio, and two-dimensional geometry of graphene-based fillers. Compared with one-dimensional fillers, two-dimensional GNPs may exhibit reduced buckling and improved stability during abrasion, allowing them to contribute more effectively to wear-activated surface features [88]. However, the effectiveness of GNP reinforcement depends strongly on exfoliation, dispersion, filler loading, and interfacial adhesion. Poorly dispersed or weakly bonded GNPs may behave as defects or self-lubricating sites, whereas well-dispersed and functionalized GNPs can improve mechanical performance, abrasion resistance, and tribological response. Therefore, controlling the structure-interface-property relationship is essential for developing GNP-reinforced elastomeric composites for durable anti-slip surfaces.

2-6- Abrasion Resistance and Wear Mechanisms in TPU/Rubber Systems

Abrasion resistance is a critical property for rubber and TPU-based materials used in applications involving repeated sliding, rubbing, or contact with rough surfaces. In footwear outsoles, tires,

automotive components, and biomedical devices, abrasive wear can lead to material loss, surface damage, dimensional instability, and reduced functional lifetime [89]. For anti-slip applications, abrasion is particularly important because the surface features responsible for traction may gradually wear away during service, reducing ice-gripping performance over time.

The application scope of thermoplastic polyurethane (TPU) frequently involves exposure to abrasive environments, making tribological evaluation essential. Assessing the wear resistance of TPU is important for estimating the service life of components such as automotive suspension units, medical catheters used inside the human body, and footwear outsoles exposed to repeated contact with walking surfaces. Therefore, abrasion-focused tribological testing is necessary for predicting the operational durability of TPU-based parts under specific service conditions [69]. The abrasion resistance of rubbers and elastomers is commonly evaluated by measuring volume loss after standardized wear testing. Several standards define procedures for abrasion-resistance testing of rubber materials [90]. In these tests, abrasion resistance is typically determined from the amount of material removed during contact with an abrasive surface. To enable comparison between materials, the Abrasion Resistance Index (ARI) is introduced in standardized methods [91]. The ARI is calculated as:

$$ARI = \frac{\Delta m_1 . \rho_2}{\Delta m_2 . \rho_1} \times 100 \qquad \text{Equation (2-6)}$$

where Δm_1 is the mass loss of the standard rubber in milligrams, Δm_2 is the mass loss of the test sample in milligrams, ρ_1 is the density of the standard rubber, and ρ_2 is the density of the sample. This index normalizes mass loss by density, allowing abrasion performance to be compared between materials with different densities.

Various experimental methods have been used to evaluate the abrasion resistance of rubber and elastomeric composites. A rotary cylindrical drum abrader following ISO 4649/DIN 53516 is commonly used to measure the abrasion resistance of rubber composites [35]. Other wear-testing configurations can also be used depending on the dominant contact condition and target wear mechanism. For example, rotating drum tests are commonly associated with abrasive wear against rough surfaces, while pin-on-disk configurations are used to evaluate sliding contact wear [92]. Namdari et al. developed a wear-test setup using aluminum abrasive paper fixed on a flat sheet to establish a standardized protocol for comparing the abrasion resistance of composites [54].

In the present research context for footwear, abrasive wear against rough surfaces is relevant for evaluating the durability of the synthesized composites. In the standard rotary drum approach, prepared specimens are abraded against a rotating drum covered with abrasive paper, and the resulting volume loss is used to quantify abrasion resistance [91]. The volume-loss calculation requires accurate density measurement of the sample, which can be conducted according to ISO 2781 using an Archimedes setup [93]. The abrasion testing duration and sliding speed can be defined based on the total sliding distance and speed specified in ISO 4649, allowing the method to remain connected to established abrasion standards.

The dominant wear mechanism in elastomeric systems depends on material properties, filler morphology, interfacial adhesion, surface roughness, normal load, sliding distance, and counter-surface characteristics. In filled elastomers and composite surfaces, interfacial bonding between reinforcing particles and the polymer matrix is especially important. Weak interfacial adhesion may promote particle pull-out, phase separation, and localized stress concentration, which can accelerate material removal during abrasion [94].

In this project, insufficient interfacial bonding between reinforcing particles and the elastomeric matrix is considered a possible contributor to the poor wear performance of some damage-induced surface-textured composites. Weak filler-matrix adhesion may prevent particles from being effectively anchored within the elastomer, leading to particle detachment, surface degradation, and reduced abrasion resistance. This mechanism is particularly important for ice-traction composites, where protruding or exposed reinforcing phases are intended to improve mechanical interaction with ice. If these features are rapidly removed during abrasion, the material may lose its anti-slip functionality.

For TPU systems, abrasion resistance is closely linked to mechanical and viscoelastic properties such as hardness, modulus, tensile strength, elongation at break, resilience, and energy dissipation [95]. The segmented structure of TPU, consisting of hard and soft domains, influences resistance to deformation, crack initiation, and material removal under sliding contact [96]. Therefore, abrasion resistance in TPU should be understood as a combined response of molecular structure, phase morphology, mechanical properties, and contact conditions.

Despite the importance of abrasion testing, experimental evaluation can be time-consuming and resource intensive. Standardized tests such as ISO 4649/DIN 53516 require controlled specimen

preparation, post-production density measurement, precise mass-loss measurement, and repeated testing to obtain reliable data. Consequently, predictive approaches that estimate abrasion resistance before extensive experimental validation are valuable for accelerating materials development. The ability to predict abrasion performance can help determine whether a TPU or composite formulation is likely to meet target requirements for durability, service life, and functional performance.

Overall, abrasion resistance in TPU/rubber systems is a key factor controlling the long-term performance of durable anti-slip surfaces. For ice-traction materials, wear mechanisms are especially important because abrasion can modify or remove the surface features responsible for friction enhancement. Therefore, understanding abrasion mechanisms, quantifying wear through standardized methods, and developing predictive tools for abrasion performance are essential steps toward designing TPU and rubber-based composites with improved durability and sustained traction.

2-7- Machine Learning and Triboinformatics for Materials Design

The development of advanced materials traditionally relies on iterative cycles of formulation, processing, characterization, and performance evaluation. Although this approach provides valuable experimental insight, it is often time-consuming, resource-intensive, and limited by the number of material variables that can be practically explored. In materials research, the path from initial discovery to commercial use may require many years, partly because material design still depends heavily on trial-and-error experimentation and repeated characterization loops [97]. This challenge is particularly important for polymers and elastomeric materials, where material performance is controlled by complex interactions among chemistry, processing conditions, morphology, mechanical properties, and service environment [98].

Machine learning (ML), a subfield of artificial intelligence (AI), offers a data-driven approach for accelerating materials design and property prediction. Instead of relying only on explicit analytical models, ML algorithms learn relationships between input descriptors and target properties from available data. In materials science, ML has been applied to property prediction, materials discovery, process optimization, and performance monitoring [99]. For mechanical and tribological applications, this approach is especially valuable because experimental testing can be

destructive, expensive, and time-intensive, while material behavior is often nonlinear and difficult to capture using simple empirical models [23].

A typical ML-based materials design workflow consists of three major elements: a structured materials database, a predictive model, and a clearly defined research problem [100]. The database may be generated from experiments, simulations, published literature, or open-source material platforms. The predictive model is then trained to map relevant input descriptors to target outputs, such as tensile strength, modulus, fatigue life, friction coefficient, or abrasion volume loss. The research problem defines the purpose of the model and determines which descriptors, algorithms, and evaluation metrics are appropriate. Therefore, successful ML implementation requires both domain knowledge in materials science and technical understanding of data-driven modeling [98].

Data quality is one of the most important factors affecting ML model performance. Materials datasets are often limited, heterogeneous, noisy, or incomplete, especially when collected from multiple sources. Therefore, data preprocessing is a critical step before model development [101]. Preprocessing may include removing outliers, handling missing values, normalizing or standardizing variables, balancing datasets, and converting raw information into meaningful numerical descriptors. In some cases, data augmentation or simulation-generated data may be used to expand the available dataset and improve model robustness [98], [102].

ML approaches are commonly categorized into supervised learning, unsupervised learning, and reinforcement learning [103]. In supervised learning, the model is trained using labeled data, where both input descriptors and target outputs are known. This approach is widely used in mechanical property prediction because measured material properties can serve as output labels [100]. Unsupervised learning is used to identify patterns, clusters, or hidden structures in unlabeled datasets, while reinforcement learning is based on sequential decision-making through interaction with an environment [104]. For abrasion resistance and mechanical property prediction, supervised regression models are particularly relevant because the goal is often to predict a continuous output variable.

Several ML algorithms can be used for materials property prediction. Linear regression provides a simple baseline for identifying linear relationships between descriptors and target properties. Polynomial regression extends this approach by including nonlinear terms. Support vector regression (SVR), decision tree regression (DTR), random forest regression (RFR), gradient

boosting regression (GBR), and artificial neural networks (ANNs) are commonly used to capture more complex and nonlinear material behavior [100]. Ensemble methods, such as random forest and gradient boosting, combine multiple learners to improve predictive stability and reduce sensitivity to individual model limitations [105]. The selection of an appropriate model depends on dataset size, feature complexity, nonlinearity, interpretability requirements, and the risk of overfitting. Figure 2-7 schematically illustrates the workflow of artificial intelligence utilization in materials design systems.

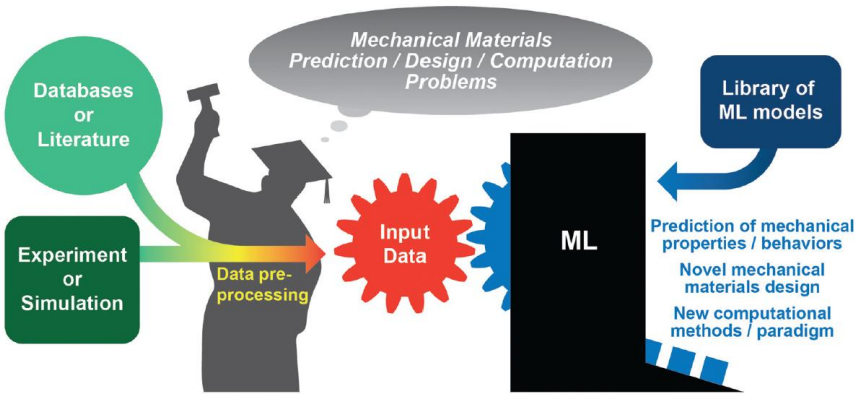


Fig. 2- 7- Machine learning workflow for mechanical materials prediction, design, and computational modeling [100].

Model validation is essential to ensure that ML predictions are reliable beyond the training dataset. Common validation strategies include train–test splitting, k-fold cross-validation, and leave-one-out cross-validation [106]. These approaches evaluate whether the model can generalize to unseen data rather than simply memorize the training set. Model performance is commonly assessed using regression metrics such as coefficient of determination, R^2, mean absolute error (MAE), mean squared error (MSE), and root mean squared error (RMSE) [107]. Reporting multiple metrics provides a more complete assessment of prediction accuracy, error magnitude, and model robustness.

In tribology, the application of ML has led to the emerging field of triboinformatics [108]. Triboinformatics applies data-driven methods to friction, wear, lubrication, and surface-interaction problems. Tribological behavior is particularly suitable for data-driven analysis because friction and wear are influenced by many interacting variables, including material properties, surface roughness, contact pressure, sliding speed, temperature, humidity, lubrication state, and counter-surface characteristics. Despite extensive experimental and theoretical research, tribology remains

highly empirical, and universal predictive laws for friction and wear are difficult to establish. Therefore, ML provides a promising tool for identifying hidden relationships between material descriptors and tribological performance.

For elastomeric materials, triboinformatics can support the prediction of wear and abrasion behavior from measurable mechanical and viscoelastic properties. Abrasion resistance is commonly evaluated through standardized experimental tests, such as ISO 4649, but these tests require specimen preparation, specialized equipment, density measurement, and controlled testing procedures. ML-based models can reduce the experimental burden by enabling early-stage screening of candidate materials before extensive laboratory validation [109]. This is particularly useful for TPU systems, where abrasion performance depends on complex relationships among hardness, modulus, tensile properties, tear strength, resilience, density, and viscoelastic response.

In the context of TPU abrasion resistance, ML can be used to correlate mechanical and viscoelastic descriptors with abrasion volume loss. Rather than directly modeling molecular structure or filler formulation, this approach focuses on identifying how measurable property descriptors relate to wear performance. Such a framework can help identify the most influential features controlling abrasion resistance and support more efficient material selection for applications requiring durability under repeated mechanical contact. Previous ML-based work on TPU abrasion prediction has shown that supervised regression models can capture structure-property-wear relationships and provide a cost- and time-efficient alternative for early-stage screening of TPU grades [110].

Overall, machine learning and triboinformatics provide a complementary framework to experimental tribology. While experimental testing remains essential for validation and material qualification, ML can accelerate the design process by identifying trends, ranking important descriptors, and predicting material performance before extensive testing. In this dissertation, the triboinformatics approach is applied to predict TPU abrasion resistance from mechanical and viscoelastic properties, supporting the broader goal of developing durable elastomeric materials for anti-slip and wear-resistant applications.

In summary, this chapter provides the fundamental background for the design of durable elastomeric materials for ice-traction applications. The discussion integrates key concepts in ice tribology, rubber friction, bioinspired surface texturing, TPU-based materials, graphene

nanoplatelet-reinforced composites, abrasion mechanisms, and machine-learning-assisted materials design. Together, these topics establish the framework for understanding how interfacial lubrication, surface morphology, filler geometry, matrix properties, and wear evolution govern both the initial frictional response and the long-term durability of anti-slip elastomeric surfaces.

2-8- References

[1] U. M. R. Paturi, S. T. Palakurthy, and N. S. Reddy, The Role of Machine Learning in Tribology: A Systematic Review, vol. 30, no. 0123456789. Springer Netherlands, 2023. doi: 10.1007/s11831-022-09841-5.

[2] A. Shinde et al., "The impacts of graphene dosage on the friction and wear performance of a graphene-reinforced silicone rubber nano composite," J. Mater. Res. Technol., vol. 21, pp. 1570–1580, 2022, doi: 10.1016/j.jmrt.2022.10.007.

[3] R. W. Liefferink, F. C. Hsia, B. Weber, and D. Bonn, "Friction on Ice: How Temperature, Pressure, and Speed Control the Slipperiness of Ice," Phys. Rev. X, vol. 11, no. 1, p. 11025, 2021, doi: 10.1103/PhysRevX.11.011025.

[4] K. Mielonen, "Hierarchically structured polymer surfaces : Curved surfaces and sliding behavior on ice," University of Eastern Finland, 2019.

[5] S. Babaee, S. Pajovic, A. Rafsanjani, Y. Shi, K. Bertoldi, and G. Traverso, "Bioinspired kirigami metasurfaces as assistive shoe grips," Nat. Biomed. Eng., vol. 4, no. 8, pp. 778–786, 2020, doi: 10.1038/s41551-020-0564-3.

[6] R. Rosenberg, "Why is ice slippery," Phys. Today, vol. 58, no. 12, pp. 50–55, 2005, doi: 10.1063/1.2169444.

[7] X. Zhang et al., "A common supersolid skin covering both water and ice," Phys. Chem. Chem. Phys., vol. 16, no. 42, pp. 22987–22994, 2014, doi: 10.1039/c4cp02516d.

[8] A. M. Kietzig, S. G. Hatzikiriakos, and P. Englezos, "Physics of ice friction," J. Appl. Phys., vol. 107, no. 8, 2010, doi: 10.1063/1.3340792.

[9] J. G. Dash, A. W. Rempel, and J. S. Wettlaufer, "The physics of premelted ice and its geophysical consequences," Rev. Mod. Phys., vol. 78, no. 3, pp. 695–741, 2006, doi: 10.1103/RevModPhys.78.695.

[10] A. M. Kietzig, S. G. Hatzikiriakos, and P. Englezos, "Ice friction: The effects of surface roughness, structure, and hydrophobicity," J. Appl. Phys., vol. 106, no. 2, 2009, doi: 10.1063/1.3173346.

[11] S. Zahmatkesh and R. Rizvi, "Evaluating surface texturing technologies of rubber composites on ice using a novel high-velocity tribotest method," Tribol. Int., vol. 206, no. October 2024, p. 110538, 2025, doi: 10.1016/j.triboint.2025.110538.

[12] M. Kandeva and N. Dishovsky, "Friction behavior produced in the course of a contact enabled between composite materials and eco-friendly soles prototypes made of elastomeric material with regard to ice-covered surface," Tribol. Ind., vol. 41, no. 1, pp. 90–99, 2019, doi: 10.24874/ti.2019.41.01.10.

[13] S. Islam, K. Gide, T. Dutta, and Z. S. Bagheri, "The effect of tread patterns on slip resistance of footwear outsoles based on composite materials in icy conditions," J. Safety Res., vol. 87, pp. 453–464, 2023, doi: 10.1016/j.jsr.2023.08.017.

[14] S. Provided and I. S. O. No, "INTERNATIONAL STANDARD Personal protective equipment — Footwear — Test method for slip resistance," vol. 2012, 2013.

[15] "ASTM F2913: Standard Test Method for Measuring the Coefficient of Friction for Evaluation of Slip Performance of Footwear and Test Surfaces/Flooring Using a Whole Shoe Tester, 2019, American Society of Testing Materials."

[16] S. T. Centre, "Slip resistance guide".

[17] “SATRA TM144: Friction (slip resistance) of footwear and floorings.” https://www.satra.com/test_methods/detail.php?id=107&msclkid=302d2127c81711ec9f7629a03a21a70f

[18] “SATRA STM 603 Slip resistance tester.” https://www.satra.com/test_equipment/machine.php?id=74&msclkid=76e88f9bc81711ecb4808b94702cf995

[19] “The SATRA STM 633 Martindale abrasion tester.” https://www.satra.com/test_equipment/machine.php?id=19&msclkid=287528d5c81811ecba223a0511cc7516

[20] B. N. J. Persson and M. Scaraggi, “Theory of adhesion: Role of surface roughness,” J. Chem. Phys., vol. 141, no. 12, 2014, doi: 10.1063/1.4895789.

[21] A. Tiwari, N. Miyashita, N. Espallargas, and B. N. J. Persson, “Rubber friction: The contribution from the area of real contact,” J. Chem. Phys., vol. 148, no. 22, 2018, doi: 10.1063/1.5037136.

[22] V. Richhariya, A. Tripathy, O. Carvalho, M. Julker Nine, D. Losic, and F. S. Silva, “Unravelling the physics and mechanisms behind slips and falls on icy surfaces: A comprehensive review and nature-inspired solutions,” Mater. Des., vol. 234, p. 112335, 2023, doi: 10.1016/j.matdes.2023.112335.

[23] M. S. Hasan, A. Kordijazi, P. K. Rohatgi, and M. Nosonovsky, “Triboinformatics approach for friction and wear prediction of Al-graphite composites using machine learning methods,” J. Tribol., vol. 144, no. 1, pp. 1–13, 2022, doi: 10.1115/1.4050525.

[24] S. P. Ammineni, D. Lingaraju, and C. Nagaraju, “The effects of physical aging on the quasi-static and dynamic viscoelastic properties of Nitrile Butadiene Rubber,” Mech. Time-Dependent Mater., vol. 27, no. 3, pp. 765–789, 2023, doi: 10.1007/s11043-023-09591-2.

[25] K. Mielonen et al., “Sliding friction of hierarchically micro–micro textured polymer surfaces on ice,” Cold Reg. Sci. Technol., vol. 163, no. April, pp. 8–18, 2019, doi: 10.1016/j.coldregions.2019.04.002.

[26] J. Lungevics, E. Jansons, I. Boiko, I. Velkavrh, J. Voyer, and T. Wright, “A Holistic Approach Towards Surface Topography Analyses for Ice Tribology Applications,” Front. Mech. Eng., vol. 7, no. June, pp. 1–14, 2021, doi: 10.3389/fmech.2021.691485.

[27] S. B. Kunal Gide, Sabrina Islam, Tilak Dutta, “Design of Tread Patterns for Us with Novel Composite Outsole Materials for Slip-Resistant Footwear,” Hum. Factors Appar. Text. Engineeing, vol. 32, pp. 89–93, 2022.

[28] Y. Zhang, J. Gao, and Q. Li, “Experimental study on friction coefficients between tire tread rubber and ice,” AIP Adv., vol. 8, no. 7, 2018, doi: 10.1063/1.5041049.

[29] J. Hale, A. O’Connell, R. Lewis, M. J. Carré, and J. A. Rongong, “An Evaluation of Shoe Tread Parameters using FEM,” Tribol. Int., vol. 153, no. August 2020, 2021, doi: 10.1016/j.triboint.2020.106570.

[30] A. Kurdi, N. Alhazmi, H. Alhazmi, and T. Tabbakh, “Practice of simulation and life cycle assessment in tribology-A review,” Materials (Basel)., vol. 13, no. 16, 2020, doi: 10.3390/MA13163489.

[31] J. M. J. Van Leeuwen, “Skating on slippery ice,” SciPost Phys., vol. 3, no. 6, 2017, doi: 10.21468/SciPostPhys.3.6.042.

[32] E. Ciulli, A. Betti, and P. Forte, “The Applicability of the Hertzian Formulas to Point Contacts of Spheres and Spherical Caps,” Lubricants, vol. 10, no. 10, 2022, doi: 10.3390/lubricants10100233.

[33] N. Thirunavukkarasu, S. Peng, H. B. Gunasekaran, Z. Yang, L. Wu, and Z. Weng, “Responsive friction modulation of 3D printed elastomeric bioinspired structures,” Tribol. Int., vol. 175, no. January, p. 107823, 2022, doi: 10.1016/j.triboint.2022.107823.

[34] W. Wang, Y. Liu, and Z. Xie, Gecko-Like Dry Adhesive Surfaces and Their Applications: A Review, vol. 18, no. 5. Springer Singapore, 2021. doi: 10.1007/s42235-021-00088-7.

[35] M. Nosonovsky and B. Bhushan, “Roughness optimization for biomimetic superhydrophobic surfaces,” Microsyst. Technol., vol. 11, no. 7, pp. 535–549, 2005, doi: 10.1007/s00542-005-0602-9.

[36] J. Oeffner and G. V. Lauder, “The hydrodynamic function of shark skin and two biomimetic applications,” J. Exp. Biol., vol. 215, no. 5, pp. 785–795, 2012, doi: 10.1242/jeb.063040.

[37] N. Orndorf, A. M. Garner, and A. Dhinojwala, “Polar bear paw pad surface roughness and its relevance to contact mechanics on snow,” J. R. Soc. Interface, vol. 19, no. 196, 2022, doi: 10.1098/rsif.2022.0466.

[38] S. Bapat, C. Tiner, K. Rajurkar, S. Nath, S. Atre, and A. Malshe, “Understanding biologicalisation of the snake-skin inspired textures through additive manufacturing for mechanical traction,” CIRP Ann., vol. 69, no. 1, pp. 201–204, 2020, doi: 10.1016/j.cirp.2020.04.109.

[39] H. H. Stutz, A. Martinez, L. Heepe, H. T. Tramsen, and S. N. Gorb, “Strength anisotropy at soil-structure interfaces with snake skin inspired structural surfaces,” E3S Web Conf., vol. 92, pp. 1–6, 2019, doi: 10.1051/e3sconf/20199213008.

[40] S. Gernay, W. Federle, P. Lambert, and T. Gilet, “Elasto-capillarity in insect fibrillar adhesion,” J. R. Soc. Interface, vol. 13, no. 121, 2016, doi: 10.1098/rsif.2016.0371.

[41] G. Gard and G. Lundborg, “Test of Swedish anti-skid devices on five different slippery surfaces,” Accid. Anal. Prev., vol. 33, no. 1, pp. 1–8, 2001, doi: 10.1016/S0001-4575(00)00002-6.

[42] S. Wang et al., “Icephobicity of Penguins Spheniscus Humboldti and an Artificial Replica of Penguin Feather with Air-Infused Hierarchical Rough Structures,” J. Phys. Chem. C, vol. 120, no. 29, pp. 15923–15929, 2016, doi: 10.1021/acs.jpcc.5b12298.

[43] M. Sedlaček, B. Podgornik, A. Ramalho, and D. Česnik, “Influence of geometry and the sequence of surface texturing process on tribological properties,” Tribol. Int., vol. 115, pp. 268–273, 2017, doi: 10.1016/j.triboint.2017.06.001.

[44] N. Naat, Y. Boutar, S. Naïmi, S. Mezlini, and L. F. M. Da Silva, “Effect of surface texture on the mechanical performance of bonded joints: a review,” J. Adhes., vol. 99, no. 2, pp. 166–258, 2023, doi: 10.1080/00218464.2021.2008370.

[45] A. F. Obilor, M. Pacella, A. Wilson, and V. V. Silberschmidt, Micro-texturing of polymer surfaces using lasers: a review, vol. 120, no. 1–2. Springer London, 2022. doi: 10.1007/s00170-022-08731-1.

[46] S. Heydarian, K. Maghsoudi, R. Jafari, H. Gauthier, and G. Momen, “Fabrication of liquid-infused textured surfaces (LITS): The effect of surface textures on anti-icing properties and durability,” Mater. Today Commun., vol. 32, no. February, p. 103935, 2022, doi: 10.1016/j.mtcomm.2022.103935.

[47] C. de K. L. Ecam Rennes - Louis de Broglie, Plasma Modification of Polyolefins: Plasma Texturing of Polymers. Jean-François Coulon, France, 2021.

[48] R. Rizvi, A. Anwer, G. Fernie, T. Dutta, and H. Naguib, “Multifunctional Textured Surfaces with Enhanced Friction and Hydrophobic Behaviors Produced by Fiber Debonding and Pullout,” ACS Appl. Mater. Interfaces, vol. 8, no. 43, pp. 29818–29826, 2016, doi: 10.1021/acsami.6b11497.

[49] N. Namdari and R. Rizvi, “Damage induced surface texturing of short fiber-PDMS composite materials,” Annu. Tech. Conf. - ANTEC, Conf. Proc., vol. 2018-May, no. May 2018, 2018.

[50] R. Rizvi, H. Naguib, G. Fernie, and T. Dutta, “High friction on ice provided by elastomeric fiber composites with textured surfaces,” Appl. Phys. Lett., vol. 106, no. 11, 2015, doi: 10.1063/1.4913676.

[51] N. Namdari et al., “Advanced functional surfaces through controlled damage and instabilities,” Mater. Horizons, vol. 7, no. 2, pp. 366–396, 2020, doi: 10.1039/c9mh01516g.

[52] Z. S. Bagheri, Y. Li, A. R. Fekr, and T. Dutta, “The effect of wear on slip-resistance of winter footwear with composite outsoles: A pilot study,” Appl. Ergon., vol. 99, p. 103611, 2022, doi: 10.1016/j.apergo.2021.103611.

[53] Vibram, “VIBRAM ARCTIC GRIP,” THE MOST ADVANCED COLD WEATHER GRIPPING SYSTEM EVER CREATED BY VIBRAM. https://www.vibram.com/ca/technology/lifestyle/TECH_arctic_grip.html

[54] N. Namdari, G. J. Otto, G. Guo, H. Sojoudi, and R. Rizvi, “Nanotextured surfaces with enhanced ice-traction and wear-resistance,” Compos. Part B Eng., vol. 238, p. 109916, 2022, doi: 10.1016/j.compositesb.2022.109916.

[55] M. Asensio, V. Costa, A. Nohales, O. Bianchi, and C. M. Gómez, “Tunable structure and properties of segmented thermoplastic polyurethanes as a function offlexible segment,” Polymers (Basel)., vol. 11, no. 12, 2019, doi: 10.3390/polym11121910.

[56] M. Mo et al., “Excellent tribological and anti-corrosion performance of polyurethane composite coatings reinforced with functionalized graphene and graphene oxide nanosheets,” RSC Adv., vol. 5, no. 70, pp. 56486–56497, 2015, doi: 10.1039/c5ra10494g.

[57] D. Nichetti and N. Grizzuti, “Determination of the phase transition behavior of thermoplastic polyurethanes from coupled rheology/DSC measurements,” Polym. Eng. Sci., vol. 44, no. 8, pp. 1514–1521, 2004, doi: 10.1002/pen.20148.

[58] P. Properties, “Elastollan,” p. 2020, 2020.

[59] J. M. M. Jesse L. Gadley , Ricardo J. Andrade, “Effect of Soft-to-Hard Segment Ratio on Viscoelastic Behavior of Model Thermoplastic Polyurethanes during Phase Transitions,” Macromol. Mater. Eng., vol. 301, pp. 953–963, 2016.

[60] F. N. Cogswell, Thermoplastic Aromatic Polymer Composites A Study of the Structure, Processing and Properties of Carbon Fibre Reinforced Polyetheretherketone and Related Materials, 1st ed. Elsevier, 2013.

[61] C. Lozano-Pérez, J. V. Cauich-Rodríguez, and F. Avilés, “Influence of rigid segment and carbon nanotube concentration on the cyclic piezoresistive and hysteretic behavior of multiwall carbon nanotube/segmented polyurethane composites,” Compos. Sci. Technol., vol. 128, pp. 25–32, 2016, doi: 10.1016/j.compscitech.2016.03.010.

[62] K. N. Raftopoulos et al., “Effects of Segment Length and Crosslinking via POSS on the Calorimetric and Dynamic Glass Transition of Polyurethanes with Aliphatic Hard Segments,” Int. J. Mol. Sci., vol. 24, no. 22, 2023, doi: 10.3390/ijms242216540.

[63] L. Jakobsen, F. G. Lysdal, T. Bagehorn, U. G. Kersting, and I. M. Sivebaek, “The effect of footwear outsole material on slip resistance on dry and contaminated surfaces with geometrically controlled outsoles,” Ergonomics, vol. 0, no. 0, pp. 1–8, 2022, doi: 10.1080/00140139.2022.2081364.

[64] K. Junik et al., “Impact of the hardness on the selected mechanical properties of rigid polyurethane elastomers commonly used in suspension systems,” Eng. Fail. Anal., vol. 121, no. October 2020, 2021, doi: 10.1016/j.engfailanal.2020.105201.

[65] S. Chibani and F. X. Coudert, “Machine learning approaches for the prediction of materials properties,” APL Mater., vol. 8, no. 8, 2020, doi: 10.1063/5.0018384.

[66] E. Aslan and G. Akincioglu, “Investigation of The Wear And Friction Profile of TPU-Based Polymers at Different Infill Ratios,” Int. J. Automot. Sci. Technol., vol. 8, no. 1, pp. 125–131, 2024, doi: 10.30939/ijastech..1398109.

[67] A. M. Onas, I. E. Biru, A. Petca, and R. C. Petca, “The Aging Behavior of Polyurethane-based Ureteral Catheters,” Mater. Plast., vol. 58, no. 4, pp. 65–72, 2021, doi: 10.37358/MP.21.4.5532.

[68] L. Tian et al., “A bioinspired design approach for biomechanically matched tracheal stents,” Virtual Phys. Prototyp., vol. 19, no. 1, pp. 1–17, 2024, doi: 10.1080/17452759.2024.2437510.

[69] K. Friedrich, “Polymer composites for tribological applications,” Adv. Ind. Eng. Polym. Res., vol. 1, no. 1, pp. 3–39, 2018, doi: 10.1016/j.aiepr.2018.05.001.

[70] J. H. Kim and G. H. Kim, “Effect of rubber content on abrasion resistance and tensile properties of thermoplastic polyurethane (TPU)/rubber blends,” Macromol. Res., vol. 22, no. 5, pp. 523–527, 2014, doi: 10.1007/s13233-014-2077-y.

[71] 1 L. Torre1 E. Fortunati , 1 F. Luzi, 1 A. Janke, 2 L. H€außler, 2 J. Pionteck, 2 J.M. Kenny, “Reinforcement Effect of Cellulose Nanocrystals in Thermoplastic Polyurethane Matrices Characterized by Different Soft/Hard Segment Ratio,” Polym. Eng. Sci., vol. 51, no. 7, pp. 1–10, 2017, doi: 10.1002/pen.

[72] L. M. Veca et al., “Polymer functionalization and solubilization of carbon nanosheets,” Chem. Commun., no. 18, pp. 2565–2567, 2009, doi: 10.1039/b900590k.

[73] S. K. Yadav and J. W. Cho, “Functionalized graphene nanoplatelets for enhanced mechanical and thermal properties of polyurethane nanocomposites,” Appl. Surf. Sci., vol. 266, pp. 360–367, 2013, doi: 10.1016/j.apsusc.2012.12.028.

[74] M. Albozahid, H. Z. Naji, Z. K. Alobad, J. K. Wychowaniec, and A. Saiani, “Thermal, Mechanical, and Morphological Characterisations of Graphene Nanoplatelet/Graphene Oxide/High-Hard-Segment Polyurethane Nanocomposite: A Comparative Study,” Polymers (Basel)., vol. 14, no. 19, 2022, doi: 10.3390/polym14194224.

[75] J. H. Los, A. Fasolino, and M. I. Katsnelson, “Mechanics of thermally fluctuating membranes,” npj 2D Mater. Appl., vol. 1, no. 1, pp. 1–5, 2017, doi: 10.1038/s41699-017-0009-3.

[76] J. R. Potts, D. R. Dreyer, C. W. Bielawski, and R. S. Ruoff, “Graphene-based polymer nanocomposites,” Polymer (Guildf)., vol. 52, no. 1, pp. 5–25, 2011, doi: 10.1016/j.polymer.2010.11.042.

[77] J. Wu, G. Huang, H. Li, S. Wu, Y. Liu, and J. Zheng, “Enhanced mechanical and gas barrier properties of rubber nanocomposites with surface functionalized graphene oxide at low content,” Polymer (Guildf)., vol. 54, no. 7, pp. 1930–1937, 2013, doi: 10.1016/j.polymer.2013.01.049.

[78] M. Li, H. Zhou, Y. Zhang, Y. Liao, and H. Zhou, “The effect of defects on the interfacial mechanical properties of graphene/epoxy composites,” RSC Adv., vol. 7, no. 73, pp. 46101–46108, 2017, doi: 10.1039/c7ra08243f.

[79] M. Moniruzzaman and K. I. Winey, “Polymer nanocomposites containing carbon nanotubes,” Macromolecules, vol. 39, no. 16, pp. 5194–5205, 2006, doi: 10.1021/ma060733p.

[80] S. Paszkiewicz and A. Szymczyk, Graphene-Based Nanomaterials and Their Polymer Nanocomposites. Elsevier Inc., 2019. doi: 10.1016/B978-0-12-814615-6.00006-0.

[81] M. Fang, K. Wang, H. Lu, Y. Yang, and S. Nutt, “Covalent polymer functionalization of graphene nanosheets and mechanical properties of composites,” J. Mater. Chem., vol. 19, no. 38, pp. 7098–7105, 2009, doi: 10.1039/b908220d.

[82] Y. Yang, J. Wang, J. Zhang, J. Liu, X. Yang, and H. Zhao, “Exfoliated graphite oxide decorated by PDMAEMA chains and polymer particles,” Langmuir, vol. 25, no. 19, pp. 11808–11814, 2009, doi: 10.1021/la901441p.

[83] J. H. Park and B. K. Kim, “Infrared light actuated shape memory effects in crystalline polyurethane/graphene chemical hybrids,” Smart Mater. Struct., vol. 23, no. 2, 2014, doi: 10.1088/0964-1726/23/2/025038.

[84] A. Rostami, H. Nazockdast, and M. Karimi, “Graphene induced microstructural changes of PLA/MWCNT biodegradable nanocomposites: Rheological, morphological, thermal and electrical properties,” RSC Adv., vol. 6, no. 55, pp. 49747–49759, 2016, doi: 10.1039/c6ra08345e.

[85] M. Liu, J. H. Hui, I. A. Kinloch, R. J. Young, and D. G. Papageorgiou, “Deformation and tearing of graphene-reinforced elastomer nanocomposites,” Compos. Commun., vol. 25, no. April, p. 100764, 2021, doi: 10.1016/j.coco.2021.100764.

[86] A. Spagni, A. Berardo, D. Marchetto, E. Gualtieri, N. M. Pugno, and S. Valeri, “Friction of rough surfaces on ice: Experiments and modeling,” Wear, vol. 368–369, pp. 258–266, 2016, doi: 10.1016/j.wear.2016.10.001.

[87] D. Verma, P. C. Gope, A. Shandilya, and A. Gupta, “Mechanical-Thermal-Electrical and Morphological Properties of Graphene Reinforced Polymer Composites: A Review,” Trans. Indian Inst. Met., vol. 67, pp. 803–816, 2014, doi: 10.1007/s12666-014-0408-5.

[88] D. G. Papageorgiou, I. A. Kinloch, and R. J. Young, “Mechanical properties of graphene and graphene-based nanocomposites,” Prog. Mater. Sci., vol. 90, pp. 75–127, 2017, doi: 10.1016/j.pmatsci.2017.07.004.

[89] R. Xu and W. S. F. Z. B. N. J. Persson, “Rubber Wear: History, Mechanisms, and Perspectives,” 2025.

[90] ISO, “ISO 20871 Footwear — Test methods for outsoles — Abrasion resistance,” 2021

[91] I. O. for Standardization, “INTERNATIONAL STANDARD ISO 4649 Rubbers, vulcanized or thermoplastic -Determination of abrasion resistance using a rotating cylindrical drum device,” ISO, vol. 2017, 2017.

[92] ASTM G99, “Standard Test Method for Wear Testing with a Pin-on-Disk Standard Test Method for Wear Testing with a Pin-on-Disk Apparatus,” ASTM Int., vol. 14, no. 2016, pp. 1–6, 2017, doi: 10.1520/G0099-17.2.

[93] ISO International Standard, “Rubber, vulcanized or thermoplastic - Determination of density,” 2008.

[94] G. Y. Lee, C. K. H. Dharan, and R. O. Ritchie, “A physically-based abrasive wear model for composite materials,” Wear, vol. 252, no. 3–4, pp. 322–331, 2002, doi: 10.1016/S0043-1648(01)00896-1.

[95] M. F. Sonnenschein, Polyurethanes: Science, Technology, Markets, and Trends, 2nd Editio. Wiley, 2021.

[96] K. Kwiatkowski and M. Nachman, “The abrasive wear resistance of the segmented linear polyurethane elastomers based on a variety of polyols as soft segments,” Polymers (Basel)., vol. 9, no. 12, 2017, doi: 10.3390/polym9120705.

[97] “National Science and Technology Council (US). Materials genome initiative for global competitiveness. Executive Office of the President, National Science and Technology Council; 2011.”

[98] R. Ramprasad, R. Batra, G. Pilania, A. Mannodi-Kanakkithodi, and C. Kim, “Machine learning in materials informatics: Recent applications and prospects,” npj Comput. Mater., vol. 3, no. 1, 2017, doi: 10.1038/s41524-017-0056-5.

[99] H. Esmaeili and R. Rizvi, “An accelerated strategy to characterize mechanical properties of polymer composites using the ensemble learning approach,” Comput. Mater. Sci., vol. 229, no. June, p. 112432, 2023, doi: 10.1016/j.commatsci.2023.112432.

[100] K. Guo, Z. Yang, C. H. Yu, and M. J. Buehler, “Artificial intelligence and machine learning in design of mechanical materials,” Mater. Horizons, vol. 8, no. 4, pp. 1153–1172, 2021, doi: 10.1039/d0mh01451f.

[101] P. Xu, X. Ji, and M. Li, “Small data machine learning in materials science,” pp. 1–15, 2023, doi: 10.1038/s41524-023-01000-z.

[102] S. G. Baird, M. Liu, H. M. Sayeed, and T. D. Sparks, “Data-driven materials discovery and synthesis using machine learning methods,” Compr. Inorg. Chem. III, Third Ed., vol. 1–10, no. September 2020, pp. 3–23, 2023, doi: 10.1016/B978-0-12-823144-9.00079-0.

[103] C. M. Bishop, Pattern Recognition and Machine Learning. Springer Nature Link, 2006.

[104] A. G. B. Richard S Sutton, Reinforcement Learning: An Introduction, 2nd Editio. 2015.

[105] M. A. Ganaie, M. Hu, A. K. Malik, M. Tanveer, and P. N. Suganthan, “Ensemble deep learning: A review,” Eng. Appl. Artif. Intell., vol. 115, no. March, p. 105151, 2022, doi: 10.1016/j.engappai.2022.105151.

[106] A. Y. T. Wang et al., “Machine Learning for Materials Scientists: An Introductory Guide toward Best Practices,” Chem. Mater., vol. 32, no. 12, pp. 4954–4965, 2020, doi: 10.1021/acs.chemmater.0c01907.

[107] S. Raschka, “Model Evaluation, Model Selection, and Algorithm Selection in Machine Learning,” 2020, [Online]. Available: http://arxiv.org/abs/1811.12808

[108] M. S. Hasan, A. Kordijazi, P. K. Rohatgi, and M. Nosonovsky, “Triboinformatic modeling of dry friction and wear of aluminum base alloys using machine learning algorithms,” Tribol. Int., vol. 161, no. March, p. 107065, 2021, doi: 10.1016/j.triboint.2021.107065.

[109] R. R. Esmaeili Hamed, Avateffazeli Maryam, Haghshenas Meysam, “Fatigue Fract Eng Mat Struct - 2024 - Esmaeili - A Hybrid Framework for Characterizing and Benchmarking Fatigue S-N Curves.pdf.” 2024.

[110] M. B. Prasad and S. K. Sahu, “Taguchi and machine learning integration for tribological analysis of polyurethane/nanodiamond nanocomposites,” Proc. Inst. Mech. Eng. Part J J. Eng. Tribol., pp. 1–17, 2025, doi: 10.1177/13506501251362067.

Chapter 3:
Evaluating Surface Texturing Technologies of Rubber Composites on Ice Using a Novel High-Velocity Tribotest Method

3-1- Chapter Preface

The findings presented here are partly based on the following peer-reviewed publication:

- *S. Zahmatkesh and R. Rizvi," Evaluating Surface Texturing Technologies of Rubber Composites on Ice Using a Novel High-Velocity Tribotest Method" Tribology International, vol. 206, p. 110538, June 2025. Available online.*

Portions of this study have been presented at the following conferences:

- *S. Zahmatkesh and R. Rizvi," Effect of sliding speed on tribological responses of ice traction in surface-damaged elastomeric composites", Progress in Canadian Mechanical Engineering, CSME Conference, Université de Sherbrooke, May 2023. Available online.*
- *S. Zahmatkesh and R. Rizvi," Bioinspired rubber composites for superior ice traction: enhancing winter safety through innovative laboratory testing in tribology", SPIE Smart Structures + Non-Destructive Evaluations, Biologically Inspired Materials, Processes, and Systems (BIMPS) 2025; Proceedings Volume 13430, Vancouver, March 2025. Available online.*

3-2- Abstract

This study presents a high-velocity tribotest using Bruker UMT Tribolab to evaluate the ice traction of rubber composites. Lab-scale tribotests are essential for developing anti-slip materials for footwear. Reciprocating and rotational movements were studied on ice, along with the physical phenomena influencing friction, optimizing dwell time and load control parameters. GF-TPU composites and commercial winter boots (Green Diamond® and Arctic Grip Vibram®) were tested for validation. The addition of 10 wt.% glass fibers to TPU increased static friction by 300% and

kinetic friction by 400%, enhancing stick-slip behavior. SiC-based texturing in Green Diamond composites improved static friction by 160% and kinetic friction by 970%. Arctic Grip samples showed a 440% increase in static friction and over 1000% in kinetic friction. Overall, the developed high-velocity tribotest provides a scalable and reproducible laboratory framework for evaluating ice-traction performance, supporting rapid screening of anti-slip footwear materials and guiding the development of durable rubber composite surfaces for winter safety applications.

Keywords: slip-resistant composites, stick-slip behavior, ice friction, tribotest.

3-3- Literature Review and Research Gaps

According to the latest statistics, ice slipping is the number-one cause of winter injuries in Canada [1]. When it comes to vulnerable communities, ice slips and falls become an important factor that impedes their Activity of Daily Living (ADL). According to population projections in Canada, the population of seniors aged 80 and over will grow from 1.6 million in 2018 to between 4.7- 6.3 million by 2068 [2].

Elastomers and rubbers are mainly used in footwear and automobile tires. Due to their hyper-elasticity, rubbers can undergo significant deformation and recovery when they are pushed against the rough points of a hard surface such as asphalt or concrete (Fig. 3-1-a) [3]. Their major drawback is their low traction in the presence of a lubrication layer, like ice (Fig. 3-1-b,c) [4]. This drawback will result in slipping of pedestrians and cars in winter. Many car accidents and several human injuries have been reported annually due to this problem [5].

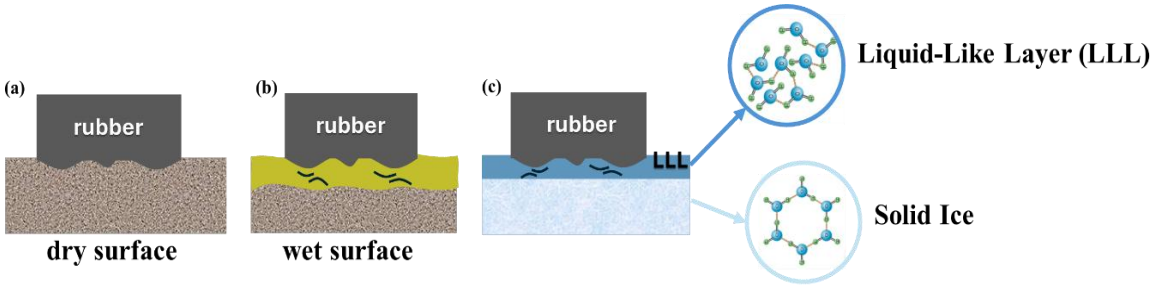


Fig. 3- 1- a) rubbers' dry interaction with roadbeds, vs. b) rubbers' wet interaction with roadbeds, and c) presence of a liquid-like-layer on the surface of ice

Evaluating tribological behavior on ice poses significant challenges due to the dynamic nature of ice. Despite its solid crystalline structure, ice retains a thin, quasi-liquid layer on its surface, even at subfreezing temperatures. As the ice approaches its melting point, this surface layer becomes

prominent, reducing friction and increasing slipperiness. This phenomenon is attributed to the weakening of hydrogen bonds in the O-H groups, leading to partial molecular mobility at the interface [6]. This interfacial water layer is critical in ice tribology, acting as a primary lubricating medium [7] (see Fig. 3-1-c). The reduction in friction on ice is primarily attributed to this thin water film, which results from surface melting induced by applied pressure or frictional heating. As the pressure or frictional force increases, a thicker quasi-liquid layer is generated, leading to a substantial reduction in friction due to hydrodynamic effects [8]. The frictional responses on icy surfaces are typically characterized by two distinct modes: smooth sliding and stick–slip behavior. In smooth sliding, the friction force exhibits an initial peak (static friction force, F_s) followed by a steady-state value (kinetic friction force, F_k). Conversely, in stick-slip behavior, the friction force oscillates periodically between a maximum (F_s) and a minimum (F_k) [9].

To create non-slip surfaces, extensive research has focused on developing anti-slip elastomers for applications such as footwear and winter tires. Rizvi et al. have proposed using destructive techniques to produce significantly damaged surfaces where glass fibers are exposed on the surfaces of Thermoplastic Polyurethane (TPU) composites. Their method, known as Damage Induced Surface Texturing (DIST), demonstrates a substantial potential for enhancing the slip resistance of elastomeric composite surfaces on ice, achieving an almost 900% improvement in efficiency compared to a pristine, untextured surface [10]. The debonding of glass fibers at the surface results in protruding hard fibers, which effectively grip the ice surface [11]. To address the issue of weak abrasion resistance in glass fiber-filled composites, Namdari and his team incorporated 2D materials to fabricate elastomeric composites using the DIST method. They evaluated the ice traction performance of Styrene Ethylene/Butylene Styrene (SEBS) rubber composites incorporating both 1D (carbon fibers) and 2D (graphene nanoplatelets (GNPs) and boron nitride nanosheets (BNNs) fillers at micro- and nanoscale levels [5]. However, their study was limited by the ice tribology setup, which was constrained to low-speed testing conditions.

To evaluate the coefficient of friction (CoF), loads must be accurately measured in both vertical and horizontal directions. Key parameters influencing tribology on icy surfaces include the contacting surface area, movement speed, applied normal pressure, and temperature [12]. The Shoe and Allied Trades Research Association (SATRA), based in the United Kingdom, is globally recognized as the leading authority for testing the slip resistance of footwear, utilizing their SATRA

Test Method (STM 603) [13][14]. However, this large and expensive device requires whole-size shoe test specimens, making it impractical for high-throughput laboratory testing. At the laboratory scale, ice friction is typically assessed using custom-built linear or rotational friction testers, often referred to as tribometers [15]. Lungevics et al. introduced two methods for evaluating ice friction. The first method uses an Inclined Plane Tribometer, where samples slide down an inclined plane without additional load. Sliding velocity was measured using eight optical sensors, and it was found that higher velocities resulted in better sliding ability on the plane. The second method involves an Oscillating Tribometer, where samples oscillate on ice under a normal load of 52 N. Their findings indicated that high-frequency oscillation on the same ice surface leads to greater penetration into the ice as it melts, thereby increasing lubrication on the ice [16]. Stamboulides and colleagues developed a fixture with parallel plate geometry to use a rotational rheometer as an ice tribometer. Their study on the ice friction of various polymers revealed that as the temperature of the ice increases from -25°C to 0°C, the coefficient of friction decreases as the ice transitions into the plastic deformation region. As temperature increases, ice softens, leading to plastic deformation under compressive stresses exerted by the slider [17].

The evaluation of tribological performance on ice requires meticulous attention to detail, particularly regarding the adherence to standardized testing protocols for controlling critical parameters. Pressure applied to the ice significantly influences physical phenomena, particularly at its melting temperature. Consequently, the contact area must be determined based on the normal force exerted on the specimen in contact with the ice [18]. In prior studies, Rizvi et al. applied substantial loads (~500 N) to small sample pieces (3 cm × 1.5 cm), although ASTM F2913 specifies that such a large load is only necessary for full-sized shoe samples (US size 7.5 men's and 8.5 women's). Namdari et al. employed a tensile machine, capable of controlled velocities and load measurements. In their approach, a pulley system was incorporated to convert vertical force into horizontal force, with a dead-weight placed on the sample surface, which was then dragged across an ice surface. However, the speed of their setup was limited to 500 $mm.min^{-1}$ (0.008 $m.s^{-1}$), significantly slower than the sliding speeds typically encountered in human gait (0.3-0.8 $m.s^{-1}$) [12].

Despite aforementioned advancements, a gap exists in laboratory-scale ice tribology setups that can simultaneously maintain consistent sliding velocities and pressures experienced during gait. Furthermore, such tests should be capable of high throughput testing of new materials without the

need for large volumes of costly sample preparations. This research is dedicated to addressing this gap by developing a novel ice tribotest and establishing a comprehensive testing protocol for ice friction evaluation. The innovative approach utilizes a modified Bruker Universal Mechanical Tester (UMT) Tribolab (Brucker Nano Analytics, Germany) that is capable of high-throughput screening rubber composites' ice traction properties, thereby advancing the accuracy and efficiency of ice friction testing in a lab setting.

3-4- Development of Lab-Scale Ice Friction Tester

Bruker's UMT Tribolab is an advanced instrument engineered for in-depth tribological studies, including the assessment of friction, wear, and lubrication effects. This machine features separate units for measuring normal and shear loads, with distinct software modules for script definition and result analysis. The UMT Tribolab is equipped with both reciprocating and rotary lower drives. Normal load is applied using a ball scratcher connected to a load cell. For ice tribology analysis, the device requires specific design adaptations, modifications, and script configurations to meet the experimental needs.

3-4-1- Mold Designing and Installation

A sample holder was designed and manufactured using 3D printing technology, replacing the machine's standard stainless-steel ball holder with this custom component. Two testing modes were developed and investigated for ice friction evaluation: reciprocating and rotational. Custom-designed ice trays were engineered for easy assembly on the instrument's lower drives, each consisting of two parts: a plate that attaches to the lower drive's plate and an adjustable ice tray. Several pyramid-shaped spike patterns were incorporated into the design of ice trays to prevent ice displacement during high-speed sliding. Figure 3-2 illustrates the 3D-printed components and the complete motion drives and molds.

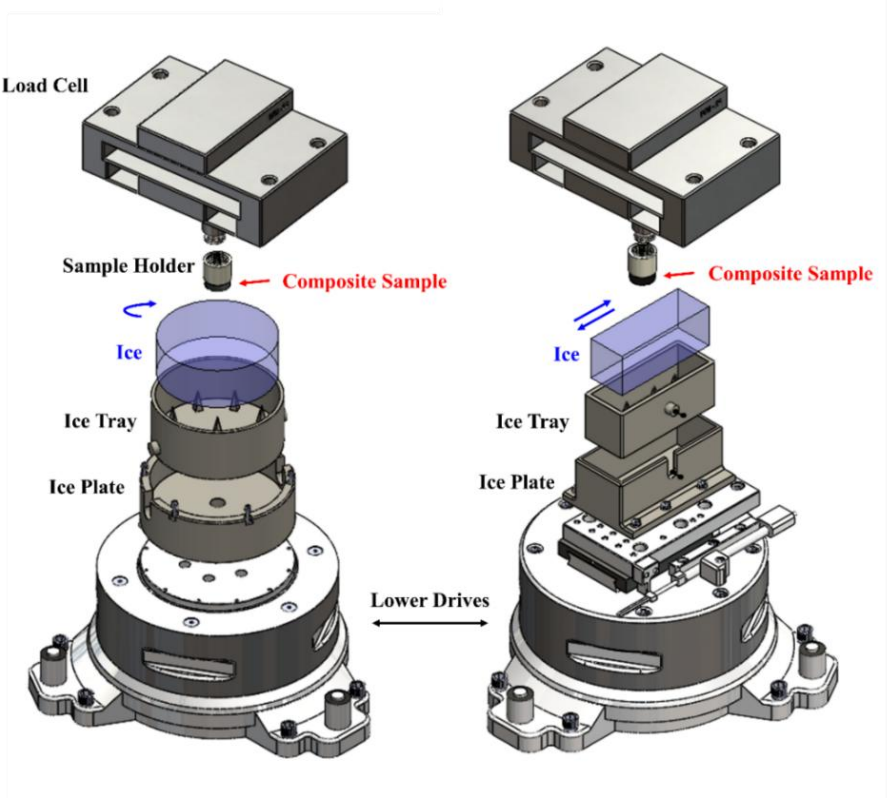


Fig. 3- 2- Testing setup featuring two-part ice molds mounted on separate rotary drives, with rubber samples secured in a 3D-printed holder, which is mounted on the load cell. Configurations are shown for: a) rotary motion and b) reciprocating motion.

3-4-2- Sample Preparations

The feasibility of the UMT Bruker Tribolab for ice tribology analyses was assessed through evaluating the ice-friction performance of three different samples materials. The first sample consisted of Thermoplastic Polyurethane Glass Fiber (TPU-GF) composites, which were previously manufactured using the DIST method as reported in Rizvi et al [19]. These composites feature TPU reinforced with linear glass fibers (2.5 wt.% and 10wt.%) and were cut transversely to create micro cleats of glass fibers on the surface [19]. The other two specimens were outsoles sourced from the top-performing commercial slip-resistant winter boots, which have exhibited superior slip resistance in field testing: Dakota WorkPro 8901 Series IceFX composite with Green Diamond® technology, and Merrell Coldpack 3 Thermo Arctic Grip composite with Vibram® technology, which from this point forward will be referred as ‘IceFX’ and ‘Arctic Grip’, respectively. These outsoles were chosen based on Tilak et al.'s [20] evaluation reports of the Maximum Achievable Angle that a volunteer could traverse both upward and downward while

wearing these boots. The outsoles were initially sectioned using a bandsaw, then cut into 17 mm diameter circular samples using a hollow drill bit. A custom fixture was designed and fabricated via 3D printing to securely hold the circular samples during further processing with a diamond wire saw, yielding flat, circular specimens. The criteria for specimen selection and the chosen anti-slip shoes are illustrated in Fig. 3-3.

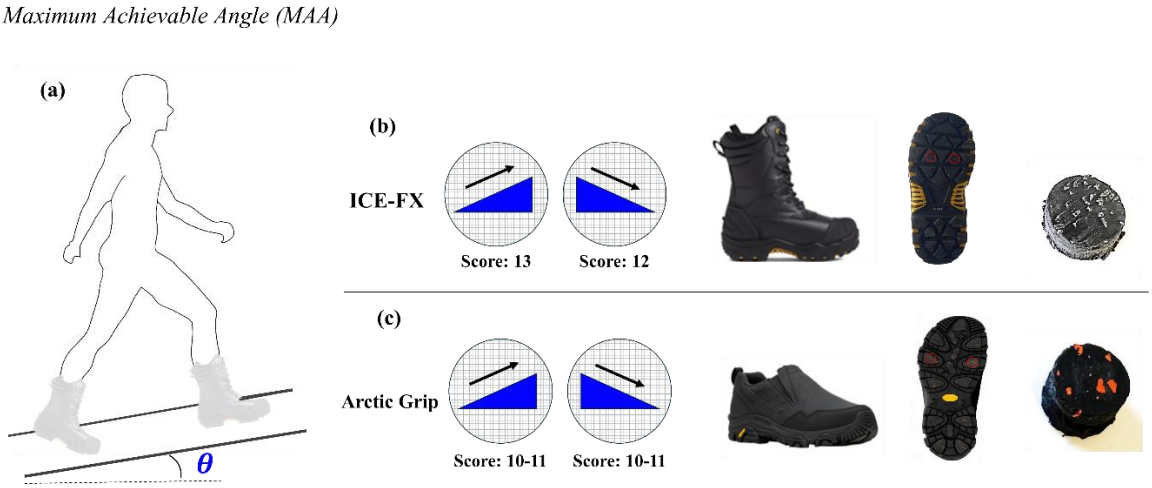


Fig. 3- 3- Sample preparation of commercial slip-resistant footwear: a) Selection based on the maximum achievable angle for walking on an icy surface, as tested by an individual wearing the boots [21], b) IceFX, including slip resistance scores and an outsole sample, and c) Arctic Grip, with reported slip resistance scores and an outsole sample.

3-4-3- Surface Characterization of Samples

The surface morphology of the samples was analyzed using Scanning Electron Microscopy (SEM). SEM and Energy Dispersive Spectroscopy (EDS) characterization was performed with a Thermo Fisher Quanta 3D-EDS (Thermo Fisher Scientific, USA) system. Prior to analysis, samples were coated with a thin platinum layer to enhance conductivity, using a Denton V Sputter Coater (Denton Vacuum, LLC, USA) at a working voltage of 20 kV.

3-4-4- Ice Surface Preparation

Creating ice in trays presents several challenges due to the presence of heterogeneous nucleation centers and impurities in the water, resulting in uneven and irregular ice surfaces. These imperfections can introduce significant variability in experimental results [5]. To mitigate this, the trays were filled with deionized water and covered with a 3D-printed lid containing a hole to accommodate expansion during solidification. A heavy, flat steel body was placed on top to stabilize the trays during the freezing process at -18°C. Before conducting friction tests, the ice

surfaces were meticulously smoothed and polished using a flat stainless-steel disc to achieve maximum flatness, followed by wiping with a wet towel to absorb any molten water and ensure consistency in the liquid-like layer thickness across all tests [21].

3-4-5- Definition of Ice Friction Testing Parameters

Evaluating the tribological behavior of ice necessitates the consideration of key parameters such as sliding velocity, ice hardness, slider geometry, and applied normal force [22][12]. Therefore, it is essential to develop a specific testing script to ensure consistent and reliable comparisons of composite performance. Existing international standards for tribology testing, such as ASTM F2913-19, primarily focus on whole-size shoe specimens [23]. However, friction on ice is significantly influenced by the pressure applied to the contact surface. As described by Poiseuille's flow (Equation 3-1), the applied pressure induces pressure heating, which subsequently increases the depth of the lubricating layer on the ice surface [24].

$$\frac{h_{lll}}{L} = \left(\frac{24hK_2}{\rho h_{sf} C L^2}\right)^{1/4} \times \left(\varepsilon - \varepsilon^2\right)^{1/4} \qquad \text{Equation (3-1)}$$

Where, h_{lll} is the height of the Liquid-Like Layer (LLL) on the ice, L: length of the contact, h: viscosity of liquid water, K_2: thermal conductivity of LLL, ρ: density of liquid water, h_{sf}: latent heat of melting, C: physical constant, and $\varepsilon = \frac{x}{L}$.

To ensure consistent control of physical phenomena, modifications to the sample size are necessary for lab-scale testing protocols. The ASTM standard specifies a normal force of 400 N for testing full-size shoe specimens, corresponding to sizes below US men's 7.5 and women's 8.5. Under these conditions, a surface pressure of roughly 22 kPa is applied to the ice during friction measurements. For the specimen size used in this study (D=17 mm), achieving the same surface pressure on the ice requires a normal force of ~5 N. Furthermore, the sliding speed was set to 0.3 m/s, as recommended by the ASTM standard for consistent testing conditions.

To simulate walking gait, the ice friction testing protocol is structured into two phases: first, the rubber composite and ice make contact under a controlled load; second, the lower drive begins movement at a predefined speed. The specific parameters for the testing are detailed in Table 3-1. Following this standardized script ensures consistent evaluation of frictional response on ice, enabling reliable comparisons between different composite materials.

Table 3- 1- Friction script definition

Normal Load (ASTM)	Applied Normal Load	Slider Tracking Radius (in rotary mode)	Sliding Speed
400 ± 20 (N) *Over whole shoe size* *(7.5 women)*	~ 5 (N) *over sample size* *(D= 17 mm)*	2 (cm)	300 (mm/sec.) ~ 145 RPM

3-4-5-1- Load Tuning

The contact dynamics were systematically analyzed across six load-tuning parameters to optimize the stability of the normal force exerted on the ice surface while maintaining consistent pace and motion. These parameters encompass three speed-related variables: pre-touch speed, touch speed, and tracking speed, and three force-related variables: touch force, set force, and tolerance. The influence of these was parametrically investigated and is described in following section.

3-5- Results and Discussion

3-5-1- SEM/EDS Morphological Analysis of Sample Surfaces

Figure 3-4 presents SEM images illustrating the morphological characteristics of IceFX and Arctic Grip outsoles, as well as TPU-GF composites. The IceFX outsole features hard, irregularly shaped additives embedded within the rubber substrate and exhibits lamellar surface waviness, likely achieved through intentional abrading of the surface. In contrast, the Arctic Grip outsole incorporates glass fiber additives within the rubber matrix, with a mean fiber diameter of approximately 11 μm, as determined by ImageJ analysis. Figure 3-5 shows EDS analysis results for the additives in the commercial anti-slip rubber formulations. The IceFX outsole contains SiC hard additives, while the Arctic Grip outsole is predominantly composed of glass fibers. The orange flake-shaped occurrences observed on Arctic Grip samples are rubber-only, suggesting they are unlikely to significantly influence the tribological performance.

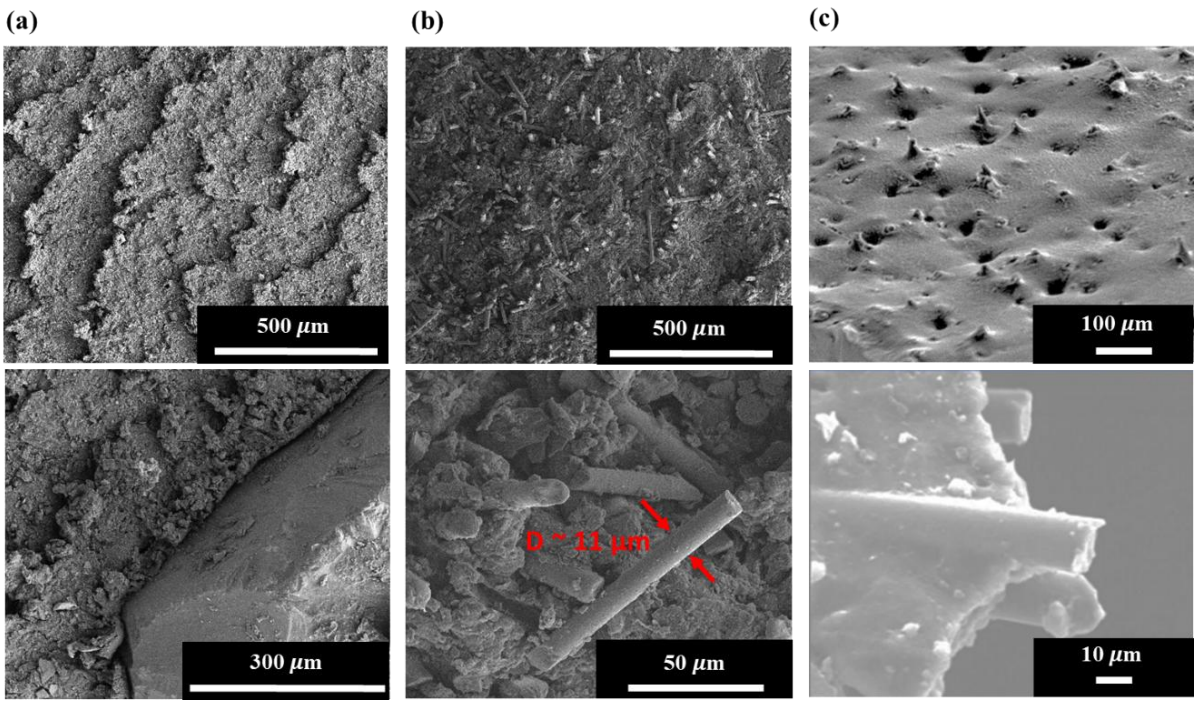


Fig. 3- 4- SEM morphology analyses of textured surfaces of specimens; a) IceFX, b) Arctic-Grip, and c) TPU-GFs[19] composites

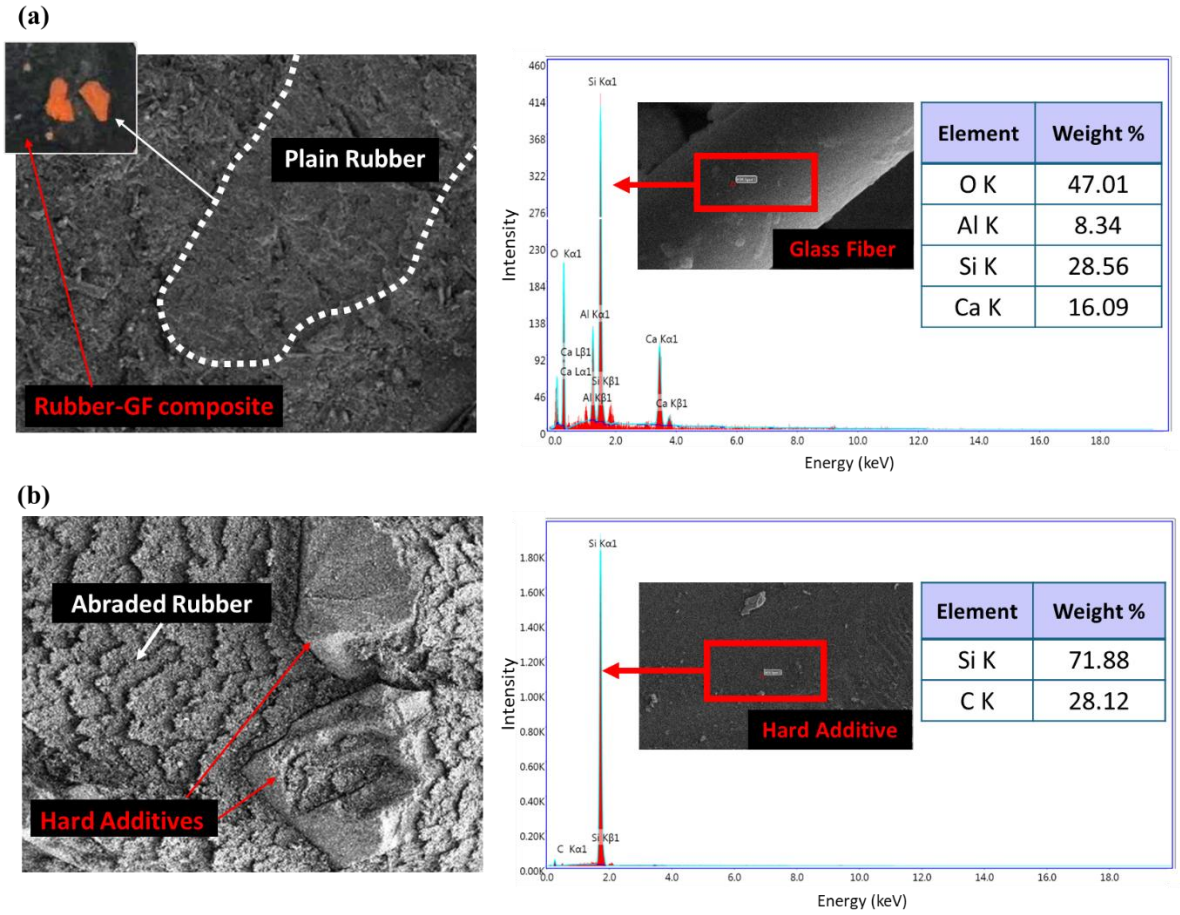


Fig. 3- 5- EDS analytical studies on the textured surfaces of a) Arctic Grip composite, and b) IceFX composite

3-5-2- Influence of Testing Parameters on Ice Tribology

Given the dynamic nature of ice as the contact surface for rubber samples, it is crucial to systematically investigate the testing protocol parameters to accurately capture the force signals from the machine. These parameters include (1) load tuning, (2) dwell time, and (3) data sampling rate, all of which are examined in detail in the following section.

3-5-2-1- Load Tuning

According to the standard guidelines for evaluating slip resistance in footwear, achieving a stabilized normal load before initiating movement is crucial [22]. This process simulates human walking, where the heel first contacts the ground, followed by full foot contact, and ends with the toe lifting off, all at a predefined speed that determines gait velocity. To ensure stable normal load

distribution across the ice surface, a detailed parametric analysis of the influencing factors is necessary. The process begins with the specimen moving at a pre-touch speed to establish initial contact with the ice surface. This is followed by deceleration to a touch speed, and further reduction in speed until the tolerance threshold for the set force is reached. Precise control of contact tuning is essential during two critical phases of the test: the initial contact between the ice and the sample, and the subsequent transverse sliding movement at a specified velocity. Load tuning variables were systematically analyzed on identical ice surfaces prepared as described in Section 3-4-4 to optimize the specimen-ice interaction during high-speed testing. This involved defining the velocity and load parameters that govern the interaction between the sample and the ice under high-speed conditions. The effects of these parameters were studied to enhance the precision and accuracy of normal load application on the ice surface. Three speed variables were sequentially adjusted, ensuring that the pre-contact speed was higher than the contact speed, and the contact speed was higher than the tracking speed. Additionally, three load control variables were employed, with the touch force set below the target force of 5 N and within a defined force tolerance range. Table 3-2 illustrates the impact of these parameters on the variation in normal force (ΔF_N), which represents the difference between the maximum and minimum forces exerted on the ice surface.

Table 3- 2- Ice-rubber contact dynamic parameters optimization

Test No.	**Speed Variables (mm/sec.)**			**Force Variables (N)**			**ΔF_N (N)**
	Pre-touch	Touch	Tracking	Touch	Set Force	Tolerance	
1	0.5	0.3	0.025	1.0	5.0	0.025	~ 5.12
2	0.5	0.3	0.025	0.2	5.0	0.025	~ 4.31
3	0.5	0.45	0.1	0.2	5.0	0.025	~ 4.68
4	0.5	0.4	0.2	0.2	5.0	0.2	~ 5.64
5	0.5	0.1	0.05	0.5	5.0	0.2	~ 8.41
6	0.5	0.3	0.1	0.2	5.0	4	~ 8.94
7	0.5	0.3	0.2	0.2	5.0	4	~ 8.46
8	0.5	0.3	0.25	0.2	5.0	4	~ 9.44
9	0.5	0.3	0.1	2	5.0	3	~ 7.54
10	0.5	0.3	0.2	2	5.0	3	~ 6.48
11	0.5	0.3	0.25	2	5.0	3	~ 6.79
12	0.5	0.3	0.25	4.85	5.0	0.1	~ 6.81
13	1.0	0.8	0.4	0.5	5.0	0.4	~ 6.40

Increasing the force tolerance results in greater instability of the normal force, whereas tighter force tolerances demonstrate improved stability in the normal load. Pre-touch speed must not be

set too high, as this can cause the two surfaces to overshoot each other and prevent the stabilization of the normal force. Other speed tuning parameters were adjusted, resulting in the corresponding ΔF values reported in Table 3-2. The optimal dynamic configuration resulted in the lowest normal force variation, recorded at 4.31 N, and the corresponding load-speed diagram is illustrated in Fig. 3-6.

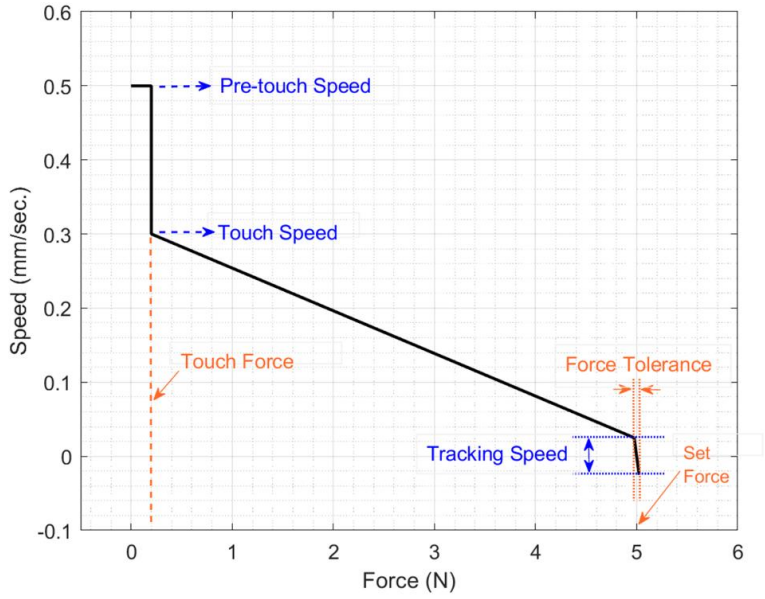


Fig. 3- 6- Optimized dynamic of contact variables for script definition

3-5-2-2- Dwell Time

Considering the dynamic behavior of ice and the room temperature testing conditions, precise control of timing in the testing procedure is critical. Figure 3-7 illustrates the effect of dwell time, comparing 10 seconds to 60 seconds, on the initiation of rotational or reciprocating movement [25][26].

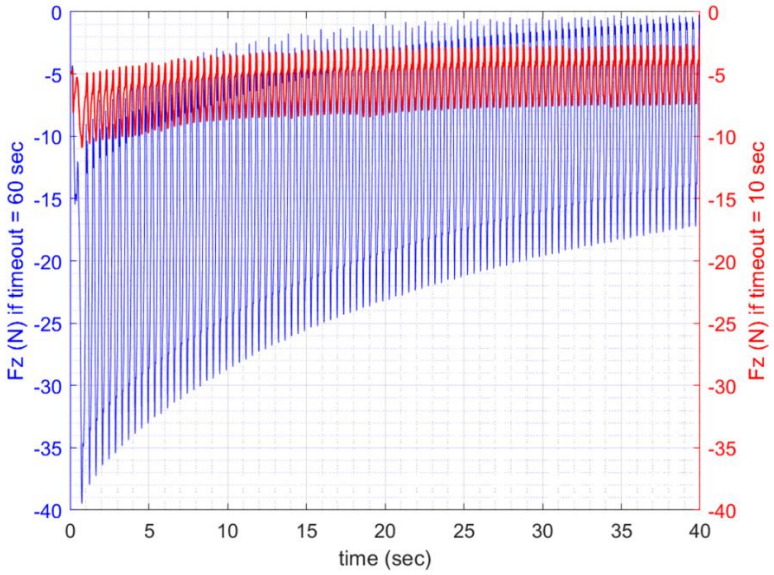


Fig. 3- 7- Influence of Contact Timing on Normal Force Stability. Blue plot represents a 60-second duration of ice-rubber initial contact before movement initiation, while the red plot illustrates a 10-second duration.

Friction on ice is significantly reduced near its melting temperature, where the ice behaves less like a solid due to the increased thickness of the liquid-like layer [23]. At lower temperatures, ice acts as a hard surface with a thinner liquid-like layer, leading to potentially higher friction [24]. Measuring friction on ice near its melting temperature thus represents a worst-case scenario, with friction likely to be higher at lower temperatures. Figure 3-7 indicate that achieving the 5 N set force between the sample and ice surface promptly is essential before commencing high-speed motion. The data demonstrates that a 10-second timing in the first phase provides better stability in the normal force and helps prevent the formation of unevenness on the ice surface. An extended dwell time of 60 seconds during the initial phase can result in the formation of a dimple on the ice surface due to localized pressure-induced melting [25]. This dimple causes significant fluctuations in the normal force signal once the test begins, with these fluctuations persisting during subsequent movements, albeit with smaller amplitudes, due to melting effects.

3-5-2-3- Data Sampling Rate

The rate of data sampling is a critical parameter in defining the test protocol [27]. Literature and previous studies indicate that frictional responses on icy surfaces typically exhibit an initial peak in static friction force, which can occur in fractions of a second at high testing speeds [9]. Consequently, capturing this static coefficient of friction requires a high sampling rate.

Furthermore, the kinetic responses are generally observed in two modes: stick-slip and smooth sliding, necessitating detailed data capture to monitor these phenomena. Figure 3-8 illustrates the effect of data sampling rate on the friction response of the Arctic Grip composite under rotational and reciprocating modes. Increasing the data sampling frequency to 1000 Hz enables the detection of intermediate stick-slip friction events of the rubber composite on ice. The static coefficient of friction was more clearly identifiable in the rotation mode as opposed to in the reciprocating mode. Lower sampling rates fail to capture intermediate stick-slip behavior, which is crucial for understanding ice traction dynamics. The sampling rate of 50 Hz is inadequate, while 2000 Hz is excessive, resulting in an excessive data volume. Therefore, a sampling frequency of 1000 Hz is optimal, effectively capturing static frictional forces and the relevant physical phenomena occurring on the ice surface.

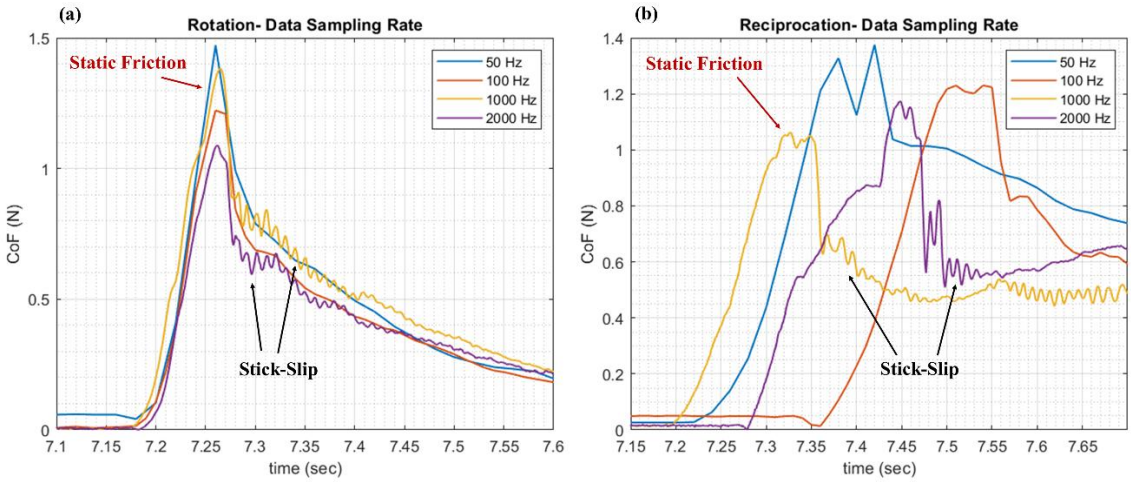


Fig. 3- 8- Effect of data sampling rate on static frictional force recognition on ice in a) rotation, and b) reciprocation test setups

3-5-3- Comparison of Reciprocating and Rotational Sliding Modes on Ice

An essential inquiry centered on determining whether reciprocating or rotational experimental setups yield more precise measurements of rubber-ice friction. Both configurations, as depicted in Figure 3-2, were subjected to a comparative analysis of their frictional responses. Figure 3-9-a illustrates the frictional behavior of the Arctic Grip composite in a reciprocating motion on ice, while Figure 3-9-b presents the corresponding behavior under rotational motion. The maximum kinetic friction force recorded in the reciprocating setup was approximately 4.3 N, significantly

higher than the approximately 0.9 N observed in the rotational setup. Figure 3-9-c provides a comparative analysis of the initial static friction peaks captured by both setups. The data reveal consistent performance in terms of static friction and intermediate stick-slip phenomena across both configurations. However, the kinetic friction profiles differ notably, with the reciprocating setup exhibiting a secondary frictional peak following the initial static peak, a behavior not observed in the rotational setup.

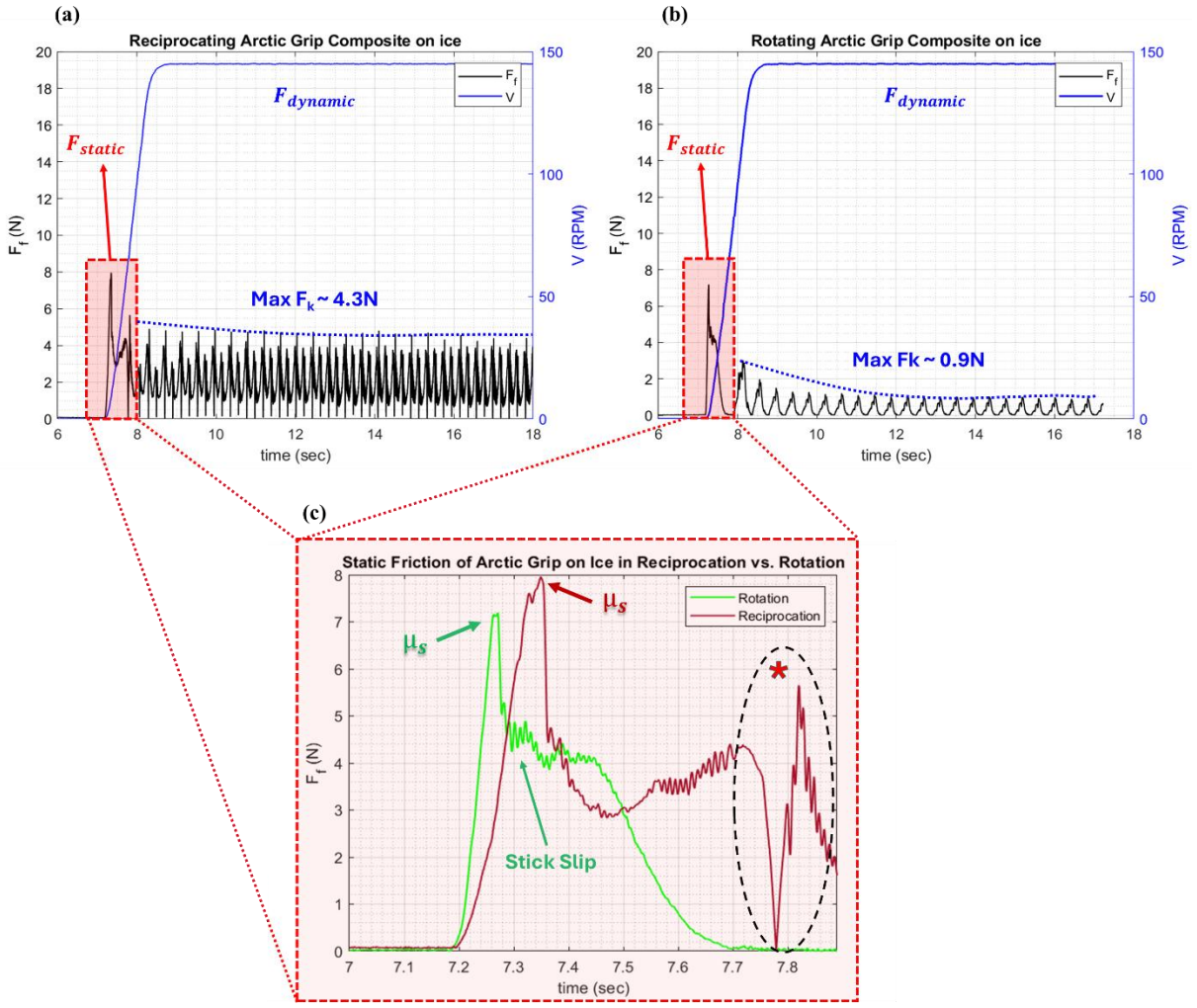


Fig. 3- 9- Static and Kinetic friction behavior of Arctic Grip composite on ice at room temperature, a) reciprocation, b) rotation, and c) comparison of static friction in rotation vs. reciprocation

In both configurations, the ice surface experiences repeated contact events, and frictional heating significantly influences the observed responses. During reciprocation, given the limited maximum stroke length (only 26 mm) of the apparatus, the ice surface is subjected to successive high-speed traversals. As the frictional sliding continues over multiple cycles, the ice progressively accumulates a thicker LLL, which suggests a transition into the hydrodynamic friction regime,

characterized by a plateauing of the friction force signal for each cycle. This behavior is also evident in the rotational setup, where the friction force decreases in intensity with successive movements. This reduction aligns with the hydrophobic nature of rubber, which minimizes the contribution of capillary forces within the hydrodynamic regime, thereby preventing an increase in friction [28]. In the hydrodynamic regime, the applied load is predominantly supported by the lubricating layer rather than the surface asperities [29].

To gain deeper insights into the physical phenomena governing each movement mode, a comparative analysis was conducted focusing on the kinetic friction responses. Due to the observed inconsistencies in the kinetic friction regions, the first several consecutive cycles of kinetic friction were selected for comparison between the rotational and reciprocating modes, as illustrated in Figures 3-10 and 3-11, respectively.

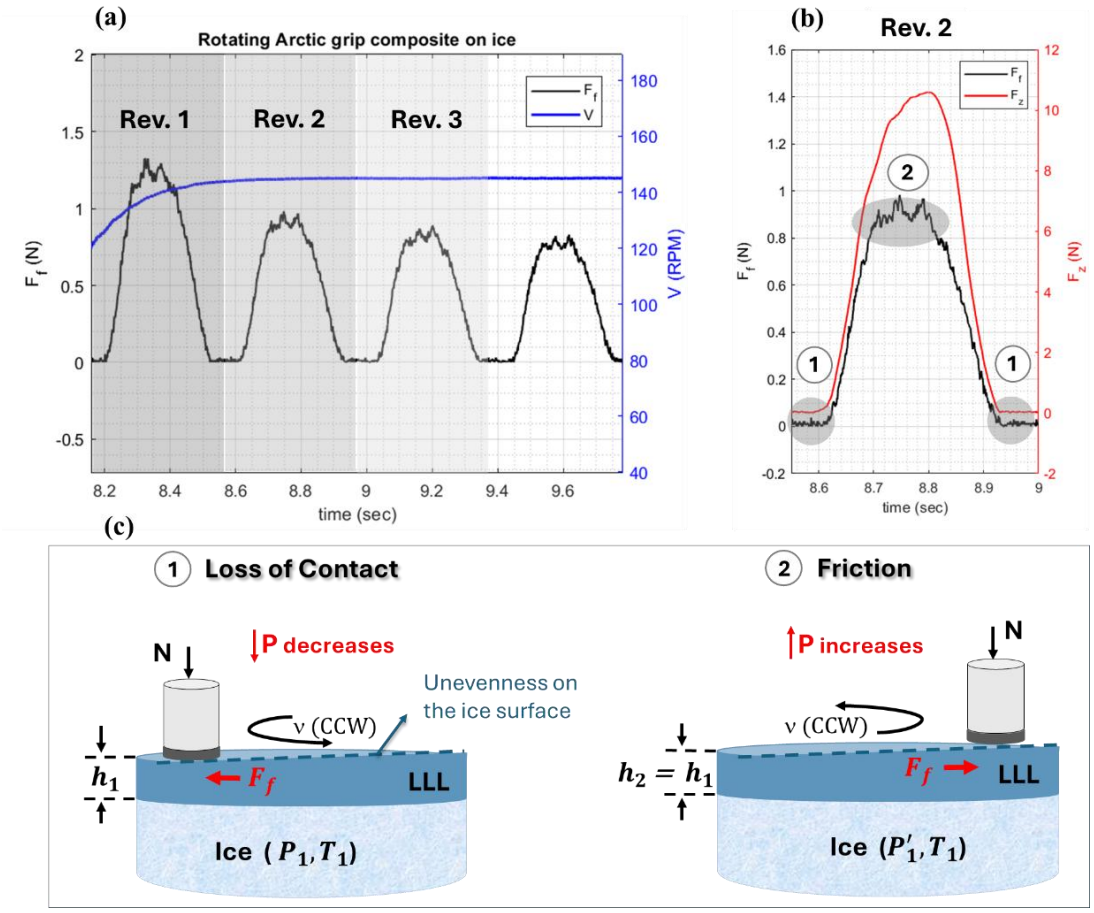


Fig. 3- 10- Kinetic friction of rubber on ice in rotational mode: a) four sequential cycles in kinetic region, b) friction and normal force signals in revolution 2 in the kinetic region, and c) schematic of the process and the contact dynamic of the machine

A thorough understanding of friction and normal force dynamics is essential for developing an effective test protocol. In this tribological test, the friction and normal force signals are influenced by the physical phenomena associated with the formation of the LLL on the ice surface, as well as the dynamic parameters set for the UMT Tribolab. In the kinetic rotational mode, each cycle produces a friction profile characterized by an initial increase with multiple stick-slip peaks, yet without a pronounced static peak, followed by a subsequent decrease (Fig. 3-10-b). The behavior of the normal force is analyzed in conjunction with the test schematic shown in Fig. 3-10-c, where the ice surface exhibits a lack of perfect evenness. As the rubber sample traverses the ice surface, it intermittently loses contact at certain locations, prompting the dynamic system to compensate by increasing the normal force to maintain the set force of 5 N. However, due to the high rotational speed of the test, the rubber quickly encounters another area of the ice with a slightly increased height. This interaction results in a cyclic fluctuation of the normal force, as depicted in Fig. 3-10-b. These fluctuations, previously mitigated by optimizing the contact dynamic parameters, do not significantly impact the slip performance, allowing the process to continue until it enters the hydrodynamic regime, where a thicker LLL forms on the ice surface [29].

Figure 3-11 presents the corresponding signal channels for the kinetic region of the same composite sample under reciprocation mode. Here, the friction signals are captured along the x-axis to differentiate between the forward and backward strokes, represented by positive and negative friction values, respectively. Each forward and backward stroke pair is defined as a cycle, providing a detailed understanding of the frictional behavior in reciprocating motion.

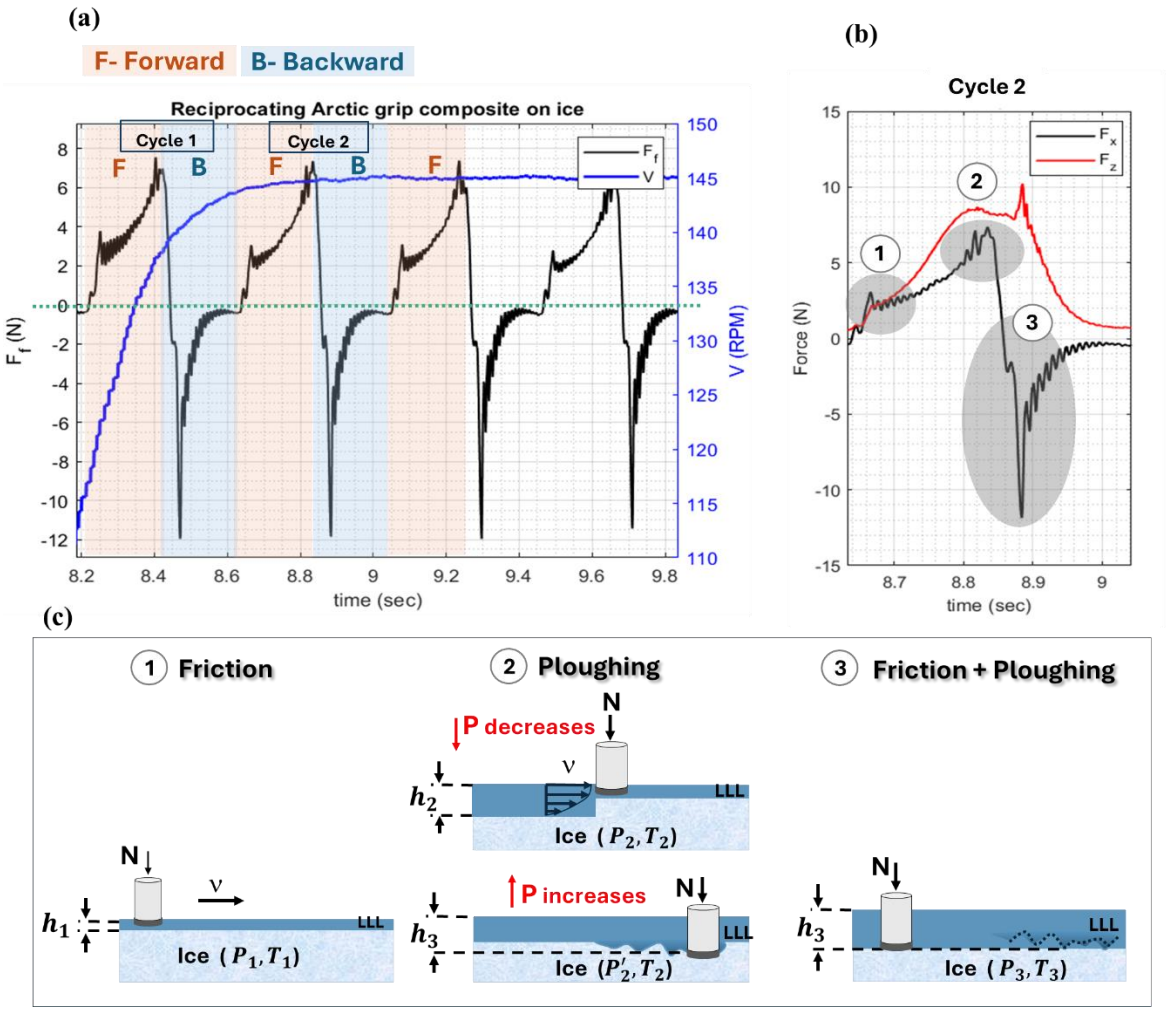


Fig. 3- 11- Kinetic friction of rubber on ice in reciprocation mode: a) four sequential cycles (forward and backward) in kinetic region, b) friction and normal force signals in cycle 2 in the kinetic region, and c) the schematic of process and physical phenomena

Reciprocating motion generates greater frictional heating on the ice surface, which influences the LLL. This frictional melting effect aligns with the principles of Couette's flow, as described by the following equation [30].

$$h = \frac{1}{h_{sf}\rho}\left(\frac{\mu N}{nb} - \sqrt{\frac{L}{2n}}\left(\Delta T_{ice}\sqrt{K_{ice}C_{ice}\rho_{ice}} + \Delta T_{sole}\sqrt{K_{sole}C_{sole}\rho_{sole}}\right)\right) \qquad \text{Equation (3-2)}$$

where h is the height of the LLL, h_{sf}: latent heat of melting, ρ: density of liquid water, μ: friction between ice and sole, N: normal force, n: number of contacts, L: length of contact, b: width of contact, n : velocity of slider, K: thermal conductivity, C: specific thermal capacity, ΔT_{ice}: temperature difference between contact surface and ice, and ΔT_{sole}: temperature difference between contact surface and sole. According to the Equation (3-2), an increase in contact velocity

leads to a thicker LLL on the ice. Additionally, increased frictional heating contributes to the transition of the ice into the plastic regime [31].

Figure 3-11-a shows that at the beginning of each forward stroke, the friction signal exhibits an initial response followed by intermediate stick-slip behavior. The friction force then increases again, and during the backward stroke, a pronounced peak in friction is observed, followed by fluctuations that eventually level off into a plateau. Figure 3-11-b presents the friction and normal force signals for a complete cycle. One cycle offers a detailed view of the dynamic interactions taking place. In Stage 1 of the forward stroke, the sample moves at high speed over the ice surface. Frictional heating leads to the formation of a thicker LLL, causing a localized reduction in normal force. To compensate for this and to maintain the force within the predefined range for contact dynamics (load tuning), there is an increase in the normal force applied by the machine. This rise in normal force, combined with the elevated ice temperature due to frictional heating in a confined area, leads to a phenomenon known as ice ploughing (Stage 2). Ice ploughing significantly contributes to the high frictional force observed in the kinetic region of reciprocation [12]. Ploughing occurs when the slider body, rather than simply sliding, plastically indents the ice in the normal direction due to the contact pressure exceeding the penetration hardness of the ice (P_h). This results in the slider sample ploughing laterally through the ice surface. The ploughing coefficient of friction (μ_p) decreases with increasing normal force, and this decrease becomes more pronounced at high velocity and temperatures near the melting point, indicating that ice enters the ploughing regime at lower friction levels. The ploughing coefficient of friction can be quantified using Equation 3-3 [12].

$$\mu_p = \frac{A_p P_h(T)}{N} \qquad \text{Equation (3-3)}$$

Where A_P is the ploughing area, P_h is the penetration hardness of the ice as a function of T, temperature, and N is the applied normal force.

During the backward stroke, the sample applies additional shear force to flatten the ploughing marks previously formed on the ice surface. This results in a sharp peak in friction force during the backward motion of reciprocation in Stage 3. Thus, reciprocating motion on the ice surface does not yield a purely accurate friction response; instead, it presents unrealistic friction values due to the combined effects of sliding and ploughing on the ice [31]. Ploughing leads to alterations

in the ice surface, which complicates the evaluation of new composites by not solely reflecting sliding behavior. In contrast, rotational movement provides a more accurate representation of sliding behavior on ice. Thus, using the Bruker UMT Tribolab with a rotational setup offers more reliable insights into the performance of rubber composites and facilitates high-throughput evaluation of new composite materials.

3-5-4- Reliability Assessment of the Testing Protocol

This tribotest allows for the systematic evaluation of various rubber composites for ice traction properties, including the comparison of static coefficients of friction, friction mechanisms, and kinetic coefficients of friction in lab-scale assessments of newly developed composites. Several composite materials were tested to assess the performance of the tribotest and the developed protocol. Each test was conducted in triplicate to evaluate the repeatability of the measured friction response.

To evaluate the reliability of the developed testing protocol, results obtained for the same TPU composites were compared with those reported by Rizvi et al., who utilized the SATRA ice friction setup, as shown in Fig. 3-12-a [19]. The new protocol demonstrated similar friction behavior for pure TPU and TPU-10% GF as observed in the SATRA setup. In both cases, the friction response started with a rapid and pronounced static friction peak, followed by multiple stick-slip peaks, and transitioned to a smoother response attributed to hydrodynamic friction.

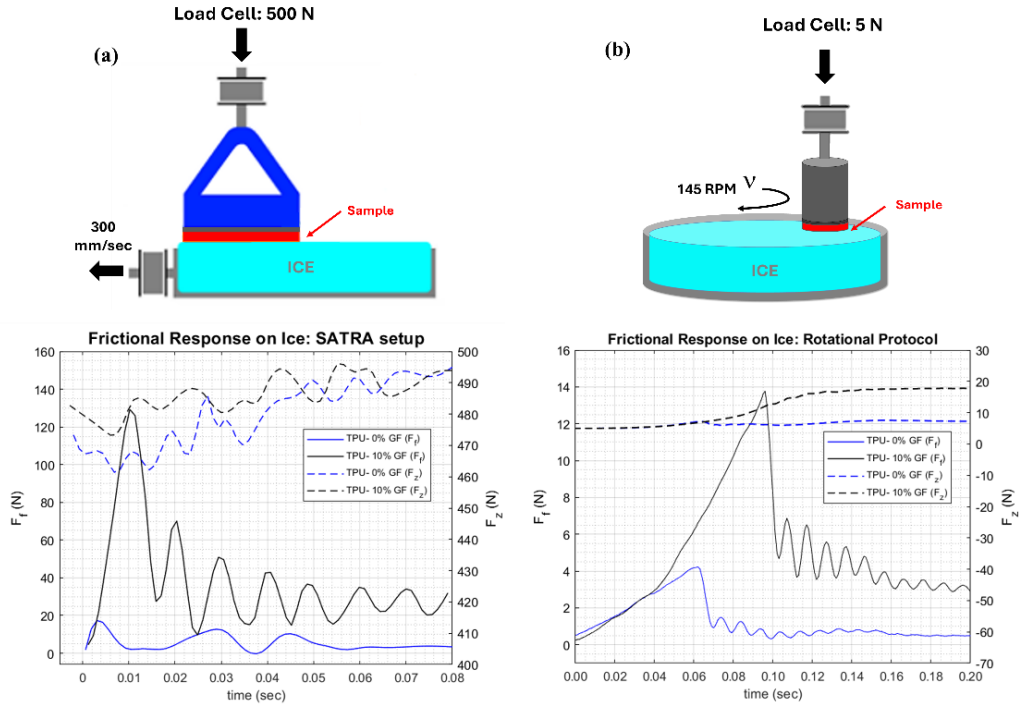


Fig. 3- 12- Friction testing protocols and obtained responses of pristine TPU and TPU-10%wt.GF obtained by: a) SATRA setup [19], and b) Newly developed rotational protocol

Different tribology tests conducted on ice surfaces produce varying results due to differences in physical and testing parameters. For instance, in the SATRA setup, a load of 500 N applies a pressure of approximately 1.11 MPa on the ice surface, whereas the new protocol applies a pressure of 0.022 MPa (refer to Section 3-4-5 for details on the effect of pressure). The higher pressure influences the measured friction response of rubber on ice [32][33].

The developed protocol provides a systematic approach to assessing the frictional responses of rubber composites with different surface texturing technologies and captures the physical phenomena underlying the friction behavior, offering a high throughput screening method for evaluating ice traction properties.

3-5-5- Ice Frictional Response of Rubber Composites

Rubber samples were analyzed at various surface texturing conditions. For the commercial boots, a sample of the midsole rubber was extracted as a plain rubber, which did not include any surface texturing technologies. This sample was tested using the rotary movement protocol developed earlier in this research and compared with the results from the textured surface composites. The outcomes of these tests, conducted according to the specified protocol, are displayed in Figure 3-13.

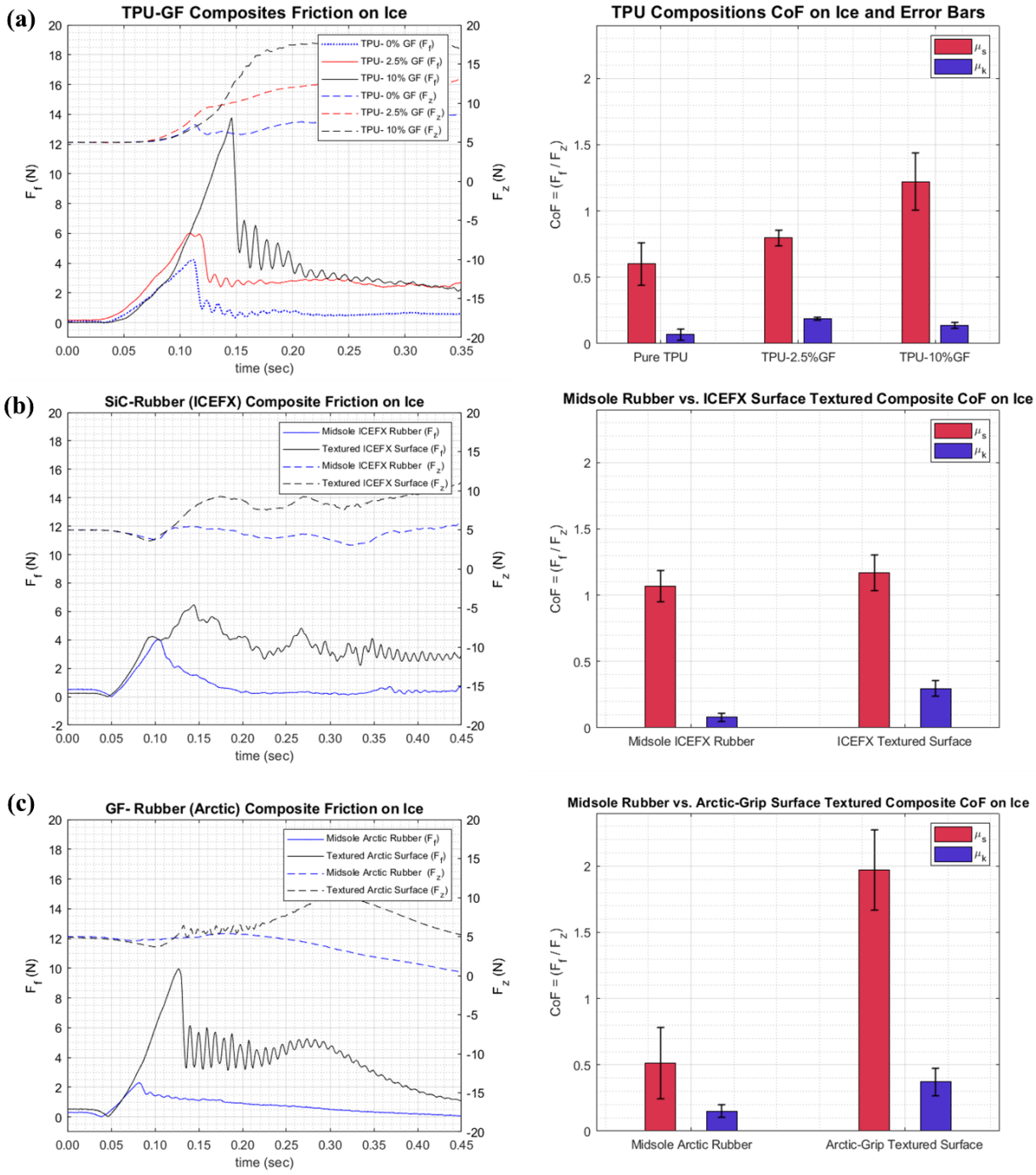


Fig. 3- 13- Specimens' friction and normal force on ice on the left, and their corresponded CoF on the right, evaluated by rotational sliding testing protocol, a) TPU and its glass-fiber composites, b) Midsole and IceFX rubber composites, and c) Midsole and Arctic-Grip composites.

In anti-slip rubber composites used for footwear and automobile tires, mechanical interlocking plays a critical role in generating frictional force between ice and rubber surfaces. This mechanism parallels natural phenomena, such as polar animals using hard claws to secure traction on ice or snakes leveraging the tilting of scales for locomotion [30]. Inspired by such natural adaptations, a

biomimetic approach to surface texturing of rubber materials in these applications aims to maximize mechanical interlocking. The observed frictional performance of the textured rubber composites corroborates this approach, and the resulting friction force generated can be described as:

$$F_f = F_{visc} + \tau_f \text{ A} \quad \text{Equation (3-4)}$$

where F_{visc} represents the pulsation deformation of the rubber material due to its viscoelastic performance, and τ_f denotes the shear stress on A, the real-contact surface[34]. An increase in the number of asperities on the surface enhances the shear stress, thereby improving grip on the ice surface. Consequently, to optimize ice grip, the second component of Equation (3-4) must be maximized.

Different surface texturing methods yield distinct frictional responses on ice by increasing shear stress at the contact interface, as illustrated by the results in Fig. 3-13. The impact of surface texturing on the static and kinetic coefficients of friction is further highlighted in the bar plots of Fig. 3-13, which demonstrate that surface texturing not only enhances grip through increased stick-slip behavior on ice but also improves the kinetic coefficient of friction, thereby suggesting enhanced ice traction performance in composite materials. The increase in glass fiber content within Thermoplastic Polyurethane (TPU) composites enhanced the static friction force and amplified stick-slip behavior, attributed to the shear forces exerted on the ice by the protruding glass fibers (see Fig. 3-4-c). Observations of commercial anti-slip footwear revealed concurrent improvements in both static and kinetic coefficients of friction due to surface texturing. The IceFX composites demonstrated enhanced ice-gripping characteristics over time, as reflected in an extended stick-slip performance domain. However, the static coefficient of friction exhibited only a slight improvement. Notably, the presence of additives other than silicon carbide (SiC) on the IceFX midsole's surface suggests that it is not composed solely of plain rubber.

The Arctic Grip material (Fig. 3-13-c) exhibited a frictional profile similar to that of TPU-GF composites (Fig. 3-13-a), which is attributed to comparable surface texturing technologies involving 1D glass fibers. These findings are consistent with predictions from Hertzian contact theory [35], which states:

$$P_{max} = \frac{3}{2}\frac{F}{\pi a^2} \quad \text{Equation (3- 5)}$$

Where P_{max} is the contact pressure that induces shear force on the surface, and a is the contact radius.

Therefore, incorporation of hard one-dimensional (1D) glass fibers enhances ice traction by reducing the contact radius on the ice surface and increasing the shear forces applied at the contact interface. These results highlight the potential of 1D additives in the fabrication of slip-resistant rubber composites. However, existing studies indicate that 1D additives in rubber composites are prone to rapid abrasion, which may lead to a decline in ice traction performance over time [36]. Consequently, abrasion resistance must also be evaluated to provide a comprehensive tribological assessment of their durability. Abrasion resistance for rubber composites can be analyzed using an abrasion drum machine in accordance with the ISO 4649 standard.

As no established standard protocol exists for assessing ice traction of small samples, this testing protocol aims to provide insights into high-throughput screening of the ice friction behavior of rubber composites in the laboratory. This approach minimizes material waste during the production of initial prototypes for new slip-resistant rubber composites. The study represents a comprehensive analysis utilizing the UMT Bruker system for ice friction investigations and outlines several directions for future research. These include reducing system errors by improving ice surface quality control, achieving precise regulation of ice temperature, and enhancing the stability of normal force application.

3-6- Conclusions

Composite technology for synthesizing anti-slip rubbers presents a promising solution for the production of ice-traction composites used in footwear outsoles and winter tires. To advance material development in this field, it is essential to implement laboratory-scale tribological testing to evaluate the tribological properties of these composites. This study successfully developed an ice tribo-testing method for evaluating the ice traction properties of rubbers using the Bruker UMT Tribolab, in accordance with ASTM F2913 standards for assessing slip resistivity in footwear. Unlike previous lab-scale setups, which were limited by low sliding velocities and unrepresentative normal loads, our protocol allows for the application and control of normal loads on the ice surface while maintaining speed levels consistent with human walking pace. Two distinct testing modes, reciprocating and rotating, were carefully designed and parametrically studied to assess the accuracy of the device's signal for ice friction analysis. The effects of the

dynamic of the contacting surfaces, dwell timing, and data sampling rates were systematically examined to establish the most accurate testing protocol for analyzing rubber-ice friction at room temperature. Samples tested included those from prior research on surface texturing, such as TPU and TPU-GF composites at various weight percentages, as well as commercial anti-skid winter shoes. The results obtained through the defined protocol demonstrate its reliability for ice tribology testing. This advancement represents a significant milestone in lab-scale ice tribology analysis, providing valuable insights for researchers involved in composite manufacturing and surface texturing projects aimed at improving ice traction performance.

3-7- References

[1] Adina Bresge, "Latest Canadian statistics on slips and falls on ice," *Can. Press*, pp. 3–7, 2019.

[2] S. Canada, "Population Projections for Canada (2018 to 2068), Provinces and Territories (2018 to 2043)," 2019.

[3] B. N. J. Persson, "Theory of rubber friction and contact mechanics," *J. Chem. Phys.*, vol. 115, no. 8, pp. 3840–3861, 2001, doi: 10.1063/1.1388626.

[4] C. H. Kang, W. Bin Jung, H. J. Kim, and H. T. Jung, "Highly enhanced tire performance achieved by using combined carbon nanotubes and soybean oil," *J. Appl. Polym. Sci.*, vol. 138, no. 10, pp. 1–13, 2021, doi: 10.1002/app.49945.

[5] N. Namdari, G. J. Otto, G. Guo, H. Sojoudi, and R. Rizvi, "Nanotextured surfaces with enhanced ice-traction and wear-resistance," *Compos. Part B Eng.*, vol. 238, p. 109916, 2022, doi: 10.1016/j.compositesb.2022.109916.

[6] X. Zhang *et al.*, "A common supersolid skin covering both water and ice," *Phys. Chem. Chem. Phys.*, vol. 16, no. 42, pp. 22987–22994, 2014, doi: 10.1039/c4cp02516d.

[7] A. M. Kietzig, S. G. Hatzikiriakos, and P. Englezos, "Physics of ice friction," *J. Appl. Phys.*, vol. 107, no. 8, 2010, doi: 10.1063/1.3340792.

[8] B. N. J. Persson, "Ice friction: Role of non-uniform frictional heating and ice premelting," *J. Chem. Phys.*, vol. 143, no. 22, 2015, doi: 10.1063/1.4936299.

[9] S. Babaee, S. Pajovic, A. Rafsanjani, Y. Shi, K. Bertoldi, and G. Traverso, "Bioinspired kirigami metasurfaces as assistive shoe grips," *Nat. Biomed. Eng.*, vol. 4, no. 8, pp. 778–786, 2020, doi: 10.1038/s41551-020-0564-3.

[10] N. Namdari *et al.*, "Advanced functional surfaces through controlled damage and instabilities," *Mater. Horizons*, vol. 7, no. 2, pp. 366–396, 2020, doi: 10.1039/c9mh01516g.

[11] N. Namdari and R. Rizvi, "Damage induced surface texturing of short fiber-PDMS composite materials," *Annu. Tech. Conf. - ANTEC, Conf. Proc.*, vol. 2018-May, no. May 2018, 2018.

[12] R. W. Liefferink, F. C. Hsia, B. Weber, and D. Bonn, "Friction on Ice: How Temperature, Pressure, and Speed Control the Slipperiness of Ice," *Phys. Rev. X*, vol. 11, no. 1, p. 11025, 2021, doi: 10.1103/PhysRevX.11.011025.

[13] "SATRA STM 603 ICE Ice tray for slip resistance tester." https://www.satra.com/test_equipment/consumable.php?id=61

[14] "SATRA STM 603 Slip resistance tester." https://www.satra.com/test_equipment/machine.php?id=74&msclkid=76e88f9bc81711ecb4808b94702cf995

[15] K. Mielonen, "Hierarchically structured polymer surfaces : Curved surfaces and sliding behavior on ice," University of Eastern Finland, 2019.

[16] J. Lungevics, E. Jansons, I. Boiko, I. Velkavrh, J. Voyer, and T. Wright, "A Holistic Approach Towards Surface Topography Analyses for Ice Tribology Applications," *Front. Mech. Eng.*, vol. 7, no. June, pp. 1–14, 2021, doi: 10.3389/fmech.2021.691485.

[17] C. Stamboulides, P. Englezos, and S. G. Hatzikiriakos, "The ice friction of polymeric substrates," *Tribol. Int.*, vol. 55, pp. 59–67, 2012, doi: 10.1016/j.triboint.2012.05.001.

[18] L. Makkonen and M. Tikanmäki, "Modeling the friction of ice," *Cold Reg. Sci. Technol.*, vol. 102, pp. 84–93, 2014, doi: 10.1016/j.coldregions.2014.03.002.

[19] R. Rizvi, H. Naguib, G. Fernie, and T. Dutta, "High friction on ice provided by elastomeric fiber composites with textured surfaces," *Appl. Phys. Lett.*, vol. 106, no. 11, 2015, doi: 10.1063/1.4913676.

[20] T. Dutta, "Rate My Tread," *Toronto Rehabilitation Institute*, 2021. https://kite-uhn.com/rmt/en

[21] A. K. Bhoopalam, C. Sandu, and S. Taheri, "Experimental investigation of pneumatic tire performance on ice: Part 2 - Outdoor study," *J. Terramechanics*, vol. 60, pp. 55–62, 2015, doi: 10.1016/j.jterra.2015.03.001.

[22] S. Zahmatkesh and R. Rizvi, "Effect of sliding speed on tribological responses of ice traction in surface-damaged elastomeric composites," in *Progress in Canadian Mechanical Engineering*, 2023, p. 357. doi: https://doi.org/10.17118/11143/21065.

[23] "ASTM F2913: Standard Test Method for Measuring the Coefficient of Friction for Evaluation of Slip Performance of Footwear and Test Surfaces/Flooring Using a Whole Shoe Tester, 2019, American Society of Testing Materials."

[24] A. Bejan and P. A. Tyvand, "The pressure melting of ice under a body with flat base," *J. Heat Transfer*, vol. 114, no. 2, pp. 529–531, 1992, doi: 10.1115/1.2911310.

[25] A. Spagni, A. Berardo, D. Marchetto, E. Gualtieri, N. M. Pugno, and S. Valeri, "Friction of rough surfaces on ice: Experiments and modeling," *Wear*, vol. 368–369, pp. 258–266, 2016, doi: 10.1016/j.wear.2016.10.001.

[26] L. Makkonen and M. Tikanmäki, "Modeling the friction of ice," *Cold Reg. Sci. Technol.*, vol. 102, pp. 84–93, 2014, doi: 10.1016/j.coldregions.2014.03.002.

[27] Y. Zhang, J. Gao, and Q. Li, "Experimental study on friction coefficients between tire tread rubber and ice," *AIP Adv.*, vol. 8, no. 7, 2018, doi: 10.1063/1.5041049.

[28] M. Nosonovsky and B. Bhushan, "Roughness optimization for biomimetic superhydrophobic surfaces," *Microsyst. Technol.*, vol. 11, no. 7, pp. 535–549, 2005, doi: 10.1007/s00542-005-0602-9.

[29] A. M. Kietzig, S. G. Hatzikiriakos, and P. Englezos, "Ice friction: The effects of surface roughness, structure, and hydrophobicity," *J. Appl. Phys.*, vol. 106, no. 2, 2009, doi: 10.1063/1.3173346.

[30] V. Richhariya, A. Tripathy, O. Carvalho, M. Julker Nine, D. Losic, and F. S. Silva, "Unravelling the physics and mechanisms behind slips and falls on icy surfaces: A comprehensive review and nature-inspired solutions," *Mater. Des.*, vol. 234, p. 112335, 2023, doi: 10.1016/j.matdes.2023.112335.

[31] K. A. Gross, "A Penetrating Look at Ice Friction," *Physics (College. Park. Md).*, vol. 14, pp. 8–10, 2021, doi: 10.1103/physics.14.20.

[32] C. Dong, Y. Meng, Y. Liu, Z. Huang, and L. Ma, "Study on the ice friction characteristics," *Cold Reg. Sci. Technol.*, vol. 216, no. August, p. 104010, 2023, doi: 10.1016/j.coldregions.2023.104010.

[33] M. Kandeva and N. Dishovsky, "Friction behavior produced in the course of a contact enabled between composite materials and eco-friendly soles prototypes made of elastomeric material with regard to ice-covered

surface," *Tribol. Ind.*, vol. 41, no. 1, pp. 90–99, 2019, doi: 10.24874/ti.2019.41.01.10.

[34] A. Tiwari, N. Miyashita, N. Espallargas, and B. N. J. Persson, "Rubber friction: The contribution from the area of real contact," *J. Chem. Phys.*, vol. 148, no. 22, 2018, doi: 10.1063/1.5037136.

[35] E. Ciulli, A. Betti, and P. Forte, "The Applicability of the Hertzian Formulas to Point Contacts of Spheres and Spherical Caps," *Lubricants*, vol. 10, no. 10, 2022, doi: 10.3390/lubricants10100233.

[36] Z. S. Bagheri, Y. Li, A. R. Fekr, and T. Dutta, "The effect of wear on slip-resistance of winter footwear with composite outsoles: A pilot study," *Appl. Ergon.*, vol. 99, p. 103611, 2022, doi: 10.1016/j.apergo.2021.103611.

Chapter 4:
Wear-Activated Surface Engineering of TPU/Graphene Nanoplatelet Nanocomposites for Ice Friction Control

4-1- Chapter Preface

The findings presented here are partly based on the following peer-reviewed publication:

- *S. Zahmatkesh, SN. Leung, R. Rizvi," Wear-Activated Surface Engineering of TPU/Graphene Nanoplatelet Nanocomposites for Ice Friction Control", Journal of Polymer Composites, Accepted and Available online.*

4-2- Abstract

Developing elastomeric composites that simultaneously provide high ice traction, and strong abrasion resistance remains a major challenge for anti-slip applications. In this study, thermoplastic polyurethane (TPU) nanocomposites reinforced with pristine and acid-functionalized graphene nanoplatelets (GNPs) were designed to address this trade-off through combined interfacial engineering and wear-activated surface design. Functionalized GNPs (*f*/GNPs) were prepared by acid treatment to introduce oxygen-containing groups and enhance filler–matrix interactions. TPU composites containing 20 and 40 phr (parts per hundred rubber) of GNPs or *f*/GNPs were fabricated by solution mixing, followed by evaluation of morphology, tensile behavior, thermal stability, ice traction, and abrasion resistance. Additionally, biomimetic surface texturing was introduced by wire brushing to generate hierarchical microfeatures, while post-abrasion surfaces were analyzed to assess wear-activated traction performance. The results confirmed successful GNP functionalization and showed that *f*/GNPs improved dispersion, interfacial adhesion, tensile stiffness, and thermal stability of TPU composites. Surface texturing consistently enhanced ice traction for all composite formulations. Post-abrasion surface analyses revealed the formation of abrasion-generated asperities and microchannels that promoted mechanical interlocking and liquid dissipation at the interface, thereby sustaining friction on ice. Among all compositions, TPU-20 *f*/GNP exhibited the best overall tribological performance, achieving the lowest abrasion volume

loss while maintaining superior post-abrasion ice traction. In contrast, higher *f*/GNP loading led to excessive interfacial constraints, reduced matrix compliance, and more brittle wear behavior. These findings demonstrate that functionalized graphene reinforcement combined with wear-activated surface engineering provides an effective pathway for tailoring the structure-property-tribology relationship of TPU nanocomposites for durable ice-traction applications.

Keywords: *TPU nanocomposites; functionalized graphene nanoplatelets; abrasion resistance; interfacial engineering; wear-activated surface texturing; ice traction*

4-3- Literature Review and Research Hypothesis

Slips and falls represent a significant global health and economic burden, particularly under icy and winter conditions. The World Health Organization reports that approximately 37.3 million fall incidents each year require medical attention, with about 684,000 fatalities annually, ranking falls as the second leading cause of unintentional injury-related death worldwide [1]. In cold-climate regions, ice- and snow-covered surfaces substantially increase injury risk; Canadian emergency-department data document 14,977 ice-related slip-and-fall events, identifying winter surface conditions as a dominant predictor of injury occurrence [2]. At the national level, unintentional falls account for nearly 654,000 emergency-department visits annually in Canada, imposing an estimated $10.3 billion per year in direct healthcare costs [3]. Although winter maintenance strategies such as mechanical plowing and chemical de-icing are routinely implemented to mitigate ice accumulation, icy surface conditions remain widespread and difficult to eliminate entirely. Consequently, slip- and fall-related injuries continue to pose a significant safety concern during winter seasons, highlighting the need for advanced surface-engineering solutions that can provide reliable traction under icy conditions.

To enhance traction of shoes on icy surfaces, Babaee et al. proposed a bioinspired kirigami-based metasurface that generates sharp protrusions under applied strain. The patterned structures, fabricated from perforated steel sheets and integrated into shoe outsoles, deform out of plane during walking to mechanically engage the ice [4]. However, the reliance on metallic spikes introduces durability concerns, as the protruding elements are subjected to repeated cyclic loading and continuous exposure to corrosive de-icing salts, which can accelerate fatigue and corrosion, leading to progressive degradation of traction performance over time.

To develop lightweight alternatives to metallic anti-slip systems, elastomeric composites and engineered surfaces have been widely explored for footwear and winter tire applications. Rizvi *et al.* [5] introduced Damage-Induced Surface Texturing (DIST) for glass fiber–reinforced thermoplastic polyurethane (TPU) composites, where controlled interfacial debonding generates surface asperities capable of mechanically engaging ice, resulting in traction improvements of up to ~900% relative to pristine surfaces. This method involves aligning chopped glass fibers within an elastomeric matrix, followed by transverse cutting to induce fiber–matrix debonding and expose hard fiber tips at the surface. Similar damage- and instability-driven strategies have been reported to create advanced functional surfaces with enhanced ice traction by Namdar *et al.* [6]. Despite significant initial performance gains, DIST-based surfaces exhibit limited durability in practical applications. The protruding glass fibers act as one-dimensional hard asperities that undergo rapid abrasion during walking on hard pavements, leading to progressive loss of surface texture and a corresponding decline in slip resistance [7].

In this context, Bagheri *et al.* [8] sought to improve the durability of damage-induced textured surfaces by developing a hybrid fiber–reinforced thermoplastic polyurethane (TPU) composite incorporating carbon fibers (CF) and poly(p-phenylene-2,6-benzobisoxazole) (PBO) fibers. By combining stiff CF with more compliant PBO fibers, the hybrid architecture enabled a textured surface that balances ice-gripping performance with improved wear tolerance, thereby sustaining a high coefficient of friction on ice surfaces over extended use. Although the results were promising and the TPU-based composite exhibited improved abrasion resistance, reliance on one-dimensional fibrous additives introduces manufacturing challenges, as achieving precise fiber alignment and controlled orientation at scale remains a significant barrier to commercialization.

Building on the DIST framework, Namdari and co-workers extended the concept to elastomeric composites incorporating two-dimensional (2D) fillers. They investigated the ice-traction behavior of SEBS rubber composites reinforced with one-dimensional (1D) and two-dimensional fillers at both micro- and nanoscales. The composites were fabricated using a solution-based process followed by compression molding and subsequent transverse cutting to generate DIST surfaces. By employing particulate 2D fillers, this approach eliminated the need for fiber alignment, thereby reducing manufacturing complexity and cost. The results demonstrated that 1D fillers exhibited inferior post-abrasion performance compared to 2D graphene nanoplatelets (GNPs) and boron

nitride nanosheets (BNNS), due to buckling and fracture of protruding 1D reinforcements under contact pressure. GNP-reinforced nanocomposites achieved the highest ice traction after abrasion; however, their reduced durability relative to other formulations suggested a persistent trade-off between traction performance and wear resistance [9].

Complementary work by Anwer *et al.* [10] further demonstrated that polyurethane-based textured composites exhibit higher abrasion resistance and sustained slip resistance on ice compared to styrene block copolymer systems, underscoring the advantage of polyurethane elastomers for durable ice-traction applications. In addition to tailoring composite composition, engineering the surface texture offers direct control over contact mechanics and interfacial engagement with ice. Nature has long served as a source of inspiration for functional surface design, providing efficient solutions that can be translated into engineered systems through biomimicry. A well-known example is the gecko, which exhibits exceptional adhesion across a wide range of surfaces. This capability originates from the hierarchical architecture of its feet, consisting of densely packed, hair-like micro- and nanoscale structures that maximize real contact area and enable strong, reversible adhesion, even on vertical and inverted surfaces [11]. Richhariya *et al.* [12] reported a bioinspired pillar-textured surface, inspired by the hierarchical micro- and nanoscale structures of gecko feet, fabricated via laser surface texturing. In their study, nanoparticle exposure enhanced surface hydrophilicity and capillary-driven fluid absorption, promoting rapid interfacial freezing and resulting in markedly increased friction on ice. Thirunavukkarasu *et al.* [13] employed 3D printing to fabricate hybrid elastomeric structures that combined claw-inspired sharp edges, amphibian-inspired supportive polygonal pillars, and springtail-inspired micro-overhang scales to enhance surface friction.

This study addresses the long-standing trade-off between ice traction and abrasion resistance in elastomeric anti-slip materials, particularly for composites incorporating two-dimensional (2D) fillers [14], [15]. Although 2D materials such as GNPs have demonstrated significant potential for enhancing ice traction, their limited abrasion resistance under repeated contact and wear remains a major challenge. This limitation hinders long-term durability, large-scale manufacturing, and commercial adoption [9]. In practical applications, premature surface degradation rapidly reduces traction, undermining the reliability of otherwise high-performing materials.

It is hypothesized that this durability limitation originates from insufficient anchoring at the GNP–elastomer interface, which promotes filler pull-out under shear and abrasive loading, accelerates surface wear, and degrades tribological performance over time. To address this gap, the present work introduces an interfacial engineering strategy based on acid-induced surface functionalization of GNPs prior to composite fabrication. By strengthening interfacial bonding between the GNPs and the elastomeric matrix, this approach mitigates filler debonding and enables simultaneous improvement of ice traction and abrasion resistance, which represent two properties that are traditionally antagonistic in elastomeric systems. Beyond compositional optimization, this study incorporates bioinspired surface texturing as a complementary design strategy. Drawing inspiration from the wear-activated, self-renewing micro-asperities of snake scales and the liquid-dissipating microchannel architecture of penguin feet, a hybrid surface design is proposed. This architecture promotes the formation of self-generated micro textures during service, such that progressive abrasion exposes new traction-enhancing asperities rather than degrading surface functionality. Through the synergistic integration of interfacial chemistry and bioinspired surface engineering, this work aims to overcome durability limitations and establish a scalable pathway toward wear-adaptive, high-performance ice-traction materials suitable for real-world applications.

4-4- Fabrication of Composites with Enhanced Tribological Behavior

4-4-1- Surface functionalization of Graphene nanoplatelets (GNPs) and Characterization

Graphene nanoplatelets (GNPs), supplied by ACS Materials, had a nominal thickness of 2–10 nm, corresponding to approximately 18 graphene layers. This grade was selected as an economical option for bulk reinforcement. The GNPs had a lateral diameter ranging from 2 to 7 μm. Figure 4-1 presents transmission electron microscopy (TEM) images of the as-received GNPs, showing their lateral dimensions and the characteristic stacked morphology composed of multiple graphene layers.

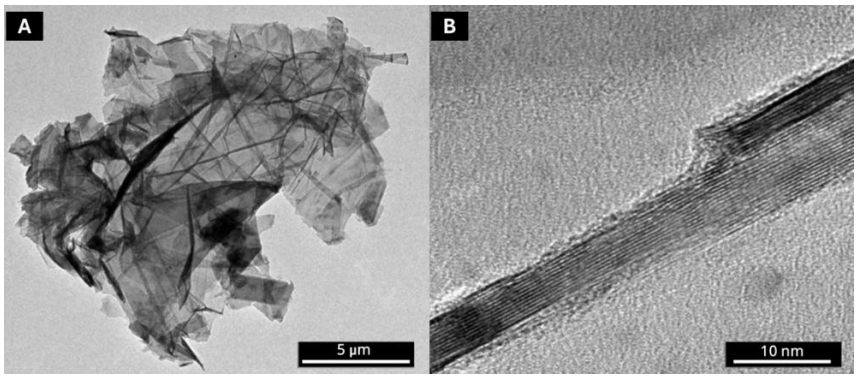


Fig. 4- 1- Transmission electron microscopy (TEM) images of graphene nanoplatelets (GNPs): (A) lateral flake morphology and size distribution; (B) stacked multilayer graphene sheets showing nanoscale thickness. The copyrighted image is used by permission of ACS Material LLC [16].

Sulfuric acid (H_2SO_4) and nitric acid (HNO_3) were purchased from Sigma-Millipore and used as received. A mixed acid solution (H_2SO_4/HNO_3 = 3:1 by volume) was prepared, and GNPs were gradually introduced at a concentration below 1 wt.% under magnetic stirring at 400 rpm. The suspension was maintained at 80 °C for 6 h to initiate oxidation, followed by an additional 12 h under the same conditions to promote surface functionalization. The resulting suspension was then added dropwise into a distilled water bath to dilute the acid mixture. The product was repeatedly washed with distilled water until a neutral pH (~7) was achieved, confirming the removal of residual acids. The acid-treated GNPs were then vacuum-dried at 80 °C for 24 h, yielding functionalized graphene nanoplatelets (*f*/GNPs) [17].

To evaluate the effects of acid functionalization, pristine GNPs and *f*/GNPs were characterized using thermogravimetric analysis (TGA) and Fourier-transform infrared spectroscopy (FTIR) to assess changes in thermal stability and surface chemistry, respectively. TGA measurements were conducted using a thermogravimetric analyzer (TGA55 Discovery, TA Instruments) under a nitrogen atmosphere. Approximately 10 mg of each sample was heated from room temperature to 800 °C at a constant rate of 10 °C min^{-1}, and the resulting weight-loss behavior was analyzed using TRIOS software. Chemical functionalization of the GNP surface was investigated by attenuated total reflectance Fourier-transform infrared (ATR-FTIR) spectroscopy (Brucker Vertex 70 spectrometer). Pristine GNPs and *f*/GNPs were mixed with potassium bromide (KBr) and pressed into pellets for examination, while a pristine KBr pellet was used as background reference. FTIR spectra were recorded in the transmittance mode over the range of 4000–500 cm^{-1}, with 16 accumulated scans.

4-4-2- Composites Synthesis

Thermoplastic polyurethane (TPU, Elastollan® C 78 A) was supplied by BASF. Dimethyl sulfoxide (DMSO) was purchased from Sigma Millipore and used as the solvent without further purification. 50 g of TPU was dissolved in 50 mL of DMSO under magnetic stirring at 400 rpm for 6 h to obtain a homogeneous polymer solution. Graphene nanoplatelets (GNPs) or acid-functionalized GNPs (*f*/GNPs) were separately dispersed in DMSO at predefined loadings and magnetically stirred at 400 rpm for 2 h. The resulting GNP or *f*/GNP dispersion was then added to the TPU solution and mixed for 1 h at 600 rpm under magnetic stirring. Composite formulations were prepared at low and high filler contents corresponding to 20 and 40phr (parts per hundred rubber) for both non-functionalized and functionalized GNP systems. To enhance filler exfoliation and dispersion, the mixtures were subsequently processed using a high-shear overhead mixer at 1200 rpm for 15 min, followed by ultrasonication for 1 h. The homogeneous composite suspensions were then added dropwise into a methanol bath, inducing polymer-filler flocculation and precipitation[18]. The precipitated composites were washed three times with methanol and subsequently immersed in distilled water to ensure complete removal of residual DMSO. The washed composites were vacuum-dried at 80 °C for 24 h. Specimens were then fabricated using Caver hydraulic hot press in custom molds at 180 °C under a pressure of 2 tons for 15 min, followed by cooling between water-cooled plates for an additional 15 min.

4-4-3- Composites Characterizations

4-4-3-1- Morphological Analysis

To evaluate the quality of interfacial bonding between graphene nanoplatelets (GNPs) and the thermoplastic polyurethane (TPU) matrix, composite specimens were sectioned to a thickness of approximately 2 mm. The samples were immersed in liquid nitrogen for 1.5 h to induce brittle behavior and subsequently fractured by rapid bending. The resulting cryo-fractured cross-sections were used for morphological investigation. The fractured surfaces were examined using scanning electron microscopy (SEM) to investigate the interfacial adhesion between GNPs and the TPU matrix, the effect of acid functionalization on interface quality, and the dispersion status of GNPs within the polymer substrate. SEM imaging was performed using Vega3 Tescan microscope operated at voltage of 30 kV. Prior to imaging, all specimens were sputter-coated with a thin gold layer using a Denton V Sputter Coater at a working voltage of 20 kV to enhance surface

conductivity. Quantitative analysis of SEM micrographs, including evaluation of platelets size distribution was carried out using ImageJ image analysis software.

4-4-3-2- Mechanical Properties Analysis

The mechanical properties of TPU–GNP and TPU–*f*/GNP composites were evaluated by uniaxial tensile testing to characterize their stress–strain behavior. Dumbbell-shaped specimens (Type V) were prepared in accordance with ASTM D638 [19] by hot pressing under the same processing conditions described in Section 4-4-2. Tensile tests were conducted following ISO 527 [20] standards using a universal testing machine (Instron 3000). All tests were performed under axial loading at a constant crosshead displacement rate of 1 mm min^{-1}. At least three specimens were tested for each composite formulation to ensure repeatability and the median curves was selected for further analysis on engineering stress–strain curves.

4-4-3-3- Thermal Analysis

Thermogravimetric Analysis (TGA) was performed to evaluate the effect of filler functionalization and composite composition on the thermal stability of the synthesized composites following the procedure reported in section 4-4-1.

4-4-4- Surface Texturing and Tribology Investigations

To introduce biomimetic surface texturing, the surfaces of the fabricated TPU-GNP and TPU-*f*/GNP composites were mechanically micro-textured using a wire-brushing technique. This process was designed to (i) protrude near-surface graphene nanoplatelets and (ii) generate microscale channels that facilitate fluid dissipation at the contact interface during sliding. The micro-wires used for surface texturing were supplied by McMaster-Carr. Multiple micro-wires were bundled and assembled into a brush using a threaded fastener to form a compact wire-brush head. The assembled brush was mounted onto a high-speed rotary tool (Dremel), and the composite surfaces were textured under identical operating conditions for all specimens. Figure 4-2(A) schematically illustrates the surface texturing concept. Three surface conditions were considered for comparative tribological evaluation: (i) the as-molded composite surface, used as the reference; (ii) the intentionally micro-textured surface produced by wire brushing; and (iii) the post-abrasion surface obtained after wear testing (See section 4-4-4-2), representing the realistic surface state of the composite when used as a shoe outsole under service conditions.

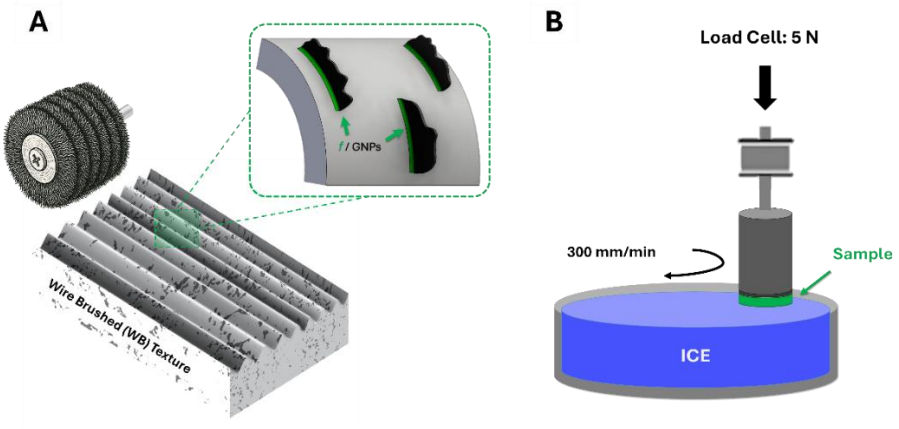


Fig. 4- 2- Schematics illustrating A) hierarchical surface texture formation induced by micro-wire brushing, the exposed and anchored functionalized GNPs, and B) the lab-scale ice traction testing method

4-4-4-1- Ice Traction Evaluation

The slip resistance performance of the composites was evaluated by measuring the static coefficient of friction (SCoF) between the composite surfaces and ice under high-velocity traction conditions. A custom ice-traction testing protocol was developed using a universal mechanical tribometer (UMT Tribolab, Bruker) to simulate real-scale footwear traction behavior under laboratory conditions, following the guidelines of ASTM F2913 for slip resistance evaluation of footwear. Disc-shaped composite specimens were hot pressed using a custom mold following instructions described in Section 4-4-2 and were rigidly bonded to a custom 3D-printed sample holder, which was mounted onto the tribometer scratcher connected to the loadcell. During testing, a composite specimen was brought into contact with a beneath flat ice surface under a normal load of 5 N [21]. Once contact was established, the ice substrate was driven at a constant sliding velocity of 0.3 m s^{-1} while maintaining the applied normal load, as specified by the ASTM F2913[22] protocol. This testing configuration was designed to replicate the mechanical conditions associated with the human gait cycle during slip initiation on icy surfaces. A schematic illustration of the experimental configuration is provided in Fig. 4-2(B). Normal and shear force signals were continuously recorded throughout the test. The initial peak in the measured shear force was identified as the static friction force, from which the static coefficient of friction was calculated. The SCoF values were used for comparative evaluation of different composite formulations and surface texturing conditions. Additional details regarding the development of the ice traction testing methodology can be found in the authors' previous work [21].

4-4-4-2- Abrasion Resistivity Evaluation

Immediately after hot-press fabrication, the density of the disc-shaped specimens was determined using the Archimedes method in accordance with ISO 2781[23]. The abrasion resistance of the TPU–GNP and TPU–*f*/GNP composites was evaluated using a rotating drum abrasion tester following ISO 4649 (Method B) [24]. Abrasion tests were performed on as-molded disc specimens with a diameter of 16 mm under a normal load of 5 N. The specimens were brought into contact with a rotating drum operating at 40 rev min^{-1}, covered with aluminum oxide abrasive paper (60 grit). Each test was conducted over a total abrasion distance of 20 m, corresponding to 42 drum revolutions. The mass of each specimen was measured before and after abrasion testing. Using the measured density values, the corresponding volumetric loss was calculated and used as a quantitative metric of abrasion resistance, where lower volume loss indicates improved wear resistance of the composite material. In addition, the Abrasion Resistance Index (ARI) was calculated to enable a proportional comparison of the wear performance of the composites relative to a reference material, which in this study was pristine TPU [10]. Figure 4-3 schematically illustrates the overall experimental workflow followed in this study for tribological investigation.

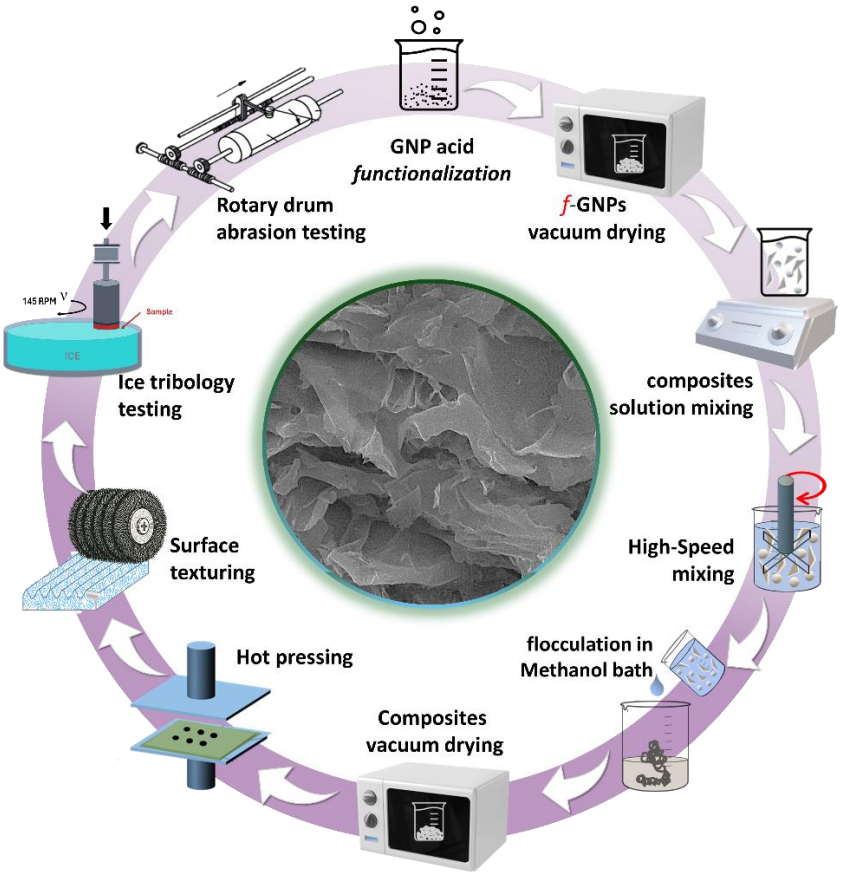


Fig. 4- 3- Schematic illustration of the fabrication, wear-activated surface texturing, and tribology testing workflow of f/GNP-reinforced TPU nanocomposites

4-5- Results and Discussion

4-5-1- FTIR Characterization of GNPs vs. *f*/GNPs

Acid treatment was employed to modify pristine graphene nanoplatelets (GNPs) by introducing oxygen- and hydrogen-containing functional groups, mainly at the platelet edges [25]. These newly generated polar sites promote secondary interactions, particularly hydrogen bonding, with the polar hard and soft segments of thermoplastic polyurethane. As schematically illustrated in Fig. 4-4(A), functionalized GNPs (*f*/GNPs) can form interfacial hydrogen bonds with TPU chains, which is expected to strengthen filler–matrix adhesion, improve stress transfer, and delay filler detachment during deformation or wear [26]. Moreover, the incorporation of surface functional groups alters the surface chemistry of GNPs, reducing their tendency to agglomerate and facilitating a more homogeneous dispersion within the TPU matrix [27]. The effectiveness of the functionalization process was assessed using Fourier Transform Infrared Spectroscopy (FTIR) and

Thermogravimetric Analysis (TGA), as shown in Fig. 4-4. The combined spectroscopic and thermal analyses confirm the successful chemical modification of the graphene nanoplatelets (GNPs), which is expected to enhance filler-matrix interactions and, consequently, improve the tribological performance of the resulting composites.

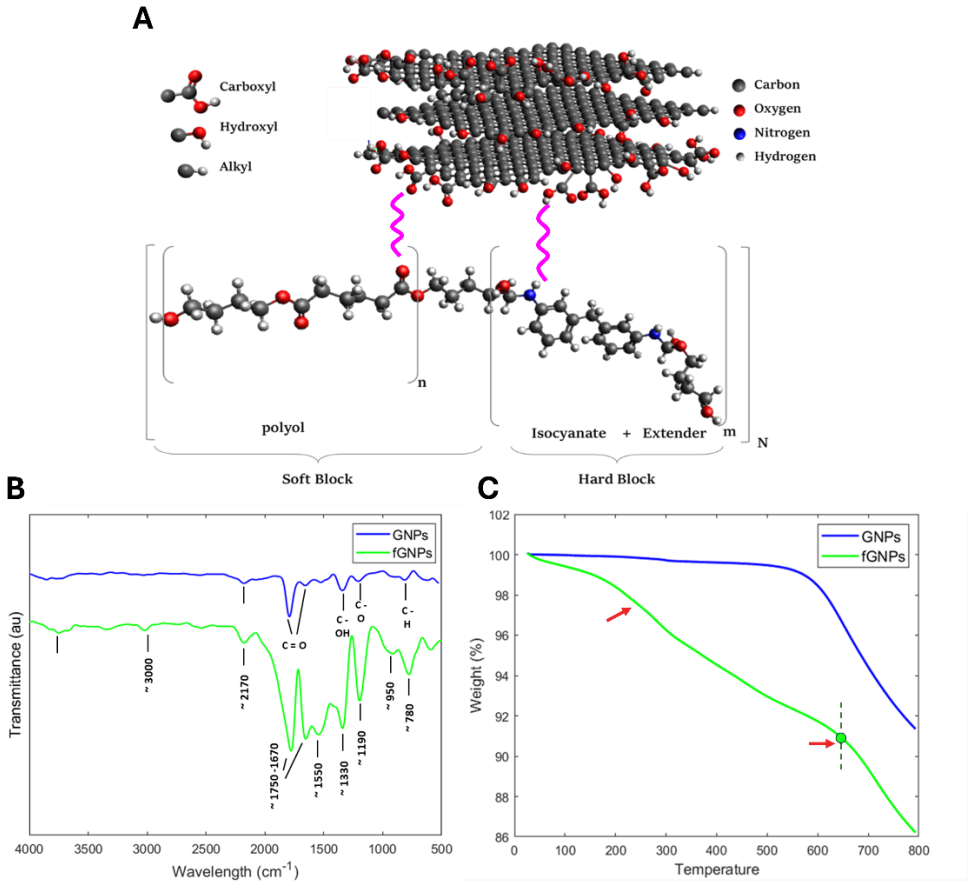


Fig. 4- 4- Surface functionalization of graphene nanoplatelets (GNPs): (A) Schematic illustration of functional group formation at GNP edges and their potential to form covalent bonds with TPU chains; (B) FTIR spectra comparing pristine GNPs and functionalized GNPs (f-GNPs), and c) TGA curves of GNPs and f-GNPs.

The FTIR spectrum of functionalized graphene nanoplatelets (*f*/GNPs) displays several characteristic absorption bands associated with oxygen-containing surface functionalities, confirming effective chemical modification of the graphene surface. A transmittance feature observed around ~3000 cm^{-1} is attributed to C–H stretching vibrations [28]. The band near 2170 cm^{-1} corresponds to skeletal vibrations of residual, non-oxidized graphitic domains [29]. Distinct transmittance peaks appearing at approximately 1750 cm^{-1} and 1670 cm^{-1} are assigned to carbonyl-related vibrations, associated with free C=O stretching and overlapping C=C/C=O stretching of carboxylic groups, respectively [28], [30]. The absorption band at ~1550 cm^{-1} is attributed to C=O

stretching vibrations [31], while the feature at ~1330 cm^{-1} corresponds to C–OH stretching modes [32]. Additionally, the band observed near 950 cm^{-1} is associated with C–O–C stretching vibrations, and the transmittance band around ~800 cm^{-1} is attributed to out-of-plane C–H bending [33]–[35]. Overall, the presence of these transmittance bands confirms the successful introduction of oxygenated functional groups onto the GNP surface via acid functionalization. Complementary TGA analysis further elucidates the thermal behavior of pristine and functionalized graphene nanoplatelets. The initial mass loss observed in *f*/GNPs plot at temperature range of approximately 200–400 °C is attributed to the thermal decomposition of oxygen-containing surface functionalities, such as carboxyl (–COOH) and hydroxyl (–OH) groups, accompanied by the release of CO_2, CO, and H_2O [36]. A subsequent mass-loss step appearing near ~600 °C under nitrogen atmosphere is associated with the thermal decomposition of sp^2-bonded carbon domains within the hexagonal graphene framework. Moreover, this high-temperature decomposition event is shifted to higher temperatures by approximately 50 °C for functionalized GNPs (*f*/GNPs), indicating enhanced thermal stability. This shift is attributed to the reduction in extended sp^2 domains and the formation of sp^3 out-of-plane bonds induced by acid functionalization, which alter the defect structure and edge chemistry of the graphene sheets [37]. These sp^3 sites are expected to serve as effective interfacial anchoring points for strong interactions with TPU chains. The FTIR and TGA results collectively confirm the successful chemical functionalization of GNPs and its role in modifying both their thermal behavior and interfacial compatibility.

4-5-2- Effect of Graphene Functionalization on TPU Nanocomposites

4-5-2-1- SEM Morphological Analysis

Scanning electron microscopy (SEM) was employed to examine the fracture-surface morphology of TPU–20GNP and TPU–20 *f*/GNP nanocomposites, with the aim of investigating the influence of GNP functionalization on particle-elastomer interfacial morphology and GNP dispersion. The size and distribution of graphene platelets were quantified using ImageJ image analysis software. The comparative morphological results are presented in Figure 4-5.

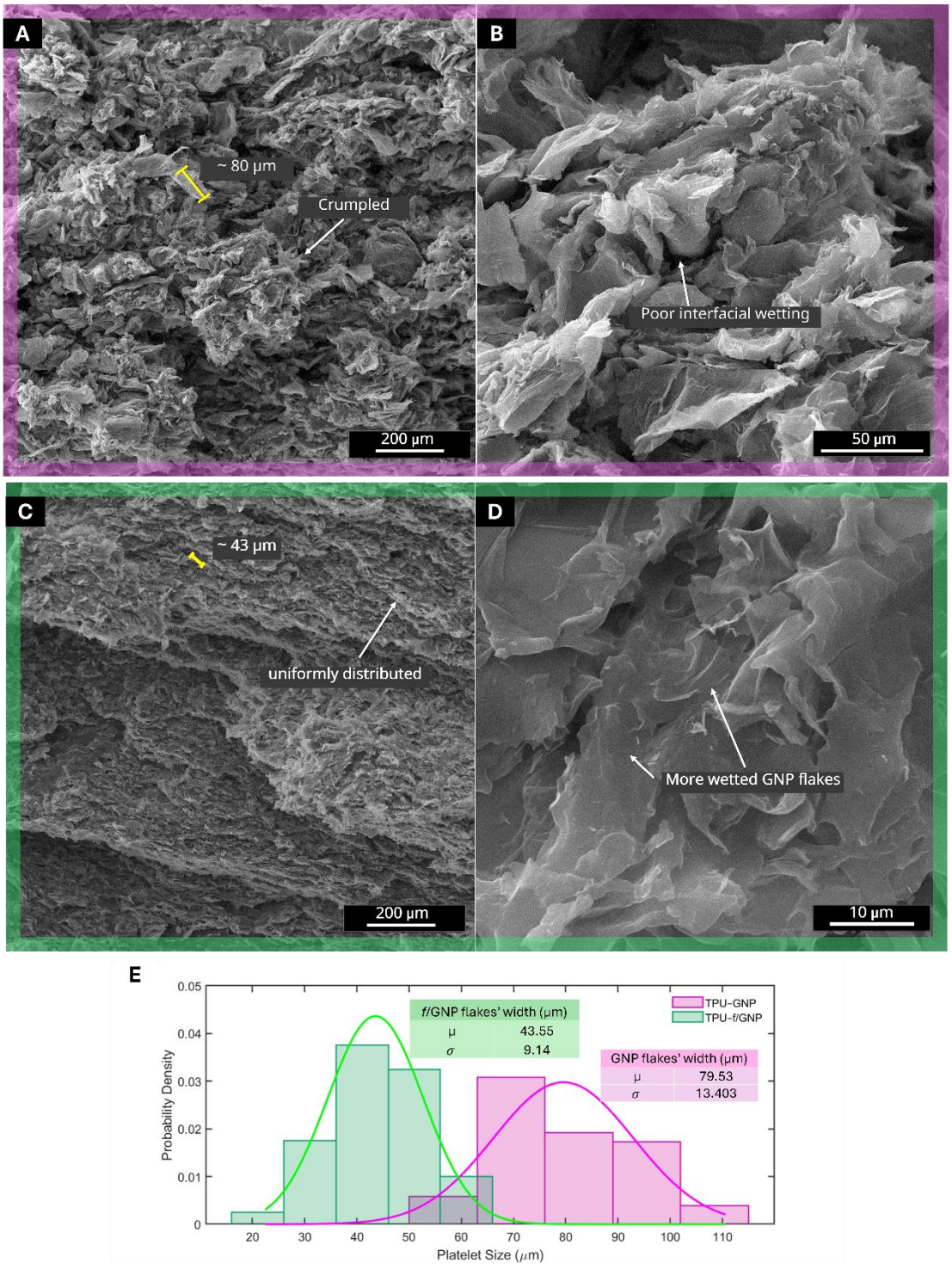


Fig. 4- 5- SEM micrographs of cryogenically fractured surfaces prepared using liquid nitrogen. (A, B) TPU–20GNP composites exhibit coarser graphene nanoplatelets and weak interfacial bonding with the TPU matrix. (C, D) TPU–20 f/GNP composites show a more uniform platelet distribution, finer particle dispersion and improved interfacial adhesion, and (E)GNPs platelet size distribution histograms.

Morphological observations of TPU nanocomposites containing an identical graphene loading (20phr) reveal pronounced differences in interfacial characteristics as a function of GNP

functionalization. In composites incorporating pristine GNPs, the fracture surfaces exhibit interfacial gaps surrounding graphene platelets, along with crumpled platelet morphologies. These features indicate limited interfacial adhesion and are attributed to the intrinsic tendency of pristine GNP sheets to restack and agglomerate due to strong π–π interactions [38]. In contrast, TPU–*f*/GNP composites display improved wetting of the graphene platelets, as evidenced by more continuous polymer coverage and reduced interfacial voids. This enhanced wetting suggests stronger interfacial interactions between functionalized graphene and the TPU matrix. Further image analysis demonstrates that f/GNPs exhibit a reduced mean platelet size of 45 µm compared to pristine GNPs, which show a mean platelet size of 90 µm, indicating improved dispersion within the elastomeric matrix. Such morphological refinement is expected to facilitate more efficient stress transfer at the filler–matrix interface, particularly under tribological loading conditions [39]. Consequently, the improved dispersion and interfacial bonding observed in TPU–*f*/GNP composites over TPU–GNP composites are anticipated to contribute to enhanced abrasion resistance, supporting the central hypothesis of this study.

4-5-2-2- Mechanical Behavior Analysis

Figure 4-6 illustrates representative engineering stress–strain curves obtained from five fabricated specimens.

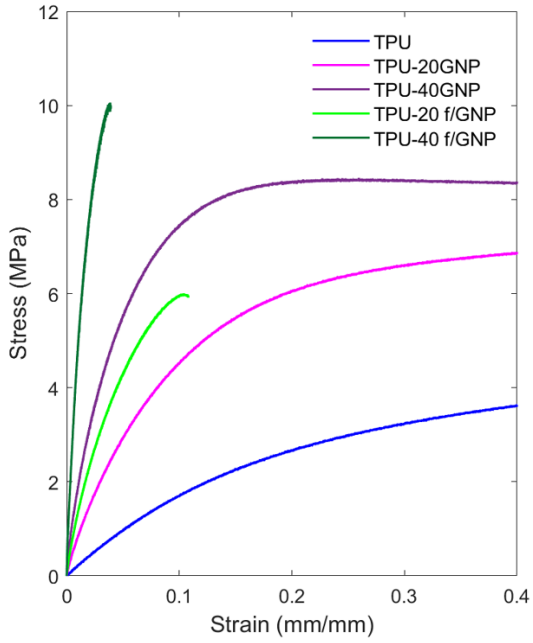


Fig. 4- 6- Engineering stress–strain curves of neat TPU and TPU–GNPs nanocomposites with non-functionalized and functionalized graphene nanoplatelets at 20phr and 40phr loadings.

According to the tensile results, neat TPU exhibits a compliant and highly deformable response characteristic of elastomeric materials. The incorporation of graphene nanoplatelets (GNPs) leads to a pronounced increase in stiffness and tensile stress, with higher filler loading resulting in greater mechanical reinforcement [40]. In composites containing pristine GNPs, interfacial adhesion is primarily governed by weak van der Waals interactions. Consequently, in TPU–40GNP composites, load transfer between TPU chains and graphene platelets becomes progressively inefficient after yielding, promoting interfacial sliding, platelet rotation, and partial pull-out. These interfacial accommodation mechanisms manifest as a post-yield stress plateau in the stress–strain response [41] [42]. Composites reinforced with functionalized GNPs exhibit a steeper initial slope and higher stress at low strains compared to their non-functionalized counterparts, indicating more effective load transfer arising from enhanced filler–matrix interactions. This behavior is consistent with prior reports by Barick et al. [40], who demonstrated that acid-functionalized multiwalled carbon nanotubes significantly improved interfacial bonding with polyurethane matrices. However, high-loaded *f*/GNP-based composites show reduced elongation at break, suggesting that stronger interfacial adhesion and improved dispersion restrict polymer chain mobility and promote earlier failure [43]. Overall, the tensile results indicate that GNP functionalization enhances stiffness and early-stage load bearing at the expense of ductility, highlighting a trade-off between strength and deformability that is closely governed by interfacial adhesion and dispersion state.

4-5-2-3- Thermal Analysis

TPU-GNP and TPU-*f*/GNP nanocomposites were investigated thermally at low and high GNP loadings to assess the influence of filler content and surface functionalization on thermal stability. The corresponding TGA results are presented in Figure 4-7.

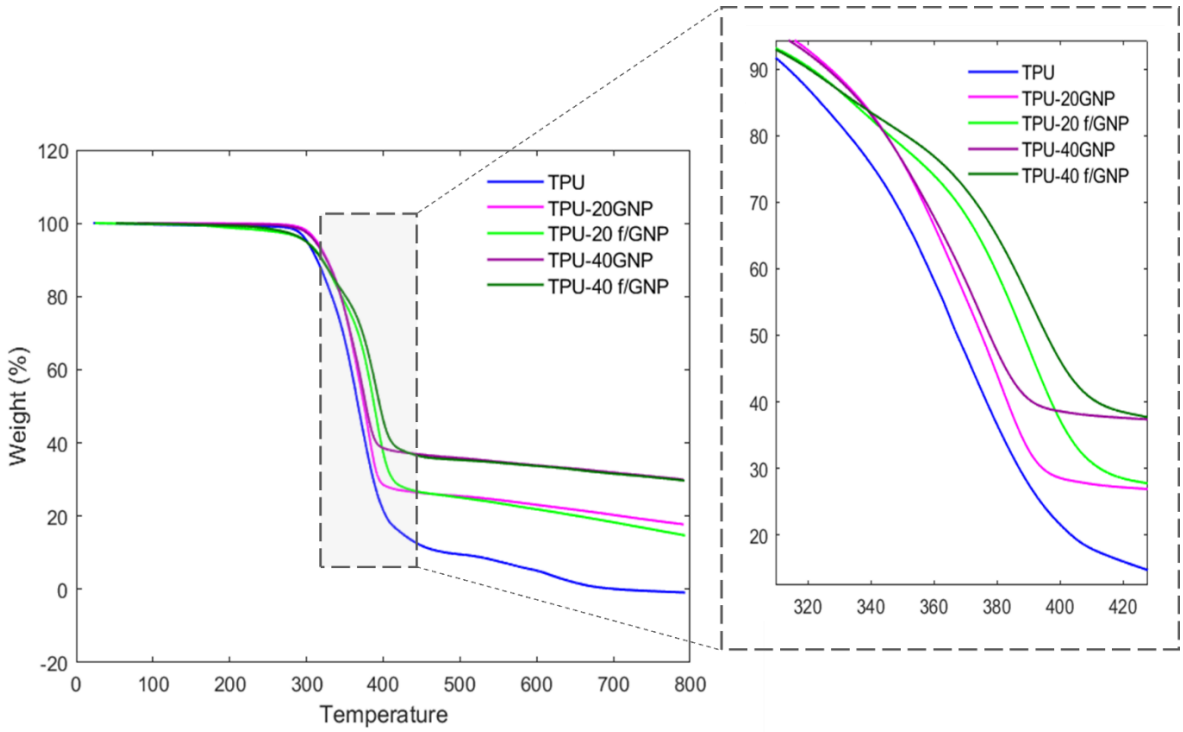


Fig. 4- 7- Thermogravimetric analysis (TGA) of fabricated nanocomposites compared with neat TPU.

Thermal degradation of polyurethane typically proceeds through two main stages: an initial degradation occurring in the range of approximately 280–400 °C, associated with decomposition of the polyol soft segments, followed by degradation of the hard isocyanate-based domains between ~400 and 600 °C [44]. This two-step degradation behavior is clearly observed in the TGA curve of neat TPU. The incorporation of GNPs enhances the thermal stability of the composites, as evidenced by a delayed onset of degradation and increased thermal resistance relative to neat TPU [45]. For composites containing 20phr GNPs, both non-functionalized and functionalized systems exhibit comparable residual weight percentages at temperatures above 450 °C. However, closer examination of the primary degradation region (350–450 °C), as highlighted in the magnified TGA plot, reveals improved thermal stability for TPU–*f*/GNP composites at both filler loadings. Within this temperature range, TPU–20GNP exhibits an approximate 33% improvement in thermal stability relative to neat TPU, while functionalization further enhances stability by an additional ~27% at the same graphene content. A similar trend is observed at higher filler loading, where the addition of 40phr GNPs results in an ~80% improvement in thermal stability, with functionalization contributing a further ~20% enhancement. The improved thermal performance of TPU–*f*/GNP composites is attributed to stronger dispersion and interfacial interactions between functionalized graphene and the TPU matrix [46]. Therefore, the TGA results demonstrate that

both graphene loading and surface functionalization significantly enhance the thermal stability of TPU nanocomposites, with functionalized GNPs providing the most effective reinforcement.

4-5-2-4- Analysis of obtained textured surface

In this study, composite design was pursued through a synergistic combination of compositional tailoring and surface engineering. Drawing inspiration from bioinspired traction mechanisms, the design strategy extended beyond establishing strong interfacial anchoring between graphene nanoplatelets (GNPs) and the TPU matrix to the intentional introduction of surface asperities and micro-channels that produce self-generating anti-slip performance (see Fig. 4-2). By reducing the persistence of a lubricating liquid layer, these micro-channels facilitate a less lubricated contact condition and consequently enhance the coefficient of friction. The presence of an interfacial liquid layer is known to act as a lubrication medium, analogous to the quasi-liquid layer (QLL) that forms on ice surfaces and contributes to reduced friction [47]. To counteract this effect, a hierarchical surface architecture was engineered such that progressive abrasion exposes subsurface micro-channels, enabling continuous renewal of the surface texture. When combined with optimized composite formulation, this wear-activated mechanism results in self-generating surface texturing, allowing the material to maintain effective liquid management throughout its service life.

As a result, the designed composites simultaneously achieve enhanced ice traction and improved abrasion durability, directly addressing a critical limitation of conventional anti-slip elastomeric materials. Figure 4-8 presents SEM micrographs of Wire Brushed (WB) surfaces of neat TPU and TPU–*f*/GNP nanocomposites at filler loadings of 20 and 40 phr.

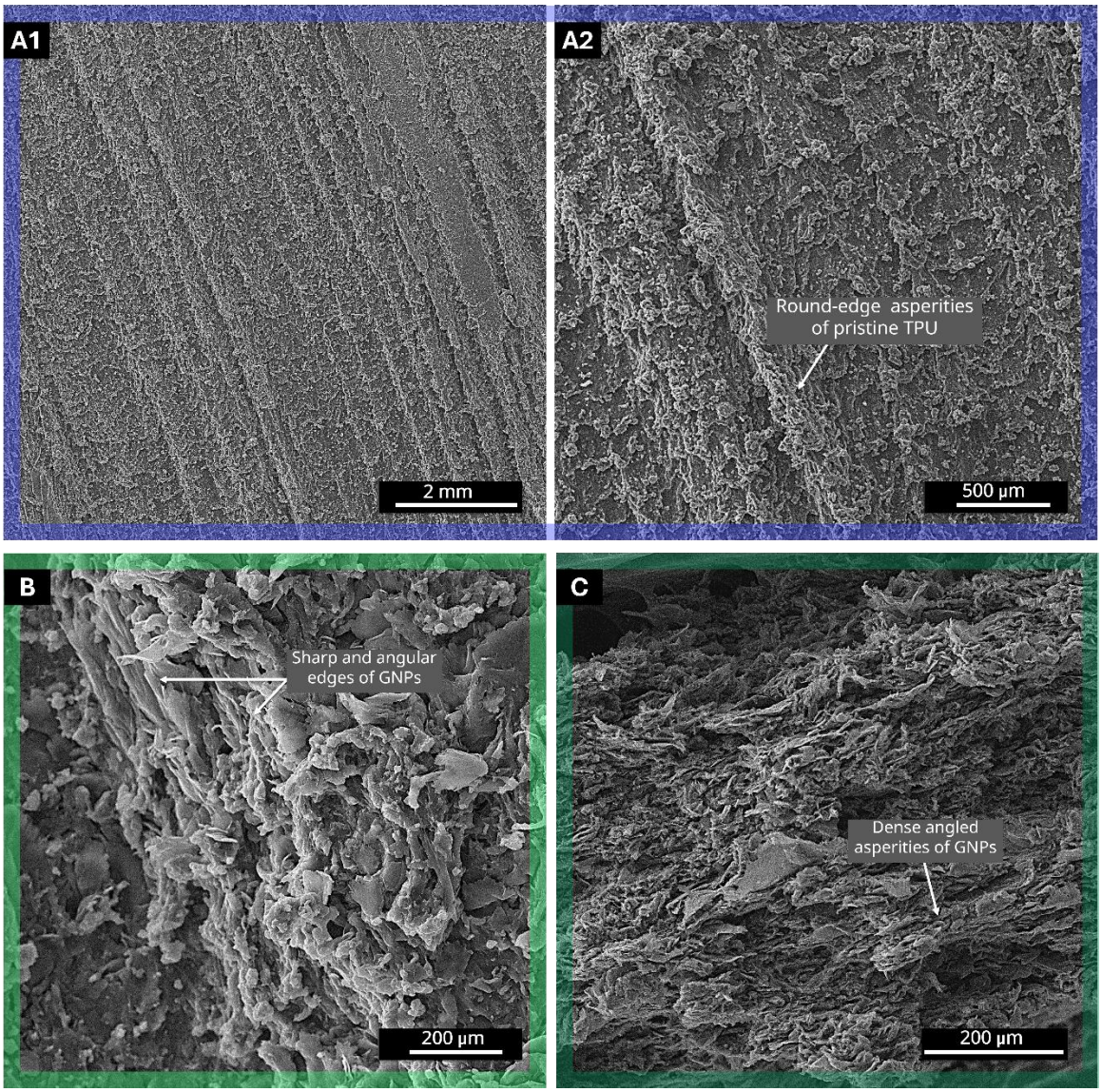


Fig. 4- 8- SEM micrographs of wire-brushed (WB) textured surfaces. (A1) Low-magnification image of wire-brushed pristine TPU, illustrating the formation of continuous, wavy surface features. (A2) Higher-magnification view of the same wire-brushed pristine TPU surface, revealing localized roughening and micro-scale asperities along the brushing direction. (B) Wire-brushed TPU–20 f/GNP nanocomposite, showing exposed 2D graphene nanoplatelets anchors within the textured surface. (C) Wire-brushed TPU–40 f/GNP nanocomposite, exhibiting a denser hierarchical texture with increased graphene-rich feature.

The frictional response of elastomeric anti-slip materials on ice is fundamentally governed by contact mechanics and interfacial stress distribution. According to Hertzian contact theory [48], the maximum contact pressure generated at the ice-rubber interface increases as the effective contact radius decreases, resulting in elevated localized stresses that promote shear resistance.

$$P_{max} = \frac{3}{2}\frac{F}{\pi a^2}$$ Equation (4-1)

where F is the applied normal load, P_{max} denotes the maximum contact pressure responsible for generating interfacial shear forces, and a is the effective contact radius. This relationship suggests that surface architectures and reinforcing phases that promote load localization over reduced contact areas can effectively increase interfacial shear stress, an effect targeted in this study through the incorporation of two-dimensional nanofillers and the controlled intercalation of their stacked structures within the elastomeric matrix. Accordingly, the frictional response of rubber composites (F_f) can be described as the combined contribution of viscoelastic energy dissipation within the bulk material and shear-dominated resistance at the true contact interface as expressed in Equation (4-2).

$$F_f = F_{visc} + \tau_f \text{ A} \qquad \text{Equation (4-2)}$$

where F_{visc} arises from viscoelastic deformation of the elastomer, and τ_f represents the shear stress acting over the true contact area (A) [49]. This shear stress increases with increasing P_{max} (as defined in Eq. 4-1), which is attributed to the formation of smaller contact areas (a). Although viscoelastic losses play a role in friction generation, traction on ice is predominantly governed by the shear-controlled component. Enhancing interfacial shear stress, most effectively achieved through an increased density of surface asperities, strengthens mechanical interlocking between the rubber surface and ice microstructures, resulting in higher static friction. This behavior is reflected in the SEM observations of the engineered wire-brushed (WB) surfaces shown in Fig. 4-8. As seen in Fig. 4-8(A), the textured surface of neat TPU lacks hard asperities capable of effective mechanical interlocking, despite the presence of compliant surface features generated by the applied texturing process. In contrast, the WB surface of TPU-20 *f*/GNP (Fig. 4-8(B)) exhibits sharp, rigid asperities that are well anchored within the viscoelastic matrix, enabling efficient load transfer and enhanced interfacial shear resistance, which directly contributes to improved traction performance. At higher filler loading, as shown for WB TPU-40 *f*/GNP in Fig. 4-8(C), the dense accumulation of two-dimensional fillers limits the effectiveness of this mechanism. Despite chemical functionalization, excessive filler content leads to closely packed rigid asperities that are insufficiently supported by the surrounding elastomer, diminishing their contribution to localized contact pressure enhancement predicted by Hertzian contact mechanics. These observations demonstrate that optimal ice traction requires a balanced integration of surface architecture and

composite formulation, where mechanically robust asperities are effectively anchored within a compliant matrix to sustain mechanical interlocking during sliding [47].

4-5-2-5- Ice Traction Investigation

The frictional behavior of rubber composites with varying compositions and engineered surface textures was evaluated on ice under high-speed sliding conditions, in accordance with a laboratory-scale protocol relevant to footwear slip-resistance assessment. Ice tribological testing was conducted using a high-kinetic testing methodology previously developed and reported by the authors [21]. During testing, the horizontal and vertical force channels of the Bruker UMT tribometer were carefully calibrated, and controlled high-velocity contact conditions were established. Upon initiation of motion, the specimen underwent a brief dwell period on the ice surface before sliding commenced. Force signals were recorded at high acquisition rates to capture the transient frictional response, as the static coefficient of friction (SCOF) is attained within the initial fraction of a second. This event is characterized by a distinct peak in both the friction force and the corresponding coefficient of friction (COF), calculated as the ratio of the measured friction force to the applied normal load of 5 N. The selected normal load was chosen to approximate the contact pressure conditions recommended in ASTM F2913 for evaluating the slip resistance of footwear on icy surfaces [22]. Figure 4-9 presents representative force and friction signal data obtained during SCOF determination for neat TPU.

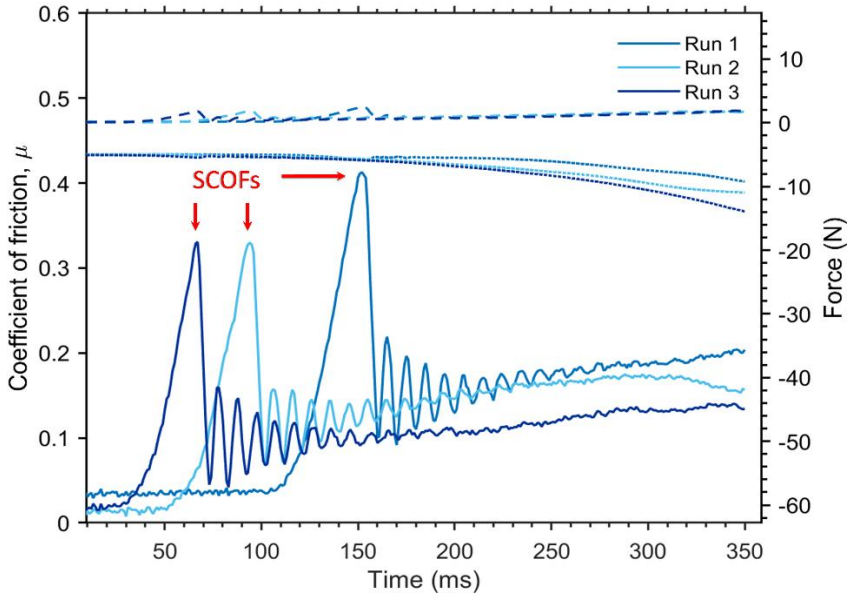


Fig. 4- 9- Static Coefficient of friction (SCOF) response of molded pure TPU, as a representative composition and surface texture, sliding on ice over repeated runs. Solid lines denote CoF, while dotted and dashed curves correspond to the normal force (Fz) and tangential friction force (Ff), respectively.

As illustrated in Fig. 4-9, the left y-axis corresponds to the coefficient of friction (COF), while the right y-axis represents the force channels, including the horizontal friction force (dashed line) and the applied normal force (dotted line). The normal load was maintained at a constant value of 5 N in accordance with standard testing recommendations at the initiation of the motion. The measured friction force reflects the resistance of the contacting surface during the onset of high-kinetic sliding on ice. Both the friction force and COF signals exhibit a distinct initial peak associated with the static friction regime, followed by multiple stick–slip events, and subsequently transition to a plateau-like response characteristic of steady-state kinetic sliding. This frictional behavior is consistent with previously reported ice–rubber interfacial responses [4]. All composite formulations and surface textures were tested in triplicate to verify the repeatability of the experiments and the reliability of the obtained measurements. The SCOFs extracted from these experiments were used for comparison of the ice-traction performance of the tailored composites. A summary of the ice-traction responses for all compositions and surface textures is presented in Fig. 4-10.

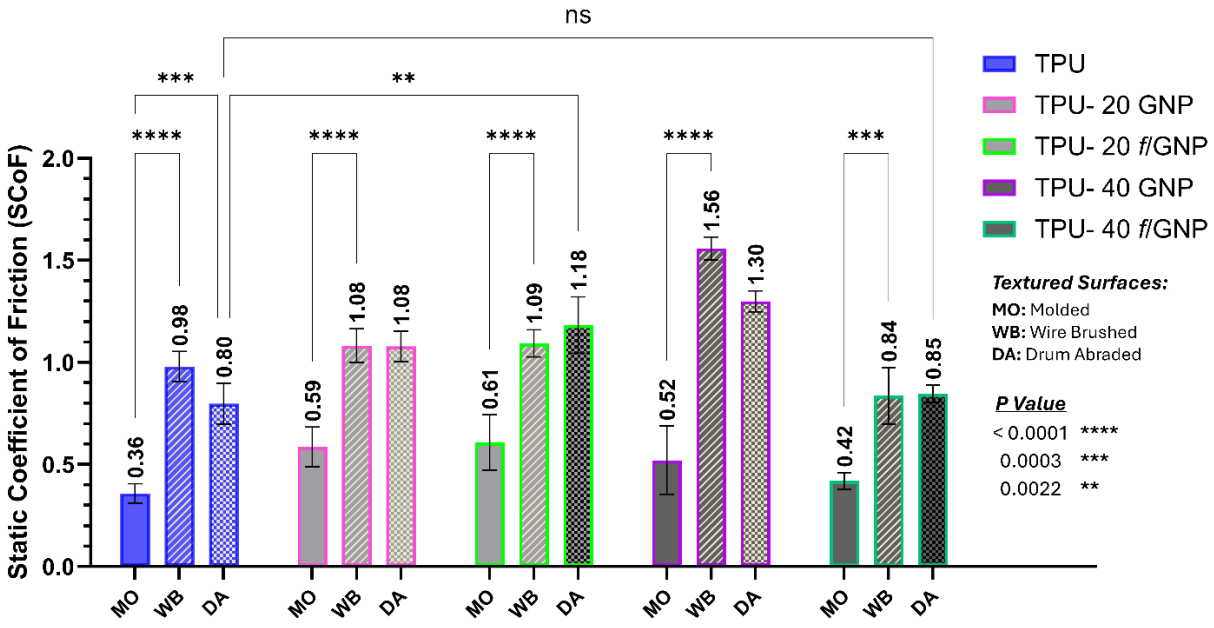


Fig. 4- 10- Static coefficient of friction of TPU–GNP composites with different surface conditions: as-molded (MO), wire-brushed (WB), and post-abrasion (DA)

The ice-traction performance of TPU–GNP and TPU–*f*/GNP composites at 20 and 40phr, processed with three different surface conditions, is summarized in Fig. 4-10. The hot-pressed

molded surface is denoted as MO, the micro-wire-brushed surface as WB, and the post-abrasion surface as DA. These results clearly demonstrate that surface texturing plays a critical role in governing the static coefficient of friction (SCOF) on ice, in addition to the effects of filler composition. For neat TPU, micro-wire brushing enhances ice traction by 172% relative to the molded surface, while a noticeable reduction in SCOF is observed after abrasion. A similar qualitative trend is maintained across all composite systems, where WB surfaces consistently outperform MO surfaces regardless of filler type or loading. This indicates that ice traction is predominantly governed by micro-scale surface topography rather than bulk composition, particularly at lower GNP contents. At higher GNP loadings, however, compositional effects become more pronounced. TPU-GNP composites at 40phr exhibit a further increase in traction for WB surfaces, which can be attributed to the higher density of hard asperities introduced by the rigid graphene platelets. These asperities enhance interfacial shear resistance and mechanical interlocking with the ice surface, thereby increasing SCOF under high-kinetic conditions. In contrast, this trend is not preserved in high-loading TPU–*f*/GNP composites. Despite similar surface texturing, the SCOF does not increase proportionally with filler content, which is attributed to the strong interfacial interactions between functionalized GNPs and the TPU matrix, which restrict polymer chain mobility and suppress the viscoelastic response of the composite. Since viscoelastic energy dissipation contributes significantly to ice traction, as described in Eq. (4-2), excessive stiffening of the elastomer compromises traction performance despite the presence of surface asperities. These results emphasize that improved ice traction cannot be achieved solely through mechanical interlocking; preservation of elastomeric viscoelasticity is equally critical. Optimal performance therefore requires a balanced design strategy that integrates surface texturing with controlled filler-matrix interactions to maintain sufficient chain mobility while enhancing interfacial shear strength. Notably, most composite systems retain relatively high traction levels after abrasion compared to neat TPU, highlighting the effectiveness of incorporating two-dimensional fillers. This observation supports previous reports suggesting that 2D nanomaterials are promising alternatives to conventional 1D fillers, such as glass fibers, which suffer from rapid wear and traction degradation in footwear applications. In the present study, functionalized GNPs enable strong interfacial bonding with the TPU matrix, facilitating a self-generating surface texturing mechanism in which abrasion exposes new micro-features without catastrophic loss of traction. Although TPU–40phr GNP with WB surface texture exhibits the highest SCOF among

the examined samples, traction performance alone is insufficient to identify the optimal material system for practical applications. Given the competing requirements of ice traction, abrasion resistance, and long-term durability, a combined tribological assessment is necessary. Accordingly, the following section evaluates the abrasion resistance of these composites to establish an integrated performance framework and identify the most durable ice-traction material system.

4-5-2-6- Abrasion Resistivity Studies

Abrasion resistivity was evaluated using the standard drum abrasion test in accordance with ISO 4649- Method A [24]. The density of all specimens was measured using the Archimedes method prior to abrasion testing [23]. Abrasion resistivity behavior was quantified in terms of abrasion volume loss (mm^3), calculated from the mass difference of samples measured before and after testing, combined with the measured density of each specimen. To enable a comparative assessment of durability, the Abrasion Resistivity Index (ARI) was determined relative to a reference material, selected here as neat TPU. The ARI provides a normalized measure of abrasion resistance, allowing direct comparison between different composite formulations. The calculation of the abrasion resistivity index is summarized in Equation (4-3):

Table 4- 1- Abrasion Resistance Index (ARI) of composites

Reference	Non-functionalized		*functionalized*	
	TPU- 20 GNP	**TPU- 40 GNP**	**TPU- 20 *f*/GNP**	**TPU- 40 *f*/GNP**
Neat TPU	168.38%	115.56%	260.25%	71.22%

$$I_{AR} = \frac{\Delta m_r \times \rho_t}{\Delta m_t \times \rho_r} \times 100 \qquad \text{Equation (4-3)}$$

where Δm_r is the mass loss (mg) of the reference compound; ρ_r is the density (mg mm^{-3}) of the reference compound; Δm_t is the mass loss (mg) of the test specimen; ρ_t is the density (mg mm^{-3}) of the test specimen.

Table 4-1 summarizes the ARI values obtained for all composite formulations. Figure 4-11(A) presents the corresponding abrasion volume loss for the investigated composites, while Figure 4-11(B) illustrates the post-abrasion ice traction performance as a function of GNP content for both non-functionalized and functionalized TPU/GNP composites.

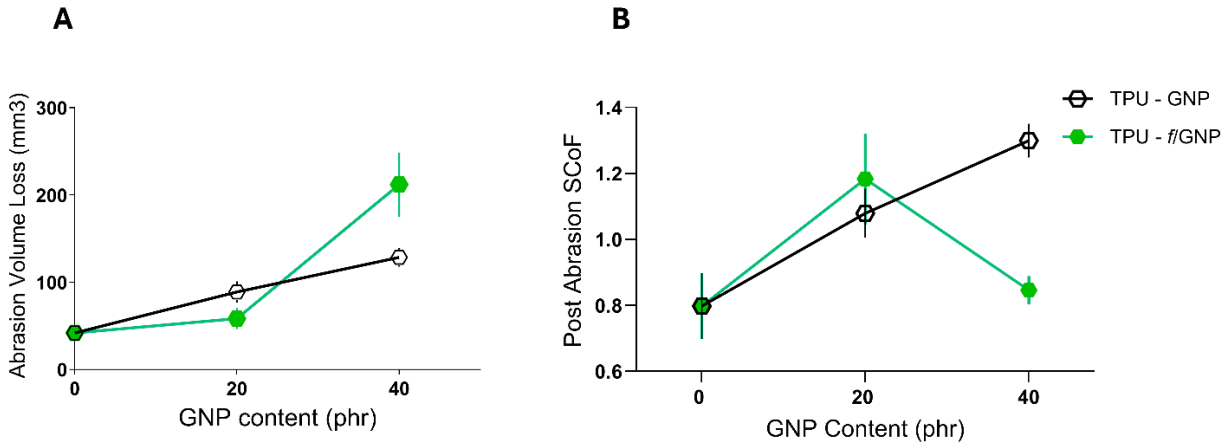


Fig. 4- 11- (A) Abrasion volume loss of TPU–GNP nanocomposites measured using the drum abrasion test in accordance with ISO 4649. (B) Ice-traction performance of the composites evaluated after abrasion, corresponding to the abraded surface state presented in Fig. 4-10.

Wear durability is evaluated using two metrics: abrasion volume loss and abrasion resistance index (ARI). While abrasion volume loss directly quantifies the extent of material removal, ARI provides a normalized measure of wear performance relative to the reference material. As reported in Table 4-1 and Fig. 4-11(A), the TPU-20 *f*/GNP composite exhibits the most favorable durability response based on both evaluation methods. At low loadings of functionalized GNPs, enhanced filler-matrix interactions improve stress transfer within the TPU, thereby limiting surface material removal under abrasive conditions [40]. In contrast, higher functionalized GNP contents introduce excessive interfacial constraints arising from strong interactions between oxygen-containing functional groups (–COOH and –OH) on the GNP surfaces and TPU chains. This over-constrained network restricts polymer chain mobility, reducing the ability of the matrix to accommodate abrasive stresses through plastic deformation. Additionally, suppressed segmental mobility of the TPU soft domains diminishes elastic recovery following deformation, which is critical for maintaining wear resistance in elastomeric materials [50][51].

Tribological analyses were performed alongside surface morphology characterization of the abraded specimens. Low-magnification SEM images of the worn surfaces for different compositions are presented in Fig. 4-12, providing an overview of abrasion-induced surface damage. Complementary high-magnification SEM micrographs shown in Fig. 4-13 reveal the underlying wear mechanisms, filler–matrix interfacial behavior, and the evolution of surface features resulting from abrasive loading.

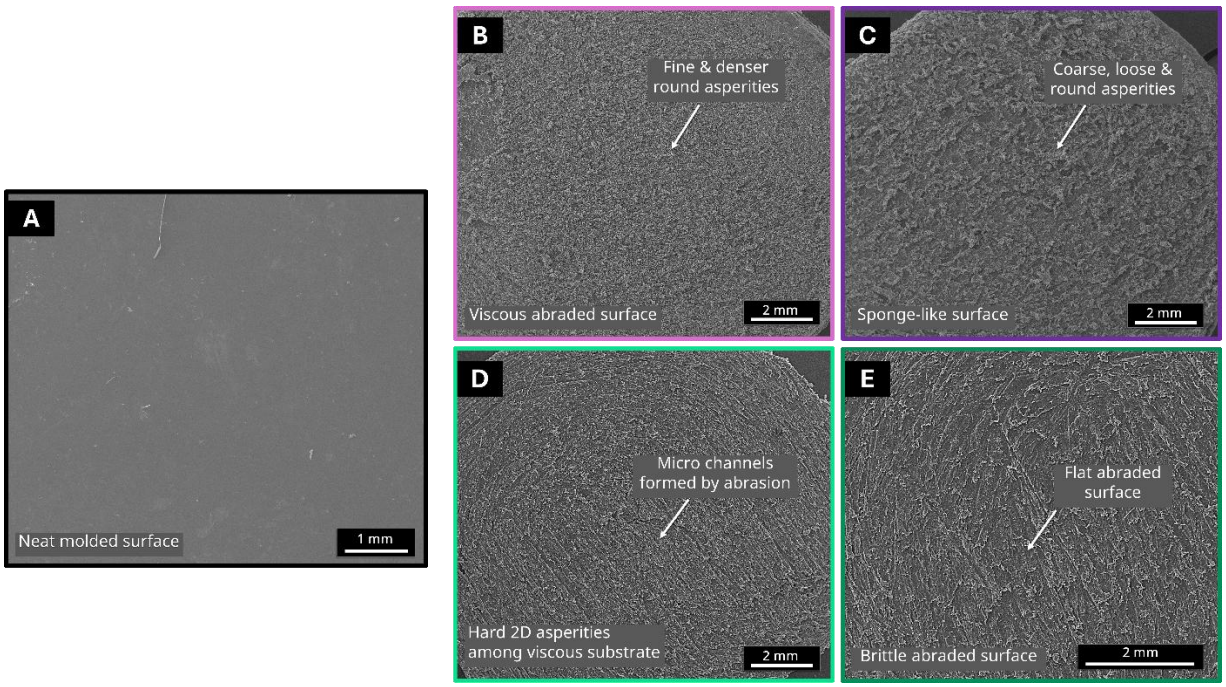


Fig. 4- 12- low magnification SEM images of TPU-GNP composites, (A) is the molded surface (MO) of the TPU-40 GNP as a representative; and post abrasion surfaces of (B) TPU- 20GNP, (C) TPU- 40GNP, (D) TPU- 20 f/GNP, and (E) TPU- 40 f/GNP

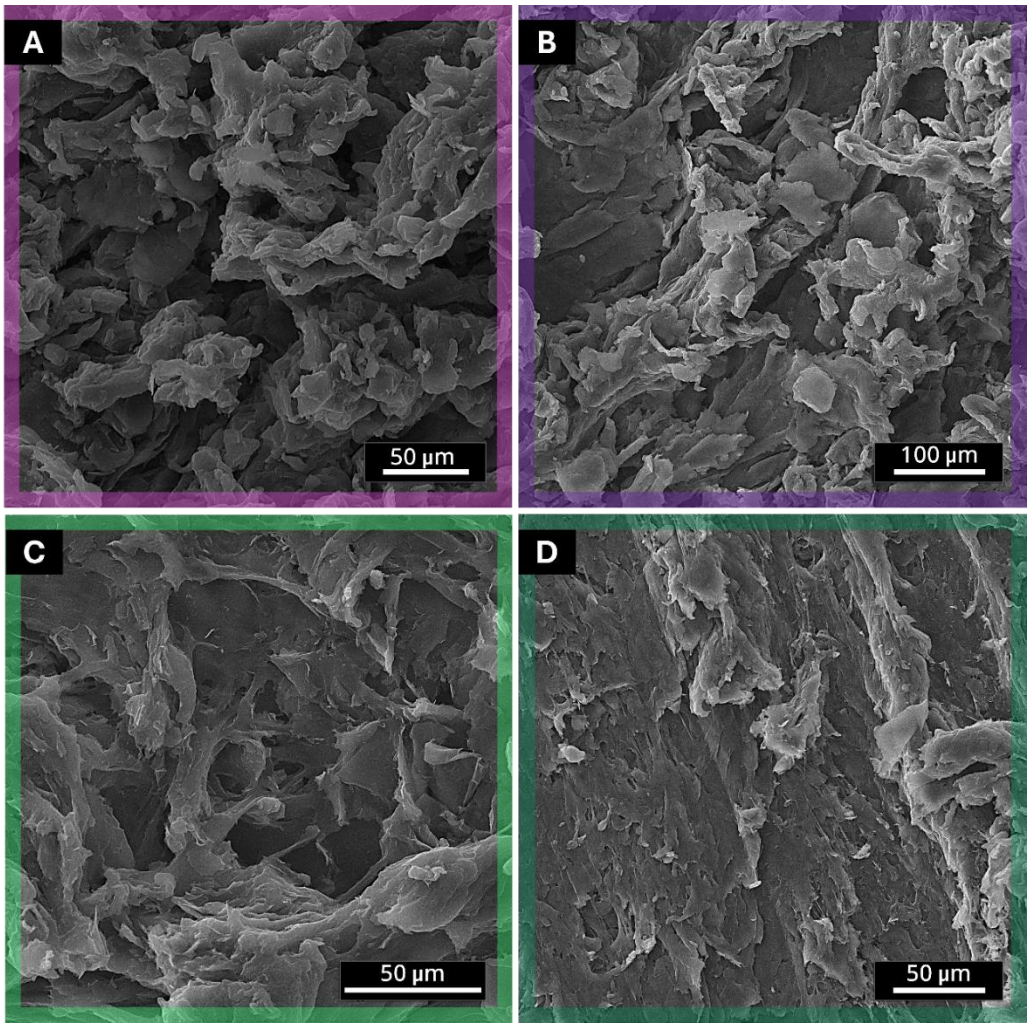


Fig. 4- 13- High magnification SEM images of post-abrasion surfaces of composites; (A) TPU- 20GNP, (B) TPU- 40GNP, (C) TPU- 20 f/GNP, (D) TPU- 40 f/GNP

The surface morphology of the abraded specimens highlights the potential of incorporating two-dimensional (2D) fillers to sustain ice traction performance after wear. Compared to the molded composite surfaces shown in Fig. 4-12(A), abrasion induces the formation of surface asperities that can contribute positively to post-abrasion ice traction. For non-functionalized TPU–GNP composites, the abraded surfaces exhibit a more ductile wear response relative to functionalized systems, particularly at higher GNP loadings. According to Fig. 4–12, TPU–GNP composites with low filler loadings exhibit fine, rounded asperities indicative of viscous-type wear. Increasing the GNP content results in the formation of coarser and more pronounced rounded abrasion features. This behavior is associated with GNP aggregation at high loading driven by π–π interactions, which promotes localized stress amplification during abrasion, leading to micro-crack formation, void generation, and the development of coarser, sponge-like surface asperities [25]. In contrast,

functionalization reduces the viscous nature of the abraded surface, resulting in a comparatively more brittle wear morphology. Among all formulations, composites with low levels of functionalized GNPs exhibit the most favorable surface characteristics, where a balance between ductile deformation and the generation of hard, finely distributed asperities is achieved following abrasion. At these filler levels, functionalization promotes strong anchoring of the 2D fillers within the TPU matrix. Given the high intrinsic hardness of GNPs, abrasion leads to the formation of micro-scale channels and asperities that enhance mechanical interlocking while facilitating fluid dissipation at the contact interface. Optimal ice-traction durability is therefore attained when abrasion-generated hard asperities are preserved without compromising the viscoelastic contribution described in Eq. (4-2). Based on a combined tribological analysis encompassing both abrasion resistance and friction behavior, TPU-20 *f*/GNP is identified as the most effective formulation. This conclusion is further supported by the post-abrasion ice-traction performance shown in Fig. 4-11(B).

4-6- Conclusions

This study addresses the persistent challenge of poor wear durability in elastomeric ice-traction composites by integrating compositional design with abrasion-activated surface evolution. TPU-based nanocomposites were fabricated via solution mixing followed by hot-press molding, incorporating controlled loadings of non-functionalized and acid-functionalized graphene nanoplatelets (GNPs). Molded, micro wire-brushed, and post-abrasion surfaces were systematically examined to capture surface states representative of real service conditions. The central hypothesis proposed that strengthening filler–matrix interfacial anchoring can suppress premature filler pull-out and interfacial damage, while enabling wear-activated surface texturing that sustains ice traction without compromising the viscoelastic response required for ice friction. To evaluate this hypothesis, comprehensive mechanical, thermal, abrasion, ice-tribology, and surface morphology analyses were conducted. Among all compositions, TPU-20 *f*/GNP demonstrated the lowest abrasion-induced material loss and the highest abrasion resistance index (ARI), underscoring the critical role of GNP functionalization in enhancing composite durability for outsole-relevant applications. At higher functionalized GNP contents, however, excessive interfacial constraints restricted polymer chain mobility, resulting in embrittled wear behavior and reduced elastic recovery. Surface morphology analysis revealed that abrasion promoted the

formation of functional asperities capable of sustaining ice traction after wear. While non-functionalized systems exhibited a more ductile abrasion response, excessive filler loading led to GNP agglomeration, stress concentration, micro-cracking, and void formation. In contrast, over-functionalized systems suffered from polymer chain locking due to dense hydrogen-bonding networks, sacrificing the viscous dissipation essential for effective ice friction. Notably, TPU-20 *f*/GNP achieved a balanced abrasion-driven surface evolution, combining mechanically robust asperities and micro-channels with sufficient matrix compliance to preserve viscoelastic energy dissipation. Post-abrasion ice-traction measurements confirmed that this formulation retained superior traction performance after wear, validating the proposed design strategy.

Overall, this work demonstrates that abrasion durability and ice traction are not inherently conflicting properties. Instead, their coexistence can be achieved through deliberate interfacial engineering and wear-activated surface design. The findings establish a materials design framework for durable, self-texturing, ice-traction-enhanced elastomeric composites suitable for footwear and related anti-slip applications. Future studies will focus on fine-tuning filler chemistry and loading to further optimize the balance between abrasion resistance and ice-tribological performance in functionalized TPU-GNP systems.

4-7- References

[1] WHO, "World Health Organization, Falls – Fact Sheet.," 2021. https://www.who.int/news-room/fact-sheets/detail/falls%0A

[2] A. Tarcea, M. Vergouwen, E. C. Sayre, and N. J. White, "The Slip and Fall Index: Assessing the risk of slipping and falling on ice.," *Can. J. Public Health*, vol. 115, no. 2, pp. 296–304, Apr. 2024, doi: 10.17269/s41997-024-00855-z.

[3] CIHI, "Canadian Institute for Health Information / economic burden of falls in Canada." [Online]. Available: https://www.cihi.ca/en/quick-stats

[4] S. Babaee, S. Pajovic, A. Rafsanjani, Y. Shi, K. Bertoldi, and G. Traverso, "Bioinspired kirigami metasurfaces as assistive shoe grips," *Nat. Biomed. Eng.*, vol. 4, no. 8, pp. 778–786, 2020, doi: 10.1038/s41551-020-0564-3.

[5] R. Rizvi, H. Naguib, G. Fernie, and T. Dutta, "High friction on ice provided by elastomeric fiber composites with textured surfaces," *Appl. Phys. Lett.*, vol. 106, no. 11, 2015, doi: 10.1063/1.4913676.

[6] N. Namdari *et al.*, "Advanced functional surfaces through controlled damage and instabilities," *Mater. Horizons*, vol. 7, no. 2, pp. 366–396, 2020, doi: 10.1039/c9mh01516g.

[7] Z. S. Bagheri, Y. Li, A. R. Fekr, and T. Dutta, "The effect of wear on slip-resistance of winter footwear with composite outsoles: A pilot study," *Appl. Ergon.*, vol. 99, p. 103611, 2022, doi: 10.1016/j.apergo.2021.103611.

[8] Z. Shaghayegh Bagheri, A. Anwer, G. Fernie, H. E. Naguib, and T. Dutta, "Effects of multi-functional surface-

texturing on the ice friction and abrasion characteristics of hybrid composite materials for footwear," *Wear*, vol. 418–419, no. May 2018, pp. 253–264, 2019, doi: 10.1016/j.wear.2018.11.030.

[9] N. Namdari, G. J. Otto, G. Guo, H. Sojoudi, and R. Rizvi, "Nanotextured surfaces with enhanced ice-traction and wear-resistance," *Compos. Part B Eng.*, vol. 238, p. 109916, 2022, doi: 10.1016/j.compositesb.2022.109916.

[10] A. Anwer, Z. S. Bagheri, G. Fernie, T. Dutta, and H. E. Naguib, "Evolution of the Coefficient of Friction with Surface Wear for Advanced Surface Textured Composites," *Adv. Mater. Interfaces*, vol. 4, no. 6, pp. 1–11, 2017, doi: 10.1002/admi.201600983.

[11] W. Wang, Y. Liu, and Z. Xie, *Gecko-Like Dry Adhesive Surfaces and Their Applications: A Review*, vol. 18, no. 5. Springer Singapore, 2021. doi: 10.1007/s42235-021-00088-7.

[12] V. Richhariya, A. Tripathy, O. Carvalho, J. Gomes, M. J. Nine, and F. S. Silva, "Capillary-Enhanced Biomimetic Adhesion on Icy Surfaces for High-Performance Antislip Shoe-Soles," *ACS Appl. Mater. Interfaces*, 2024, doi: 10.1021/acsami.4c14496.

[13] N. Thirunavukkarasu, S. Peng, H. B. Gunasekaran, Z. Yang, L. Wu, and Z. Weng, "Responsive friction modulation of 3D printed elastomeric bioinspired structures," *Tribol. Int.*, vol. 175, no. January, p. 107823, 2022, doi: 10.1016/j.triboint.2022.107823.

[14] M. N. Shenvi, A. Verulkar, C. Sandu, and H. Mousavi, "Tread rubber compound effect in winter tires : An experimental study," *J. Terramechanics*, vol. 99, pp. 57–73, 2022, doi: 10.1016/j.jterra.2021.11.004.

[15] A. Soica and C. Gheorghe, "Tire – Road Interaction : A Comprehensive Review of Friction Mechanisms , Influencing Factors , and Future Challenges," 2025.

[16] ACS Materials, "Graphene Nanoplatelets (2-10nm)," 2026. https://www.acsmaterial.com/graphene-nanoplatelets-2-10nm.html

[17] A. Rostami, H. Nazockdast, and M. Karimi, "Graphene induced microstructural changes of PLA/MWCNT biodegradable nanocomposites: Rheological, morphological, thermal and electrical properties," *RSC Adv.*, vol. 6, no. 55, pp. 49747–49759, 2016, doi: 10.1039/c6ra08345e.

[18] H. Kim, Y. Miura, and C. W. MacOsko, "Graphene/polyurethane nanocomposites for improved gas barrier and electrical conductivity," *Chem. Mater.*, vol. 22, no. 11, pp. 3441–3450, 2010, doi: 10.1021/cm100477v.

[19] P. Materials and E. I. Materials, "Standard Test Method for Tensile Properties of Plastics 1," 2017, doi: 10.1520/D0638-14.1.

[20] ISO-527-1, "527-1: Plastics—Determination of tensile properties—Part 1: General principles," *ISO Stand.*, vol. 2012, 1997, [Online]. Available: http://scholar.google.com/scholar?hl=en&btnG=Search&q=intitle:Plastics+-+Determination+of+tensile+properties+-+Part1:+General+principles#1

[21] S. Zahmatkesh and R. Rizvi, "Evaluating surface texturing technologies of rubber composites on ice using a novel high-velocity tribotest method," *Tribol. Int.*, vol. 206, no. October 2024, 2025, doi: 10.1016/j.triboint.2025.110538.

[22] "ASTM F2913: Standard Test Method for Measuring the Coefficient of Friction for Evaluation of Slip Performance of Footwear and Test Surfaces/Flooring Using a Whole Shoe Tester, 2019, American Society of Testing Materials."

[23] ISO International Standard, "Rubber, vulcanized or thermoplastic - Determination of density," 2008.

[24] I. O. for Standardization, "INTERNATIONAL STANDARD ISO 4649 Rubbers, vulcanized or thermoplastic -Determination of abrasion resistance using a rotating cylindrical drum device," *ISO*, vol. 2017, 2017.

[25] S. Liu and A. Dahi Taleghani, "Engineering of polymer nanocomposites using acid-functionalized graphite nanoplatelets for high-temperature sealing purposes," *Compos. Part B Eng.*, vol. 306, no. July, p. 112772,

2025, doi: 10.1016/j.compositesb.2025.112772.

[26] P. Govindaraj, B. Fox, P. Aitchison, and N. Hameed, “A Review on Graphene Polymer Nanocomposites in Harsh Operating Conditions,” *Ind. Eng. Chem. Res.*, vol. 58, no. 37, pp. 17106–17129, 2019, doi: 10.1021/acs.iecr.9b01183.

[27] D. Verma, P. C. Gope, A. Shandilya, and A. Gupta, “Mechanical-Thermal-Electrical and Morphological Properties of Graphene Reinforced Polymer Composites: A Review,” *Trans. Indian Inst. Met.*, vol. 67, pp. 803–816, 2014, doi: 10.1007/s12666-014-0408-5.

[28] T. K. Gupta *et al.*, “Superior nano-mechanical properties of reduced graphene oxide reinforced polyurethane composites,” *RSC Adv.*, vol. 5, no. 22, pp. 16921–16930, 2015, doi: 10.1039/c4ra14223c.

[29] Z. M. Marković *et al.*, “Antibacterial potential of electrochemically exfoliated graphene sheets,” *J. Colloid Interface Sci.*, vol. 500, pp. 30–43, 2017, doi: 10.1016/j.jcis.2017.03.110.

[30] D. Cai, K. Yusoh, and M. Song, “The mechanical properties and morphology of a graphite oxide nanoplatelet/polyurethane composite,” *Nanotechnology*, vol. 20, no. 8, 2009, doi: 10.1088/0957-4484/20/8/085712.

[31] K. Bilisik and M. Akter, “Graphene nanoplatelets/epoxy nanocomposites: A review on functionalization, characterization techniques, properties, and applications,” *J. Reinf. Plast. Compos.*, vol. 41, no. 3–4, pp. 99–129, 2022, doi: 10.1177/07316844211049277.

[32] T. Zhang and D. Zhang, “Aqueous colloids of graphene oxide nanosheets by exfoliation of graphite oxide without ultrasonication,” *Bull. Mater. Sci*, vol. 34, no. February 2011, pp. 25–28, 2018.

[33] Q. Jing, W. Liu, Y. Pan, V. V. Silberschmidt, L. Li, and Z. L. Dong, “Chemical functionalization of graphene oxide for improving mechanical and thermal properties of polyurethane composites,” *Mater. Des.*, vol. 85, pp. 808–814, 2015, doi: 10.1016/j.matdes.2015.07.101.

[34] M. Veerapandian, M. H. Lee, K. Krishnamoorthy, and K. Yun, “Synthesis, characterization and electrochemical properties of functionalized graphene oxide,” *Carbon N. Y.*, vol. 50, no. 11, pp. 4228–4238, 2012, doi: 10.1016/j.carbon.2012.05.004.

[35] M. T. Kartel *et al.*, “Changes in the Structure and Properties of Graphene Oxide Surfaces During Reduction and Modification,” *Him. Fiz. ta Tehnol. Poverhni*, vol. 13, no. 2, pp. 179–189, 2022, doi: 10.15407/hftp13.02.179.

[36] M. Charoenchai, S. Tangbunsuk, and W. Keawwattana, “Silica-graphene oxide nanohybrids as reinforcing filler for natural rubber,” *J. Polym. Res.*, vol. 27, no. 8, 2020, doi: 10.1007/s10965-020-02209-y.

[37] F. Farivar, P. L. Yap, R. U. Karunagaran, and D. Losic, “Thermogravimetric Analysis (TGA) of Graphene Materials: Effect of Particle Size of Graphene, Graphene Oxide and Graphite on Thermal Parameters,” *J. Carbon Res.*, vol. 7, no. 2, p. 41, 2021.

[38] M. Mo *et al.*, “Excellent tribological and anti-corrosion performance of polyurethane composite coatings reinforced with functionalized graphene and graphene oxide nanosheets,” *RSC Adv.*, vol. 5, no. 70, pp. 56486–56497, 2015, doi: 10.1039/c5ra10494g.

[39] D. Cai, J. Jin, K. Yusoh, R. Rafiq, and M. Song, “High performance polyurethane/functionalized graphene nanocomposites with improved mechanical and thermal properties,” *Compos. Sci. Technol.*, vol. 72, no. 6, pp. 702–707, 2012, doi: 10.1016/j.compscitech.2012.01.020.

[40] A. K. Barick and D. K. Tripathy, “Preparation, characterization and properties of acid functionalized multi-walled carbon nanotube reinforced thermoplastic polyurethane nanocomposites,” *Mater. Sci. Eng. B Solid-State Mater. Adv. Technol.*, vol. 176, no. 18, pp. 1435–1447, 2011, doi: 10.1016/j.mseb.2011.08.001.

[41] G. Shi, S. Araby, C. T. Gibson, Q. Meng, S. Zhu, and J. Ma, “Graphene Platelets and Their Polymer Composites: Fabrication, Structure, Properties, and Applications,” *Adv. Funct. Mater.*, vol. 28, no. 19, pp. 1–44, 2018, doi: 10.1002/adfm.201706705.

[42] W. K. Chee, H. N. Lim, N. M. Huang, and I. Harrison, “Nanocomposites of graphene/polymers: a review,” *RSC Adv.*, vol. 5, no. 83, pp. 68014–68051, 2015, doi: 10.1039/c5ra07989f.

[43] X. Li *et al.*, “Graphene/thermoplastic polyurethane nanocomposites: Surface modification of graphene through oxidation, polyvinyl pyrrolidone coating and reduction,” *Compos. Part A Appl. Sci. Manuf.*, vol. 68, pp. 264–275, 2015, doi: 10.1016/j.compositesa.2014.10.016.

[44] P. Askari, Fahimeh; Barikani, Mehdi ;Barmar, Mohammad ;Shokrollahi, “Polyurethane/amino-grafted multiwalled carbon nanotube nanocomposites: Microstructure, thermal, mechanical, and rheological properties,” *J. Appl. Polym. Sci.*, vol. 134, no. 4, p. 4411, 2017.

[45] A. Navidfar and L. Trabzon, “Graphene type dependence of carbon nanotubes/graphene nanoplatelets polyurethane hybrid nanocomposites: Micromechanical modeling and mechanical properties,” *Compos. Part B Eng.*, vol. 176, 2019, doi: 10.1016/j.compositesb.2019.107337.

[46] M. Bera and P. K. Maji, “Effect of structural disparity of graphene-based materials on thermo-mechanical and surface properties of thermoplastic polyurethane nanocomposites,” *Polymer (Guildf).*, vol. 119, pp. 118–133, 2017, doi: 10.1016/j.polymer.2017.05.019.

[47] V. Richhariya, A. Tripathy, O. Carvalho, M. Julker Nine, D. Losic, and F. S. Silva, “Unravelling the physics and mechanisms behind slips and falls on icy surfaces: A comprehensive review and nature-inspired solutions,” *Mater. Des.*, vol. 234, p. 112335, 2023, doi: 10.1016/j.matdes.2023.112335.

[48] E. Ciulli, A. Betti, and P. Forte, “The Applicability of the Hertzian Formulas to Point Contacts of Spheres and Spherical Caps,” *Lubricants*, vol. 10, no. 10, 2022, doi: 10.3390/lubricants10100233.

[49] A. Tiwari, N. Miyashita, N. Espallargas, and B. N. J. Persson, “Rubber friction: The contribution from the area of real contact,” *J. Chem. Phys.*, vol. 148, no. 22, 2018, doi: 10.1063/1.5037136.

[50] S. Nitodas, R. Shah, and M. Das, “Research Advancements in the Mechanical Performance and Functional Properties of Nanocomposites Reinforced with Surface-Modified Carbon Nanotubes: A Review,” *Appl. Sci.*, vol. 15, no. 1, 2025, doi: 10.3390/app15010374.

[51] B. Ahmadi-Moghadam, M. Sharafimasooleh, S. Shadlou, and F. Taheri, “Effect of functionalization of graphene nanoplatelets on the mechanical response of graphene/epoxy composites,” *Mater. Des.*, vol. 66, no. PA, pp. 142–149, 2015, doi: 10.1016/j.matdes.2014.10.047.

Chapter 5:
Predicting Abrasion Resistance in Thermoplastic Polyurethanes Using Machine Learning

5-1- Chapter Preface

The findings presented here are partly based on the following peer-reviewed publication:

- *S. Zahmatkesh, H. Esmaeili, A.T. Valerio, R. Rizvi," Predicting Abrasion Resistance in Thermoplastic Polyurethanes Using Machine Learning" Journal of Applied Polymer Science, Volume 142, Issue 42, e57619, July 2025.* Available online.

Author Contribution Statement:

This chapter is based on a collaborative peer-reviewed publication. Sara Zahmatkesh contributed to the conceptualization of the study, development of the methodology, programming and implementation of the machine-learning models, data visualization, analysis and interpretation of the results, and preparation of the original manuscript draft. Hamed Esmaeili contributed to the methodology, data processing, and manuscript review and editing. Alfonso Tavares Valerio contributed to data collection and writing support.

Portions of this study have been presented as a poster at the following conference:

- *S. Zahmatkesh and R. Rizvi," Data-Driven Prediction of Abrasion Resistance in Thermoplastic Polyurethane Elastomers Using Machine Learning Approach", 25th International Conference on Wear of Materials (WOM), Sitges, Spain, April 2025.*

5-2- Abstract

Abrasion resistance is a critical property of thermoplastic polyurethane (TPU), especially for applications in automotive, footwear, and medical devices where durability under mechanical stress is essential. Conventional testing methods for abrasion, such as ISO 4649, are time-consuming and require specialized equipment. This study introduces a machine learning (ML)-based predictive framework to estimate TPU abrasion volume loss using mechanical and structural property data extracted from the CAMPUS database. Key features including viscoelastic moduli, tensile and tear strength, Shore hardness, and density were selected through Pearson correlation analysis. Six supervised regression models were developed and evaluated: Linear, Polynomial,

Decision Tree, Random Forest, Gradient Boosting Regressor (GBR), and Support Vector Regressor (SVR). SVR achieved the highest R^2 (0.79) on testing data, but its poor training performance indicated underfitting and sensitivity to data sparsity. In contrast, GBR demonstrated more consistent and generalizable predictions, achieving an R^2 of 0.72 and RMSE of 5.2 mm^3. The results underscore the potential of ML algorithms to model structure-property relationships in elastomers. This approach offers a cost- and time-efficient alternative for early-stage screening of TPU grades and accelerates the design of abrasion-resistant polymer formulations.

Keywords: *Machine Learning; Thermoplastic Polyurethane; Abrasion Resistance; Gradient Boosting; Polymer Tribology; Data-Driven Design; Structure–Property Prediction*

5-3- Introduction and Literature Review

Tribology, the study of interfaces, investigates the friction and wear behavior of contacting surfaces. These phenomena are strongly influenced by material properties and testing conditions, and the field remains highly empirical despite extensive efforts to establish universal rules or laws of friction and wear [1][2]. With advancements in Artificial Intelligence (AI) and Machine Learning (ML), these techniques have emerged as powerful and predictive tools for evaluating tribological performance [3]. The integration of ML into material and tribological property prediction has recently achieved significant success, unlocking new possibilities in material science and tribology [4].

Thermoplastic polyurethane (TPU) is a highly versatile elastomer that combines the elasticity of rubber with the toughness of plastic. Its unique molecular structure, composed of alternating hard and soft segments, imparts flexibility, durability, and resistance to environmental stresses [5]. The soft segment is made of long chains of polyether or polyester polymers responsible for the flexibility of TPU, while the hard segment is highly polar and act as the crosslinker in the polymer. Hard segments are obtained by reaction between isocyanates and chain extenders like hydroxyl group or 1,4-butanediol. It is an environmental-friendly polymer which has a distinguished abrasion resistivity [6][7]. By varying the chemistry and relative composition of the soft and hard segments, thermoplastic polyurethane (TPU) can achieve a broad spectrum of physical properties, ranging from soft elastomers to hard plastics. This versatility is attributed to TPU's high degree of chemical tunability, which enables precise adjustments to its properties, such as abrasion

resistance, toughness, and flexibility. As a result, TPU serves as a unique material that effectively bridges the gap between conventional rubber and plastic materials [8].

TPU has become indispensable across industries such as automotive, healthcare, electronics, and footwears [9]. Its exceptional resilience under extreme mechanical stress makes it a key material in many automotive applications, including suspension components, air bumps, and where wear resistance and mechanical stability are essential [10][11]. Additionally, TPU's lightweight and robust characteristics have driven innovation in athletic footwear and protective equipment [12]. In healthcare, TPU's biocompatibility makes it a preferred material for medical tubing, catheters, and stents, which are widely used to maintain urine drainage following kidney stone surgeries [13][14].

The application scope of thermoplastic polyurethane (TPU) frequently involves exposure to abrasive environments, necessitating detailed tribological analysis. Assessing the wear resistance of TPU is crucial in determining the operational lifespan of components such as automotive suspension units, the performance and durability of medical catheters within the human body, and the longevity of footwear. As such, tribological evaluations, particularly focused on abrasion resistance, are essential for predicting the service life of TPU-based parts under specific operating conditions [15].

The abrasion resistance of rubbers and elastomers is commonly evaluated based on their volume loss using standardized wear protocols, such as those defined in ISO 4649/DIN 53516. These protocols require the preparation of specific samples that are subjected to abrasion on an abrasion drum machine [16]. The abrasion resistance is quantified as volume loss, which necessitates accurate density measurements of the TPU part post-production. This is conducted according to ISO 2781, using an Archimedes setup [17]. However, these procedures demand significant resources, including time, specialized equipment, and human labor. Consequently, the ability to predict the properties of composite materials prior to experimental validation is of critical importance, as it helps determine whether the material can meet specific performance requirements, such as its operational lifespan.

The integration of artificial intelligence (AI) into materials characterization holds the potential to revolutionize materials development by reducing the reliance on extensive physical testing. This approach accelerates innovation, optimizes resource utilization, and enables the efficient discovery

and design of advanced materials. The application of machine learning (ML) in predicting material properties has gained significant traction among researchers in recent years. In 2023, Esmaeili et al. introduced an accelerated strategy for characterizing the mechanical properties of polymer composites using an ensemble learning approach [18]. Hasan et al. applied the Triboinformatics framework to predict the tribological properties of Al-graphite composites [19]. Likewise, Gyurova et al. employed artificial neural networks to predict the sliding friction and wear behavior of polyphenylene sulfide composites [4]. Most recently, in 2024, Deshpande and colleagues used ML techniques to forecast the wear rate of glass-filled PTFE composites [20].

ML algorithms are particularly effective at identifying nonlinear relationships between material properties and tribological behavior, offering predictive accuracy that surpasses traditional methods such as empirical and analytical models. One area where AI and machine learning (ML) tools show significant potential is tribology, particularly in the prediction of friction, wear, and component failure. By leveraging ML algorithms, the field aims to enhance the accuracy of forecasting tribological performance and service life [21]. The accelerated, data-driven approach to predicting tribological properties has been termed "Triboinformatics" [22]. Hasan et al. utilized machine learning (ML) models to predict the tribological properties of metal alloys and metal-matrix composites. Their findings highlighted that mechanical properties such as hardness, yield strength, and tensile strength significantly influence the prediction of friction and wear characteristics [19][23][24]. In the context of polymer composites, Velten et al. [25] trained an Artificial Neural Network to predict the wear properties of Nylon reinforced with glass and carbon fibers. For model training, mechanical properties including tensile and compression strengths, strain at failure, and impact properties were identified as critical input variables. Specifically for thermoplastic polyurethanes (TPUs), Kopal et al. [26] developed an artificial neural network (ANN) model to capture the relationship between the dynamic mechanical properties, including storage and loss moduli measured using Dynamic Mechanical Analysis (DMA), at different temperatures. Their model successfully predicted the viscoelastic behavior of TPUs under various thermal conditions, effectively reducing the need for time consuming and costly experimental testing.

In this study, the relationship between structural variations, such as the mechanical properties of different TPU grades, and their abrasion resistance is explored. We aimed to develop an AI-based

predictive model trained on the mechanical and physical properties of polyurethanes to estimate the lifespan of abrasion life of specific TPU grades. This novel approach offers valuable insights into durability prediction, eliminating the need for time-intensive material testing and analysis.

5-4- Mechanical and Structural Properties Influencing TPU Abrasion Resistance

5-4-1- Effect of the viscoelasticity properties

Elastomeric materials, such as thermoplastic polyurethane (TPU), exhibit viscoelastic behavior, demonstrating both viscous and elastic properties. This behavior arises from their distinct microstructure, comprising alternating soft and hard segments [5]. Experimental research has established correlations between the abrasion resistance of polyurethanes and their viscoelastic properties, typically characterized by the storage modulus (elastic component) and the loss modulus (viscous component). Sigamani [27] reported that softer TPUs, characterized by a higher loss modulus, demonstrate enhanced abrasion resistance due to their capacity to resist crack propagation. Building on this, Arena et al. [28] investigated the relationship between the viscoelastic properties of several commercial TPUs and their abrasion resistance. Figure 5-1 presents representative TEM images of select TPU samples, stained with lead citrate and uranyl acetate, which enhance the contrast of the soft segments, highlighting the distribution of their soft and hard segments.

(a)

Chemical basis	Density [g/cm^3]	Hardness [Shore A]	Elastic modulus [MPa]	Tensile stress [MPa]	Deformation at break [%]	Glass transition temperature (T_g) [°C]
ether-based TPU	1.12	86	27.8±1	47.9±3	773.3±17	-50
ester-based TPU	1.21	84	25.4±0.2	43.3±8	691.6±61	-42
carbonate-based TPU	1.15	86	28.8±3	35.6±1	647.5±10	-36

(b) (c) (d)

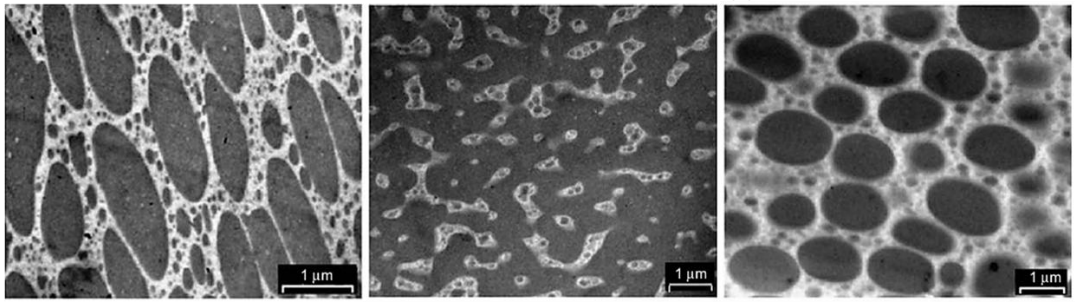


Fig. 5- 1- a) Materials properties, and TEM images of b) ether-based TPU, c) ester-based TPU, and d) carbonate-based TPU (reprinted with permission from eXPRESS Polymer Letters [28])

In the above images, soft segments are depicted in darker tones, while hard segments appear brighter. As illustrated, the distribution of soft segments within TPU matrices can vary between localized and dispersed arrangements. Additionally, the chemical nature of the soft segments can differ, being either ether- or ester-based, which influences the material's overall viscoelastic and abrasion-resistant properties. Figure 5-2 illustrates the viscoelasticity and corresponded abrasion resistivity of TPU samples reported by Arena et.al. [28].

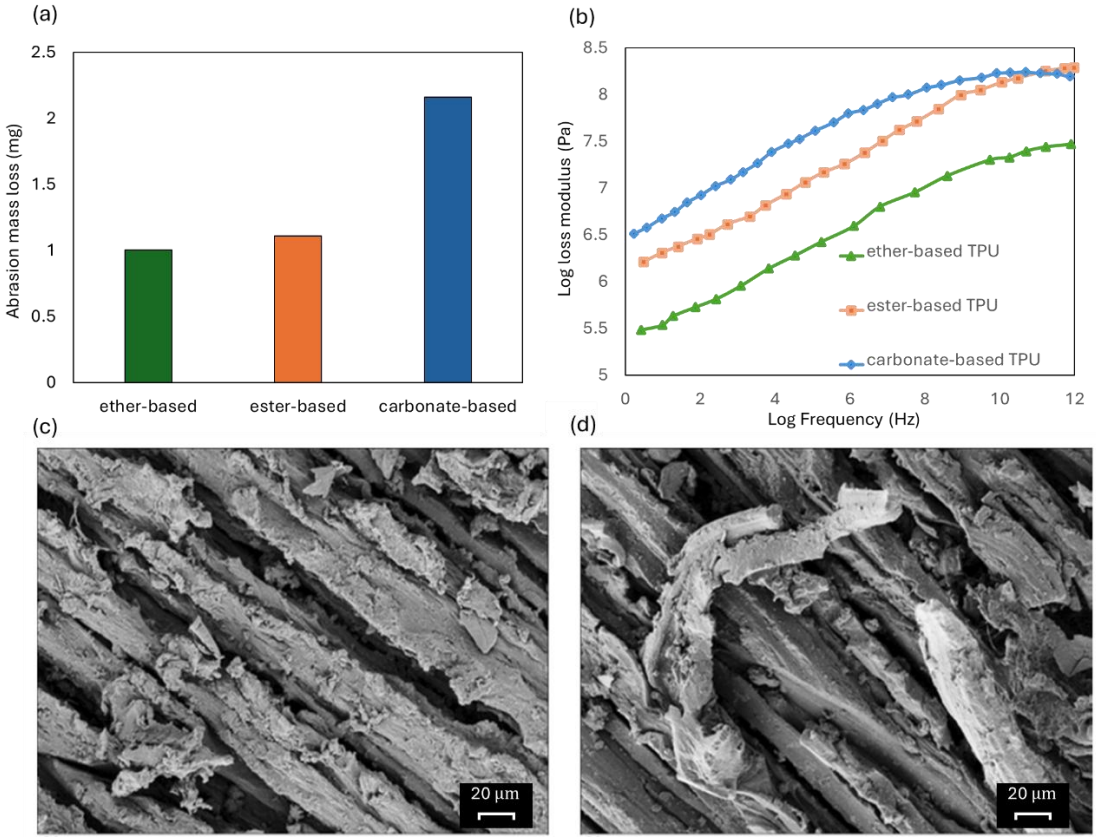


Fig. 5- 2- a) Abrasion mass loss during Abrasion test on 500 mm of P180 abrasive paper, b) master curves of E'' (loss or viscous modulus for the various TPUs, SEM images of abraded surface of c) ether-based TPU, and d) ester-based TPU (reprinted with permission from eXPRESS Polymer Letters [28]).

According to their results, the correlation between viscoelasticity and abrasion resistivity was found to be robust, persisting across a wide range of frequencies in viscoelasticity analyses. Further insights were provided by SEM analysis of abraded surfaces, which revealed that samples with lower abrasion resistance exhibited larger fragments removed from their surfaces. These findings

underscore the critical influence of viscoelastic properties on the abrasion behavior of TPUs, offering valuable guidance for material design and optimization.

5-4-2- Effect of the mechanical properties

TPUs exhibit exceptional properties beyond their elasticity, including robust mechanical performance, enhanced tear resistance, and notable abrasion resistance. The mechanical behavior of TPUs is influenced by the presence of randomly sequenced hard and soft segments. The hard segments occupy a significant volume and function as physical crosslinks, contributing to the material's structural integrity [29]. Figure 5-3 illustrates TPU chains schematically, and the chemical structure of TPU. The mechanical properties of TPU are influenced by the (I) chemical structure of the chains, (II) the chain lengths of the hard and soft segments, and (III) the degree of crystallization. Variations in the chemical structure of TPU make it suitable for a wide range of applications. [30].

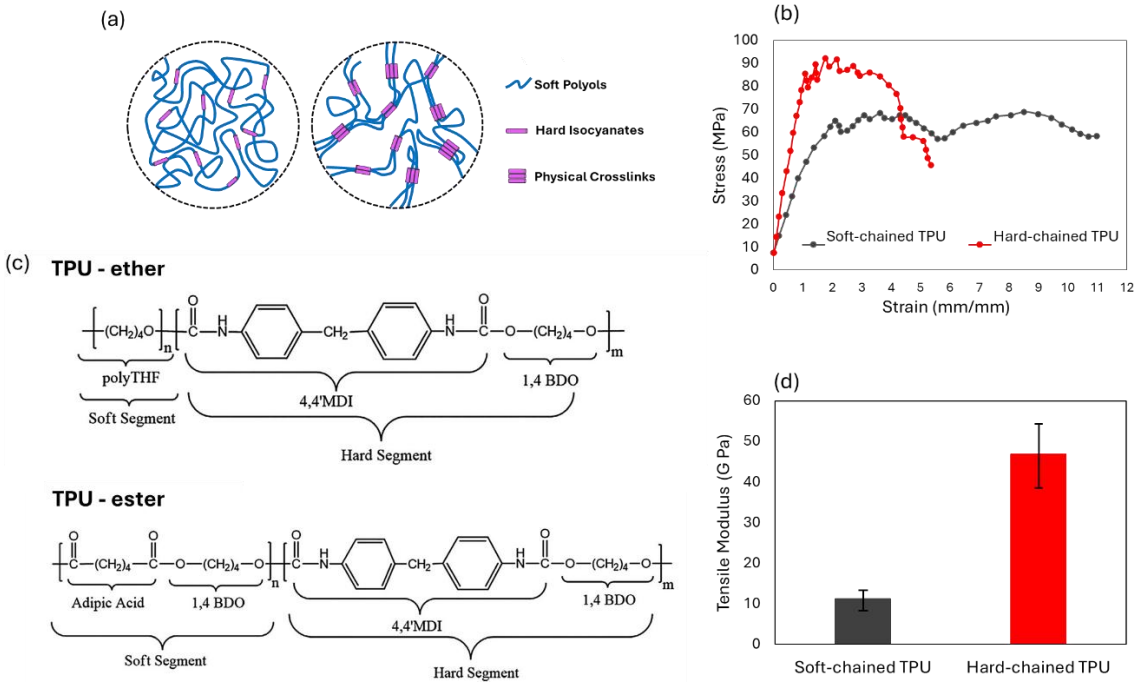


Fig. 5- 3– a) Schematic of polyol (soft) and isocyanate (hard) segments in TPU, b) how variations in ratios of soft and hard segments influence TPU stress-strain curve, c) chemical structure of TPU, comprising soft(ether or ester) and hard segments, and d) tensile moduli of soft-chained TPU and hard-chained TPU [31].

Modifications to the polyol or the isocyanate structure or any adjustment to the stoichiometric ratio in the TPU chains result in notable alterations to the morphology, forming a two-phase structure. These changes substantially enhance cross-linking behavior, thereby improving the mechanical

properties of the TPU [32]. In thermoplastic polyurethanes (TPUs), the selection of isocyanate plays a critical role in determining the rigidity and mechanical strength of the polymer [33]. The hard segments govern the degree of phase separation between the hard and soft domains, leading to variations in morphology and molecular mobility [34]. The effect of hard segment length in TPU on its mechanical properties was investigated by Wang et al. [35], who reported that increasing hard segment content enhanced tensile strength while reducing elongation at break. Kore et al. [31] investigated the mechanical properties of TPU–carbon fiber (CF-TPU) composites prepared using soft-chained (S-TPU) and hard-chained (H-TPU) variants, distinguished based on their measured hardness. Their results, presented in Fig. 5-3(b), indicate a significant difference in the initial failure strength between S-TPU (64.7 MPa) and H-TPU (85.2 MPa). This difference is attributed to the cross-linked backbone structure, which enhances the load-bearing capacity of S-TPU composites. Furthermore, tensile modulus analysis, depicted in Fig. 5-3(d), was conducted to examine the effect of segmental motion on the performance of CF-TPU composites. It was also reported by Nofar et.al. [36] that an increase in the hard segments of TPUs evokes finer morphology. On the other hand, more soft segments grant coarser morphology which is favorable to enhance the ductility and impact properties of TPUs. Their results are comparable with the TEM analysis done by Arena. et.al. [28], which suggests that mechanical responses of TPUs could be defined as a function of their morphological structure.

5-4-3- Effect of hardness

Shore hardness is a vital parameter used by manufacturers to evaluate a material's ability to withstand external forces or deformation applied by needle. Based on the durometer scale for Shore A hardness, materials are categorized as "medium hard" (60–80), "hard" (80–95), and "extra hard" (above 95) for rubber, plastics, and non-metallic substrates [37]. In thermoplastic polyurethanes, hardness is directly linked to durability, especially under repeated surface contact, which makes them prone to wear and tear [38]. Furthermore, hardness significantly impacts fracture resistance, with tearing resistance serving as a critical factor for characterizing TPU materials [10]. Research by Sun et al. [39] revealed that higher shore hardness in rubber composites enhances abrasion resistance. Figure 5-4 summarizes the results reported by Banoriya et.al. [40], who investigated the effect of shore hardness of TPU composites on their weight loss due to abrasion.

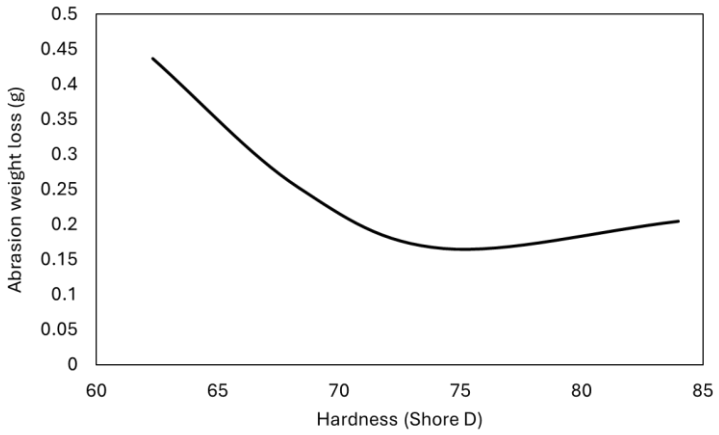


Fig. 5- 4- Abrasion weight loss as a function of shore hardness for TPU [40].

5-5- Machine Learning Model Development

Machine learning (ML) algorithms were developed in this study, to predict the abrasion resistance of various Elastollan TPU grades produced by BASF Polyurethanes GmbH. This section outlines the methodology, including data collection, preprocessing techniques, selection of input parameters, the ML algorithms employed, and the strategies used for parameter optimization.

5-5-1- Data Collection

Data can be sourced from various reliable channels, including simulations, experimental studies, and open-access databases. However, comparing the properties of similar materials becomes challenging when data originates from different sources. Even when a consistent standard is applied within a single source, variations in testing conditions permitted by that standard can lead to discrepancies in the data [41]. For instance, CAMPUS plastics [42], a registered trademark of Chemie Wirtschaftsförderungsgesellschaft mbH (CWFG) based in Frankfurt am Main, Germany, offers standardized, open-source material data for the plastics industry, measured in compliance with international protocols. In this study, data were compiled from unreinforced Elastollan TPU grades provided by BASF and produced by injection molding, as a representative case. These grades are categorized based on their composition, either as ester or ether polyol soft segments and aromatic or aliphatic isocyanate hard segments. A summary of the data collected from this open-source platform is presented in Table 5-1.

Table 5- 1- TPU grades selected from the database

Material Grade	Family	# of data	Producer

Elastollan® A B C D W 000 A: Polyether or Polyester B: Shore Hardness C: Granule Shape D: Lubricant W: Additives 000: Natural	TPU- ARES*	34	**BASF Polyurethanes Gmbh**
	TPU- ARET**	24	
	TPU- ALES***	7	

* Aromatic isocyanate, polyester polyol, ** Aromatic isocyanate, polyether polyol, *** Aliphatic isocyanate, polyester polyol

Data collection from the source was conducted to compile comprehensive information on Elastollan TPU elastomers. Key mechanical properties were evaluated as input features, including viscous and elastic moduli, their ratio (tan δ), tensile modulus, stress at 100%, and 300% elongations, as well as stress at break, measured per ISO 527[43]. Additional parameters included compression sets at 23 °C and 70 °C for 24 hours (ISO 815), tear strength (ISO 34-1)[44], density (ISO 1183)[45], shore hardness (ISO 48-4)[46], and abrasion resistivity(mm^3) as the target response (ISO 4649)[16]. All data were collected in strict adherence to the specified standards to ensure consistency and reliability.

5-5-2- Feature Selection

Feature selection is a critical process that identifies a subset of relevant features from the original dataset to enhance prediction accuracy and reduce redundancy. By minimizing noise, it improves model performance and provides domain experts with a more concise and interpretable dataset [47]. Furthermore, feature selection optimizes computational efficiency by reducing the dimensionality of data, resulting in faster execution times and more efficient resource utilization [48]. Various feature selection techniques are available for both supervised and unsupervised machine learning models. In supervised learning, feature selection methods include Filter Methods, Wrapper Methods, and Embedded Methods [49]. Filter methods are commonly employed and include statistical techniques such as Pearson, Spearman, Kendall correlations, Analysis of Variance (ANOVA), and Chi-squared test [50], [51]. These methods play a pivotal role in identifying the most relevant features while maintaining computational efficiency and predictive power.

Features most correlated with the target variable (abrasion resistivity) were identified using Pearson correlation, which quantifies the linear relationship between two variables. This method

ensures reliable and robust feature selection for the analysis [20]. The Pearson correlation coefficient is defined as [52]:

$$r_{xy} = \frac{\sum(x - \bar{x})(y - \bar{y})}{(\sqrt{\sum_1^n (x_i - \bar{x})^2}\,(\sqrt{\sum_1^n (y_i - \bar{y})^2}} \qquad \text{Equation 5-1}$$

Here, x and y are random variables, x_i and y_i denote the *i-th* values of x and y, respectively, n represents the total number of observations, and $\bar{x}$ and $\bar{y}$ are the mean values of x and y. The coefficient, r_{xy} measures the strength and direction of a linear relationship between two variables, with values ranging from -1 to +1. A positive *r* indicates both variables increase together, while a negative *r* means one increases as the other decreases. Values closer to -1 or +1 denote stronger correlations.

The most informative mechanical properties were selected as key input features, serving as a fingerprint of the material's structure and morphology to predict abrasion resistivity. To ensure the linear independence of input variables, a critical requirement for developing effective machine learning algorithms [53], certain features were excluded to ensure the input variables were both linearly independent and representative of the TPU's structural morphology. Features with the highest Pearson correlation to abrasion resistivity were identified and retained; specifically, any feature with a Pearson correlation coefficient above 0.25 was maintained as a model input. Remaining features were subsequently added stepwise, with model performance monitored at each stage. Notably, the inclusion of density as an input variable enhanced the model's predictive performance. The selected features, deemed more robust and informative, are presented in Fig. 5-5.

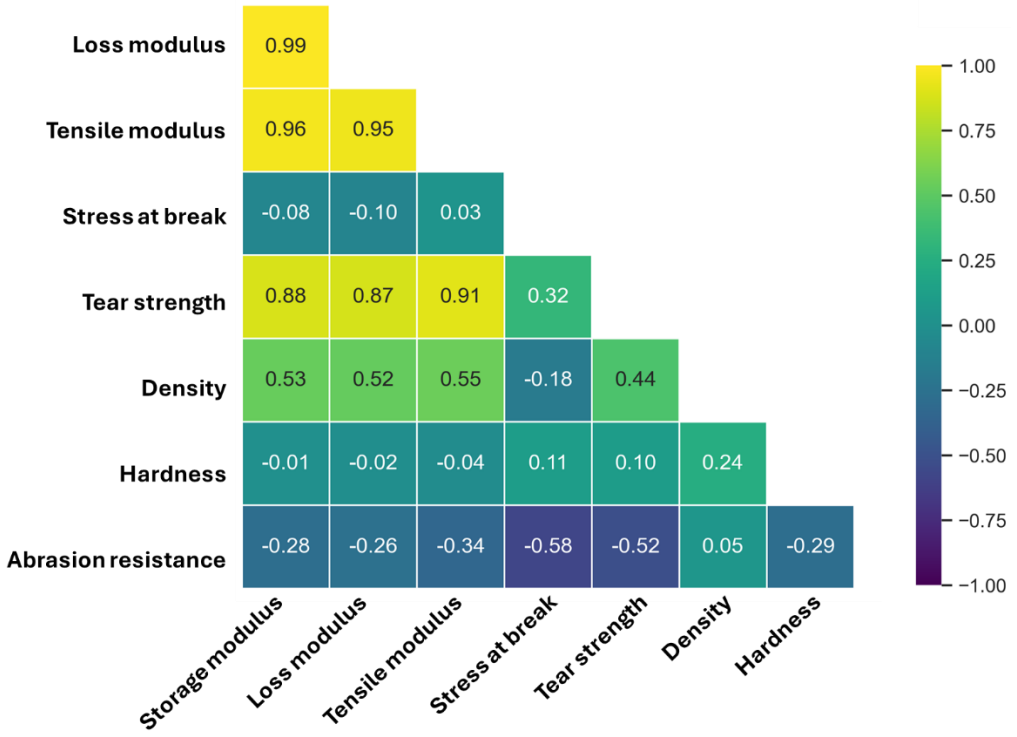


Fig. 5- 5- Selected features as most correlated inputs to the abrasion resistivity performance of TPUs

Figure 5-6 illustrates the linear relationship between abrasion resistivity and two of the most informative input features: “stress at break” and “tear strength”.

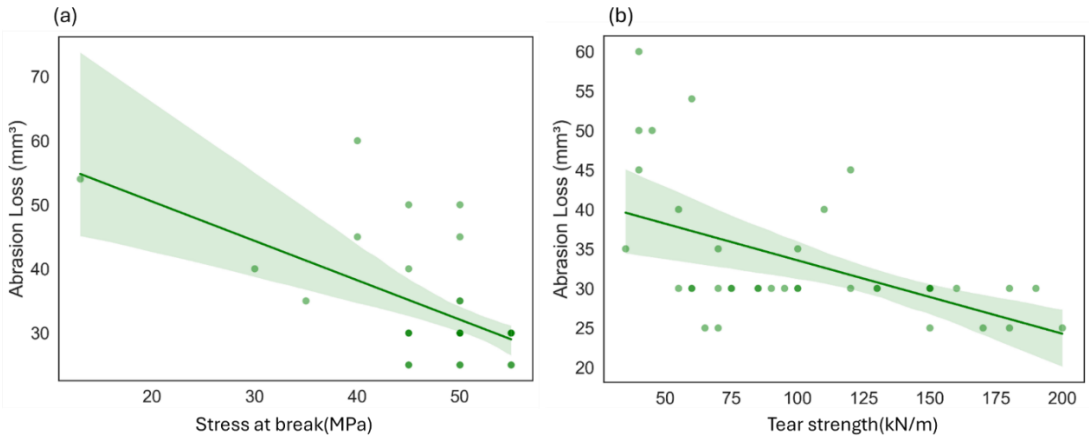


Fig. 5- 6- linear correlation between the target feature and two most correlated mechanical properties: a) stress at break, and b) tear strength.

5-5-3- Data Processing

Data preprocessing is an essential step in preparing datasets for machine learning models [18]. This process involved addressing missing values, outliers, and applying normalization through

feature scaling. Managing missing values in small datasets is essential to ensuring the accuracy of material property definitions [54]. Outliers were addressed by applying a statistical threshold of three standard deviations from the mean for each feature [55].

The data was normalized using MinMaxScaler from Scikit-learn, which scales values to a defined range (e.g., [0, 1]) while preserving their relative proportions [56]. This normalization ensures that all features have equal influence during model training and data analysis [57]. The dataset was divided into two separate subsets: a training set for model development and a test set for evaluating model performance. Machine learning models were trained on the training set, and their ability to generalize to new data was tested on the test set. The entire process was implemented using the Python programming language in the Jupyter Notebook environment (version 6.5.4).

5-5-4- Studies of Machine Learning Algorithms

Six different regression models of ML algorithms are developed on the data and evaluated. The studied algorithms are Linear Regression, Polynomial Regression, Decision Tree Regressor (DTR), Random Forest Regressor (RFR), Gradient Boosting Regressor (GBR), and Supervised Vector Regressor (SVR). The ML analyses were performed using the built-in "scikit- learn" toolkit in Python (version 3.11.5). A brief description of the ML algorithms used in this study is presented below.

5-5-4-1- Regression

Linear regression is a widely used algorithm in machine learning for predicting continuous target variables. It models the output variable by fitting a straight line to the given dataset and learns the linear relationship between the input variables $x_i = (x_{i1}, x_{i2}, \dots, x_{ij})$, where j is the number of inputs, and the output variable y_i using the least squares method. The algorithm determines the weights and bias, which are the parameters optimized to make the most accurate predictions [58]. A Multivariate Linear Regression (MLR) equation is [53]:

$$y_i = \omega_0 + \omega_{i1}x_{i1} + \omega_{i2}x_{i2} + \cdots + \omega_{ij}x_{ij} + \varepsilon_i \qquad \text{Equation 5-2}$$

Where y is the dependent variable, $x_{i1}, \dots, x_{ij}$ are the independent variables of i^{th} data, $\omega_{i1}, \dots, \omega_{ij}$ are the corresponding weights to each input variable, ω_0 is the intercept, and ε_i is the error corresponded to the i^{th} data.

Polynomial regression generalizes linear regression by representing the relationship between variables as a k^{th} degree polynomial, where k is a non-negative integer. This method fits a curve to the data, allowing for the identification of non-linear relationships. It is especially useful for capturing complex patterns in cases where the interaction between variables is not linear [59][60]. The equation for polynomial regression is [58]:

$$\begin{cases} y_1 = \omega_0 + \omega_1 x_1 + \omega_2 x_1^2 + \omega_3 x_1^3 \ldots + \omega_k x_1^k \\ y_2 = \omega_0 + \omega_1 x_2 + \omega_2 x_2^2 + \omega_3 x_2^3 \ldots + \omega_k x_2^k \\ \vdots \\ y_j = \omega_0 + \omega_1 x_j + \omega_2 x_j^2 + \omega_3 x_j^3 \ldots + \omega_k x_j^k \end{cases} \quad \text{Equation 5-3}$$

5-5-4-2- Decision Tree Regressor (DTR)

Decision tree (DT) algorithms are a cornerstone of supervised learning, known for their versatility in handling both regression and classification tasks. They operate by iteratively partitioning the feature space to minimize impurity, using a top-down approach to construct a tree-like model. While their inherent interpretability and utility make them widely applicable, decision trees are susceptible to overfitting, particularly when tree depth is not adequately constrained, or regularization techniques are omitted [61]. The splitting process in decision trees relies on specific criteria to optimize the model's performance. At each decision node, Variance Reduction (VR) is calculated, as in Eq. 5-4, to determine the optimal split, with the objective of maximizing VR across root and leaf nodes. This approach ensures that the model captures the underlying structure of the data while progressively reducing variability at each level of the tree [62][63].

$$V_R = V_{Root} - \sum_{i=1}^{n} W_i \times V_{Leaf}$$

$$V_{Root} = V_{Leaf} - \sum_{i=1}^{n} (y_i - \bar{y}_i)^2 \quad \text{Equation 5-4}$$

Where W_i denotes the weight associated with the n^{th} node, V_{Root} and V_{Leaf} represent the variances at the root and leaf nodes, respectively. Additionally, y_i refers to the observed response, while $\bar{y}_i$ corresponds to the mean predicted response within the respective node.

5-5-4-3- Random Forest Regressor (RFR)

Random Forest (RF) is a supervised machine learning algorithm that uses an ensemble of decision trees to make predictions. RF creates multiple decision trees, each trained on different subsets of the data (bootstrapped), and combines their outputs by averaging for regression or majority voting for classification to improve accuracy and reduce errors [62].

One of the main strengths of Random Forest is its ability to prevent overfitting, which is a common issue with individual decision trees. To achieve the best performance, key parameters need to be fine-tuned. These include the maximum depth of the trees (*max_depth*) to control tree complexity, the number of features considered at each split (*max_features*) to ensure tree diversity, and the total number of trees (*n_estimators*) to balance prediction accuracy and computational efficiency [20]. The RF algorithm's output can be expressed as follows[48]:

$$\hat{Y}(x) = \frac{1}{r}\sum_{j=1}^{r} f_j(x) \qquad \text{Equation 5-5}$$

Where $\hat{Y}(x)$ is the predicted output, r denotes the total number of decision trees, and $f_j(x)$ represents the output of the j^{th} decision tree.

5-5-4-4- Gradient Boosting Regressor (GBR)

Gradient Boosting Machine (GBM) is a highly effective machine learning algorithm widely used for regression and classification tasks. Like the Random Forest (RF) regressor, GBM builds upon decision tree models but employs a distinct strategy for ensemble construction. Specifically, GBM utilizes a boosting approach where decision trees are sequentially built, and each tree aims to correct the errors made by the previous ones [24][64]. The ensemble method used in GBM combines the predictions of multiple decision trees, progressively improving model accuracy. The boosting mechanism iteratively develops base models, focusing on training instances where previous models performed poorly. This process minimizes a specified loss function, such as the mean absolute error or mean squared error, which quantifies the difference between predicted and actual values [65].

$$f_t(x) = f_{t-1}(x) + \rho_t h_t(x)$$
$$(\rho_t, h_t(x)) = \arg\min \sum_{i=1}^{n} L(y_i, f_{t-1}(x_i) + \rho h(x_i)) \qquad \text{Equation 5-6}$$

Where $f_t(x)$ is the estimation function of t^{th} base learner, t = 1, 2, …, T, and ρ_t denotes its weight. L is the differentiable loss function as $L(y_i, f_t(x))$.

GBM operates in an iterative manner, where each iteration seeks to strengthen the model's predictive capabilities by refining the mapping of inputs to outputs. This is achieved by reducing the loss function value at each step [66]. Two key parameters, the learning rate and the number of boosting stages (*n_estimators*), play a critical role in defining the model's complexity. Proper tuning of these interdependent parameters is essential for optimizing GBM's performance.

5-5-4-5- Support Vector Regressor (SVR)

Support Vector Machine (SVM) is a supervised learning algorithm well-suited for both classification and regression tasks. It is particularly effective for small datasets with many input features, due to its ability to handle high-dimensional spaces and define optimal decision boundaries [67]. SVM regression (SVR) maps data into a higher-dimensional feature space using a transformation matrix ϕ(x) enabling linear separability in that space and constructing a hyperplane for prediction [24][60].

$$f(x) = \omega^T \emptyset(x) + b \qquad \text{Equation 5-7}$$

Where ω and b are weight and bias of the model, respectively.

The primary goal of SVR is to minimize the discrepancy between the predicted output *f(x)* and the actual target *y*, subject to a permissible error ε. The loss function is activated only when the absolute difference between *f(x)* and *y* exceeds ε. Within a tolerance band of width 2 ε, predictions are considered accurate, and no loss is computed. SVR constructs a hyperplane *f(x)* in the high-dimensional space that minimizes the total deviations (slack variables x_i^1 and x_i^2) for data points outside this tolerance band, while simultaneously maximizing the fit of data within the defined threshold [18] [60]. Therefore, the objective of the SVR is to minimize the following term:

$$\min \frac{1}{2} \|W\|^2 + C \sum_{i=1}^{n} (x_i^1 + x_i^2) \qquad \text{Equation 5-8}$$

Here W is the weight vector, and C is a regularization parameter, which balances the trade-off between model complexity and prediction error, enabling fine control of generalization and robustness[68].

Kernel functions, $\kappa(x,x_i)$, are essential components of the SVR algorithm, facilitating the transformation of data into higher-dimensional hyperplanes. Common kernel functions include linear, polynomial, sigmoid, and radial basis function (RBF) kernels. Equation 5-9 illustrates the form of the kernel function in SVR, where $\hat{a}_i$ and a_i represent Lagrange multipliers involved in the optimization process. [24][58][60].

$$f(x) = \sum_{i=1}^{n} (\hat{a}_i - a_i)\kappa(x, x_i) + b \qquad \text{Equation 5-9}$$

Careful tuning of these parameters is essential to achieve optimal model performance.

5-5-5- Parameters Optimization and Hyperparameters Search Space

Hyperparameter optimization is a crucial step in improving the performance of machine learning (ML) algorithms, as each dataset and model requires a specific configuration. In this study, the grid search method was used to identify optimal hyperparameters. Python scripts implemented the grid search, which systematically evaluated combinations of specified hyperparameter ranges through iterative ML analyses, ultimately determining the best configuration. GridSearchCV, a function from the Scikit-learn library, automated this process by testing all possible combinations of predefined hyperparameters and selecting the set that maximized model performance. The optimal parameters identified for each algorithm, along with their respective hyperparameter search spaces, are detailed in Table 5-2.

Table 5- 2- Hyperparameters optimization and their search space for ML models

Model	Hyperparameter type	Hyperparameter search space	Optimized parameter	Optimized train-test split size
Regression	-	-	-	0.75 – 0.25
DTR	criterion max_depth	{“squared_error”, “friedman_mse”, “absolute_error”, “poisson”} {1, 2, …, 20}	“absolute_error” 6	0.75 – 0.25
RFR	num_estimators max_depth	{10, 20, …, 200} {1, 2, …, 20}	160 6	0.75 – 0.25
GBR	num_estimators max_depth	{10, 20, …, 200} {1, 2, …, 10}	80 3	0.75 – 0.25

SVR	kernel C values	{“linear”, “poly”, “rbf”, “sigmoid”} {0.01, 0.10, 1, 10, 100}	“linear” 0.10	0.85 – 0.15

DTR: Decision Tree Regression,

RFR: Random Forest Regression,

GBR: Gradient Boosting Regression,

SVR: Support Vector Regression

Figure 5-7 illustrates the outline of the proposed approach of ML model train and evaluation for abrasion resistivity of TPU elastomers.

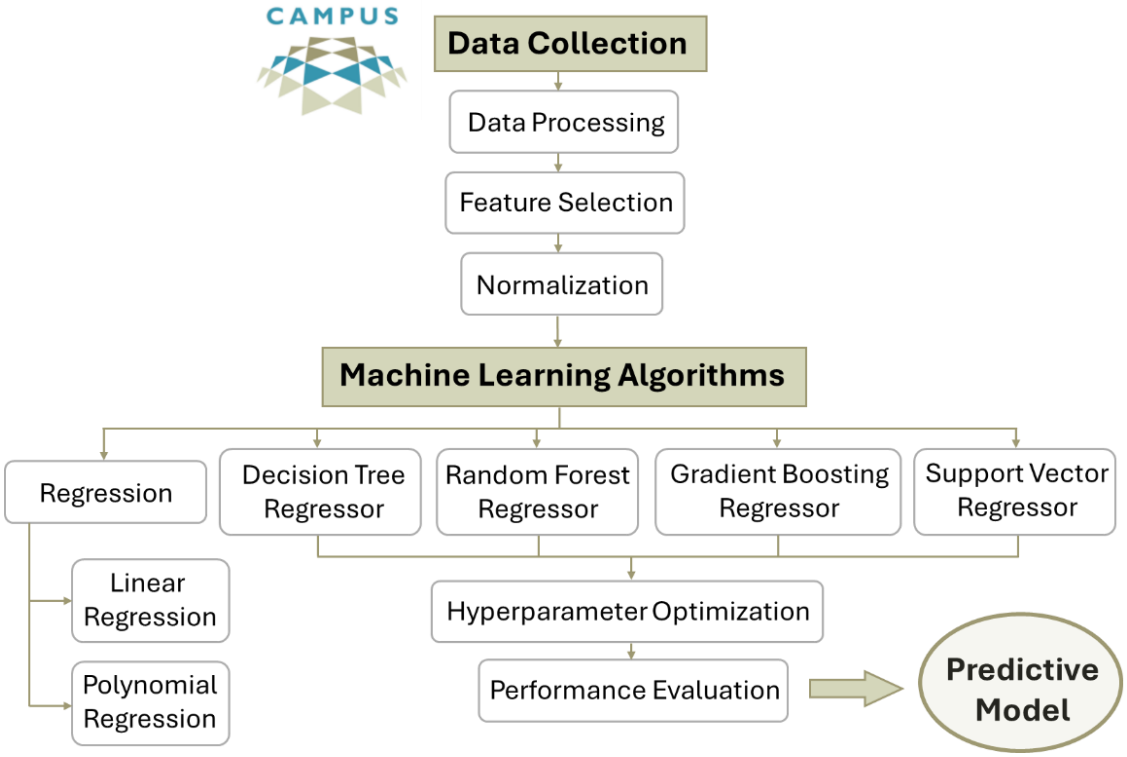


Fig. 5- 7- Flowchart outlining the approach for ML-based TPUs abrasion resistivity prediction

5-6- Results and Discussion

This section presents the results of the machine learning (ML) analysis for predicting abrasion resistance in TPU elastomers, with interpretations supported by materials science concepts. The performance of the ML models is evaluated, and the influence of individual features on abrasion resistance is analyzed.

5-6-1- Model Performance Evaluation

To evaluate the models for continuous targets, such as abrasion volume loss (mm^3), several performance metrics are used, including mean absolute error (MAE), mean squared error (MSE), root mean squared error (RMSE), mean absolute percentage error (MAPE%), and the coefficient of determination (R^2), as detailed in Table 5-3.

Table 5- 3- Evaluation metrics performed on ML models and their statistical description

Evaluation Metric	Mathematical Expression	Description
MAE	$\frac{1}{N}\sum_{i=1}^{N}\lvert y_i - \hat{y}_i\rvert$	MAE measures the absolute distance between actual (y_i) and predicted ($\hat{y}_i$) target values [58].
MSE	$\frac{1}{N}\sum_{i=1}^{N}(y_i - \hat{y}_i)^2$	Mean Squared Error (MSE) is a common cost function for regression problems, using the squared differences between predicted and actual values to avoid the influence of negative signs [18].
RMSE	$\sqrt{\frac{1}{N}\sum_{i=1}^{N}(y_i - \hat{y}_i)^2}$	Root Mean Squared Error (RMSE), the square root of MSE, measures how closely data points align with the line of best fit. A lower RMSE indicates a better fit of the model to the dataset [64].
MAPE%	$\frac{1}{N}\sum_{i=1}^{N}\left\lvert\frac{\hat{y}_i - y_i}{\hat{y}_i}\right\rvert * 100$	Mean Absolute Percentage Error (MAPE) measures the average percentage difference between predicted values and observed outcomes, reflecting the multiplicative effect of estimation errors [64].
R^2	$1 - \frac{\sum(y_i - \hat{y}_i)^2}{(y_i - \bar{y})^2}$	The coefficient of determination (R^2) represents the proportion of variance in the dependent variable that can be explained by the independent variables [69].

Performance metrics provide a quantitative assessment of how well machine learning (ML) models fit the actual data. For supervised regression tasks, the coefficient of determination (R^2) is a key metric, representing the proportion of variance in the target variable explained by the model. The coefficient of determination (R^2), which varies between 0 and 1, indicates how well the input variables account for the variation in the predicted outcomes. An R^2 value between 0.7 and 0.9 is generally considered to reflect good predictive accuracy [70]. Higher R^2 values, combined with lower MSE, RMSE, MAE, and MAPE%, indicate stronger model performance and better

predictive capability. Table 5-4 summarizes the performance evaluation of developed ML models on TPUs abrasion volume loss predictions.

Table 5- 4– ML models' performances on abrasion volume loss prediction of TPU elastomers

	Regression		DTR	RFR	GBR	SVR
	Linear	**Polynomial**				
R^2 Score	0.54	-0.99	0.719	0.579	0.718	0.79
MAE (mm^3)	4.83	11.33	2.9	4.11	3.17	4.403
MSE [$(mm^3)^2$]	46.46	202.30	27.1	40.68	27.23	22.29
RMSE (mm^3)	6.816	14.22	7.88	6.37	5.21	4.72
MAPE%	11.725	32.40	8.59	12.32	9.51	15.29

The results show that the regression models struggled to identify meaningful patterns in the data and instead appeared to memorize the training data. Even after applying 5-fold cross-validation on the data, the issue of overfitting persisted. This problem was especially evident in polynomial regression, where the R^2 score on the training data reached 1.0, indicating that the model fit the training data perfectly but failed to predict the unseen data. Figure 5-8 highlights the performance of various regression models in predicting TPU abrasion resistivity.

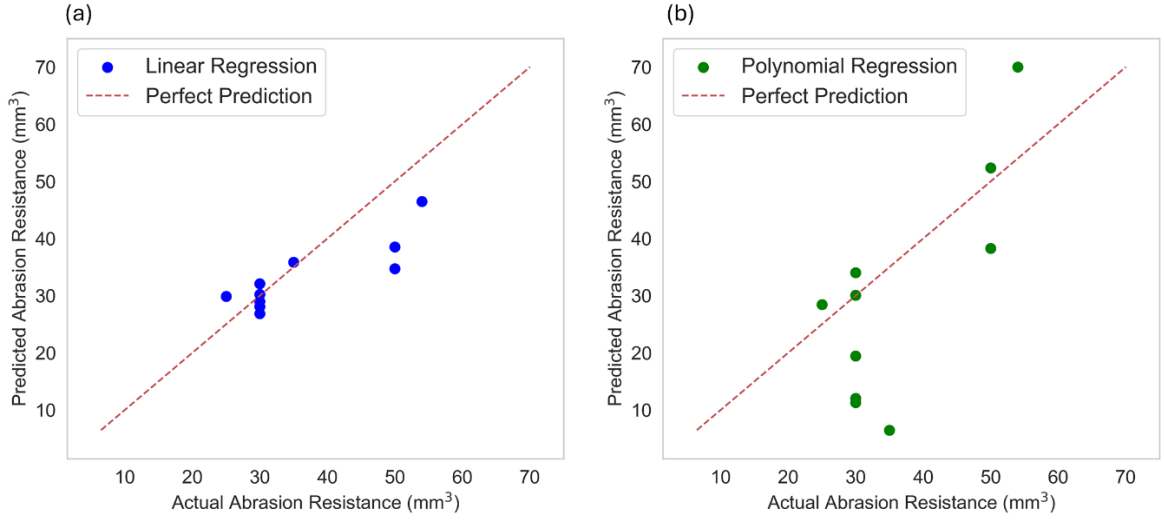


Fig. 5- 8- Regression model performance in prediction of abrasion resistivity, a) linear regression, and b) polynomial regression

The deviations between the predicted and actual abrasion volume loss values in polynomial regression demonstrate the models' inability to learn effectively from the dataset. This observation aligns with the findings of Wang et al. [60], who highlighted the limitations of polynomial

regression in small datasets. This model is prone to overfitting, especially when the dataset is limited, as it may capture noise rather than the underlying patterns in the data.

As shown in Table 5-4, the Decision Tree Regressor (DTR) achieved an R^2 score of 0.72, with a mean absolute error (MAE) of 3 mm^3, demonstrating its predictive reliability on unseen data. The Random Forest Regressor did not yield improved predictions despite increasing the number of trees in the model. The next best-performing model, the Gradient Boosting Regressor (GBR), exhibited an R^2 score of 0.718 and an MAE of 3.17 mm^3. Notably, the Support Vector Regressor (SVR) achieved the highest R^2 score of 0.79 among all models; however, it had the highest MAE at 4.4 mm^3, indicating greater variability in prediction accuracy. This could be interpreted as the model being effective at capturing trends and identifying patterns in the data, but its ability to make precise predictions is mainly hindered by the limited amount of data available. In contrast, GBR combines the predictions of multiple weak learners (decision trees), reducing overfitting and enhancing predictive performance, a key advantage when working with small datasets. Unlike SVR, which is more sensitive to noise or sparse regions in the limited data (as evidenced by its high R2 and MAE), GBR generalizes more effectively. While its R^2 is not the highest, the relatively low RMSE and MAE demonstrate GBR's strong generalization and predictive consistency in data-scarce scenarios.

The optimal predictive model is characterized by achieving the highest R^2 score while maintaining the lowest error metrics, a balance that is particularly critical when working with small-sized datasets and should be interpreted with caution [71]. To provide a more comprehensive evaluation, Figure 5-9 compares the performance of the ML models during both the training and testing phases, highlighting their consistency and generalization capabilities.

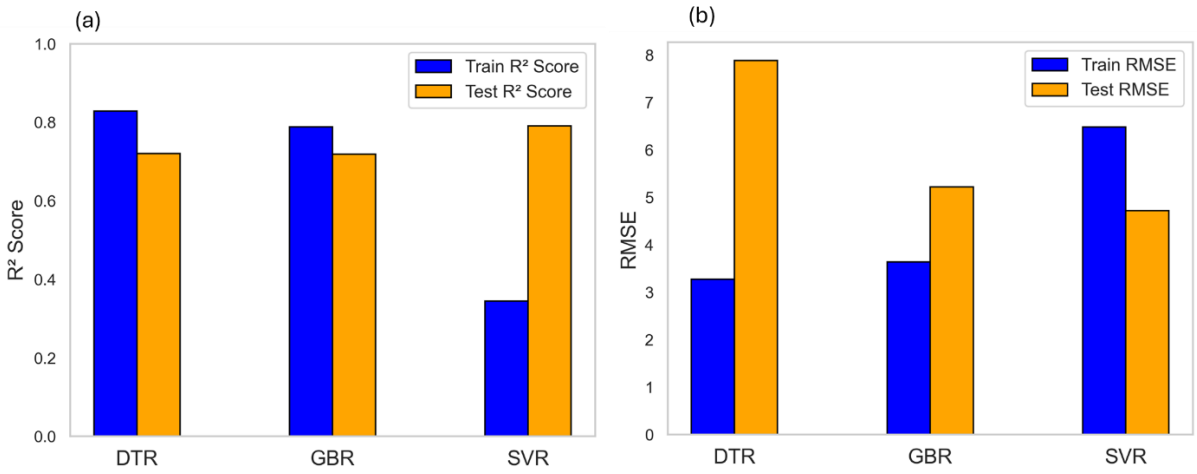


Fig. 5- 9- Evaluating ML models on training and testing performance based on: a) R^2 score and b) root mean square error

A thorough examination of evaluation metrics across both training and testing phases is essential to comprehensively analyze model performance [72]. The metrics shown in Figure 5-9(a) reveal that, while the Support Vector Regressor (SVR) demonstrates superior predictive accuracy on unseen data, its performance during training is notably lower compared to the Decision Tree Regressor (DTR) and Gradient Boosting Regressor (GBR). This discrepancy is further highlighted in Figure 5-9(b), which compares the root mean square error (RMSE) for both training and testing phases. Interestingly, the RMSE for SVR during training exceeds its error during testing, suggesting that the model is underfitting and failing to effectively learn from the dataset. SVR's sensitivity to the distribution of data points, particularly in small datasets, might contribute to this issue. However, GBR achieves more consistent results by sequentially training multiple weak learners, each correcting the errors of its predecessor. This iterative approach enables balanced learning and improved generalization, particularly in noisy or data-limited scenarios.

Figure 5-10 provides a summary of the predicted versus actual values for TPU abrasion resistivity as generated by DTR vs. GBR models.

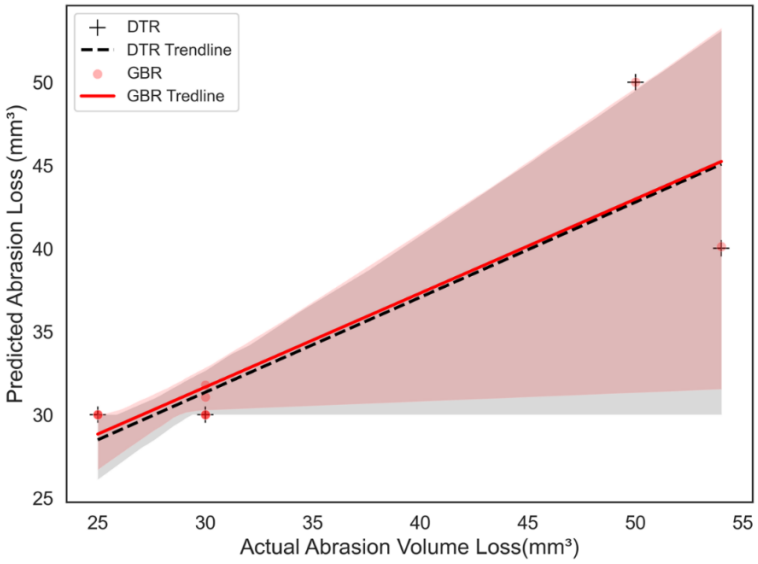


Fig. 5- 10- Evaluation analysis on Decision Tree and Gradient Boosting regressors in abrasion resistance prediction

For abrasion volume loss exceeding 45 mm^3, the dataset was sparse, as the majority of TPU elastomers exhibited abrasion loss in the range of 25-40 mm^3. This scarcity of data points in the higher range limits the ability of models to accurately recognize patterns, introducing potential uncertainties in predictions.

Abrasion loss is a critical parameter in materials design, particularly for TPU elastomers under service conditions where material degradation is a concern. An effective predictive model for this context is one that operates conservatively, yielding predicted abrasion volume loss values slightly higher than the actual values. This ensures the inclusion of safety factors in the materials design process. Based on this analysis, the Gradient Boosting Regressor (GBR) and Decision Tree Regressor (DTR) were identified as the most effective models for predicting abrasion volume loss in unreinforced TPUs and estimating the service lifespan of these elastomers. Among these, GBR demonstrated superior predictive accuracy, evidenced by a lower root mean squared error (RMSE) of 5.21mm^3 compared to DTR's RMSE of 7.88 mm^3.

This study represents an application of machine learning (ML) for predicting the performance of pristine polymeric materials, such as TPU, without the inclusion of reinforcement additives like glass fibers (GF) or carbon fibers (CF). The proposed methodology leverages the correlation between the polymer's structure, morphology, and their mechanical properties to develop predictive models. To further enhance the reliability and accuracy of this approach, future work

should focus on expanding the dataset, particularly for higher abrasion volume loss values, and incorporating reinforced TPU materials. Investigating the composition and performance of TPU composites will require extensive experimental efforts to characterize their mechanical properties. Moreover, the inclusion of filler content in TPU significantly increases the complexity of the system, demanding more sophisticated modeling strategies. This expansion would open the door to employing advanced ML architectures, such as Artificial Neural Networks (ANN), that can better capture nonlinear and multivariate interactions, ultimately improving predictive capabilities in materials design [73][74].

5-7- Conclusions

This study presents a machine learning (ML)-based framework for predicting the abrasion resistance of thermoplastic polyurethane (TPU) materials by leveraging structural and mechanical property data sourced from the CAMPUS Plastics database. Feature selection was performed using Pearson correlation analysis, identifying highly influential parameters such as viscoelastic moduli, tensile strength, elongation at break, tear resistance, hardness, and density. These variables were normalized and utilized to train six supervised regression models: Linear Regression, Polynomial Regression, Decision Tree Regressor (DTR), Random Forest Regressor (RFR), Gradient Boosting Regressor (GBR), and Support Vector Regressor (SVR). Among the models developed, Linear and Polynomial Regression exhibited limited generalizability, with significant overfitting and poor predictive accuracy, underscoring their inadequacy in handling nonlinear relationships within the dataset. Similarly, RFR failed to improve model performance, likely due to the ensemble's reduced sensitivity in small, sparse datasets. In contrast, DTR, SVR, and GBR models demonstrated enhanced predictive capabilities. SVR achieved the highest testing R^2 score (0.79), suggesting strong model-data alignment; however, its elevated MAE (4.4 mm^3) and MAPE (15.29%) values revealed sensitivity to data sparsity and noise. The GBR model, employing a sequential boosting strategy, yielded a lower RMSE (5.21 mm^3) and more stable performance across cross-validation splits, indicating superior robustness and generalization. DTR, with an R^2 of 0.72, also produced reasonably accurate predictions but was less consistent than GBR. Collectively, these results validate GBR as the most effective model for abrasion resistance prediction in data-limited scenarios, offering a reliable, cost-efficient alternative to experimental testing. Furthermore, the models successfully captured structure–property relationships in pristine TPU grades, laying a

data-centric foundation for accelerated materials selection in tribologically demanding applications, including medical devices, footwear, and automotive components.

This framework contributes to the broader field of triboinformatics, supporting predictive materials engineering through AI-enabled design, with the potential to reduce experimental load and accelerate innovation in polymeric materials. Looking ahead, future work should aim to expand the dataset, especially for TPU grades with high abrasion losses; integrate reinforcement data (e.g., carbon or glass fibers) to model composite TPU systems; and adopt more complex ML architectures, such as deep neural networks or hybrid models, to enhance nonlinear mapping and multi-feature interaction analysis.

While the current study focused on injection-molded TPU grades, future work will extend the model to account for anisotropic wear behavior in 3D-printed TPUs by incorporating print-specific parameters, such as layer orientation, raster angle, and build direction. Including such features will enhance the model's applicability to a broader range of manufacturing scenarios and support the design of functionally optimized additive parts.

5-8- References

[1] R. W. Liefferink, F. C. Hsia, B. Weber, and D. Bonn, "Friction on Ice: How Temperature, Pressure, and Speed Control the Slipperiness of Ice," *Phys. Rev. X*, vol. 11, no. 1, p. 11025, 2021, doi: 10.1103/PhysRevX.11.011025.

[2] P. Marlina *et al.*, "The rheological and mechanical properties of natural rubber/graphene composites," *IOP Conf. Ser. Earth Environ. Sci.*, vol. 963, no. 1, 2022, doi: 10.1088/1755-1315/963/1/012026.

[3] A. Rosenkranz, M. Marian, F. J. Profito, N. Aragon, and R. Shah, "The use of artificial intelligence in tribology—a perspective," *Lubricants*, vol. 9, no. 1, pp. 1–11, 2021, doi: 10.3390/lubricants9010002.

[4] L. A. Gyurova and K. Friedrich, "Artificial neural networks for predicting sliding friction and wear properties of polyphenylene sulfide composites," *Tribol. Int.*, vol. 44, no. 5, pp. 603–609, 2011, doi: 10.1016/j.triboint.2010.12.011.

[5] J. H. Kim and G. H. Kim, "Effect of rubber content on abrasion resistance and tensile properties of thermoplastic polyurethane (TPU)/rubber blends," *Macromol. Res.*, vol. 22, no. 5, pp. 523–527, 2014, doi: 10.1007/s13233-014-2077-y.

[6] M. Mo *et al.*, "Excellent tribological and anti-corrosion performance of polyurethane composite coatings reinforced with functionalized graphene and graphene oxide nanosheets," *RSC Adv.*, vol. 5, no. 70, pp. 56486–56497, 2015, doi: 10.1039/c5ra10494g.

[7] D. Nichetti and N. Grizzuti, "Determination of the phase transition behavior of thermoplastic polyurethanes from coupled rheology/DSC measurements," *Polym. Eng. Sci.*, vol. 44, no. 8, pp. 1514–1521, 2004, doi: 10.1002/pen.20148.

[8] J. M. M. Jesse L. Gadley , Ricardo J. Andrade, "Effect of Soft-to-Hard Segment Ratio on Viscoelastic Behavior of Model.pdf," *Macromol. Mater. Eng.*, vol. 301, pp. 953–963, 2016.

[9] L. Jakobsen, F. G. Lysdal, T. Bagehorn, U. G. Kersting, and I. M. Sivebaek, “The effect of footwear outsole material on slip resistance on dry and contaminated surfaces with geometrically controlled outsoles,” *Ergonomics*, vol. 0, no. 0, pp. 1–8, 2022, doi: 10.1080/00140139.2022.2081364.

[10] K. Junik *et al.*, “Impact of the hardness on the selected mechanical properties of rigid polyurethane elastomers commonly used in suspension systems,” *Eng. Fail. Anal.*, vol. 121, no. October 2020, 2021, doi: 10.1016/j.engfailanal.2020.105201.

[11] S. Chibani and F. X. Coudert, “Machine learning approaches for the prediction of materials properties,” *APL Mater.*, vol. 8, no. 8, 2020, doi: 10.1063/5.0018384.

[12] E. Aslan and G. Akincioglu, “Investigation of The Wear And Friction Profile of TPU-Based Polymers at Different Infill Ratios,” *Int. J. Automot. Sci. Technol.*, vol. 8, no. 1, pp. 125–131, 2024, doi: 10.30939/ijastech..1398109.

[13] A. M. Onas, I. E. Biru, A. Petca, and R. C. Petca, “The Aging Behavior of Polyurethane-based Ureteral Catheters,” *Mater. Plast.*, vol. 58, no. 4, pp. 65–72, 2021, doi: 10.37358/MP.21.4.5532.

[14] L. Tian *et al.*, “A bioinspired design approach for biomechanically matched tracheal stents,” *Virtual Phys. Prototyp.*, vol. 19, no. 1, pp. 1–17, 2024, doi: 10.1080/17452759.2024.2437510.

[15] K. Friedrich, “Polymer composites for tribological applications,” *Adv. Ind. Eng. Polym. Res.*, vol. 1, no. 1, pp. 3–39, 2018, doi: 10.1016/j.aiepr.2018.05.001.

[16] I. O. for Standardization, “INTERNATIONAL STANDARD ISO 4649 Rubbers, vulcanized or thermoplastic -Determination of abrasion resistance using a rotating cylindrical drum device,” *ISO*, vol. 2017, 2017.

[17] “ISO 2781-2008[10919].pdf.”

[18] H. Esmaeili and R. Rizvi, “An accelerated strategy to characterize mechanical properties of polymer composites using the ensemble learning approach,” *Comput. Mater. Sci.*, vol. 229, no. June, p. 112432, 2023, doi: 10.1016/j.commatsci.2023.112432.

[19] M. S. Hasan, A. Kordijazi, P. K. Rohatgi, and M. Nosonovsky, “Triboinformatics approach for friction and wear prediction of Al-graphite composites using machine learning methods,” *J. Tribol.*, vol. 144, no. 1, pp. 1–13, 2022, doi: 10.1115/1.4050525.

[20] A. R. Deshpande, A. P. Kulkarni, N. Wasatkar, V. Gajalkar, and M. Abdullah, “Prediction of Wear Rate of Glass-Filled PTFE Composites Based on Machine Learning Approaches,” *Polymers (Basel).*, vol. 16, no. 18, 2024, doi: 10.3390/polym16182666.

[21] R. Shah *et al.*, “Artificial Intelligence and Machine Learning in Tribology: Selected Case Studies and Overall Potential,” *Adv. Eng. Mater.*, vol. 2401944, pp. 1–14, 2025, doi: 10.1002/adem.202401944.

[22] A. Kordijazi, H. M. Roshan, A. Dhingra, M. Povolo, P. K. Rohatgi, and M. Nosonovsky, “Machine-learning methods to predict the wetting properties of iron-based composites,” *Surf. Innov.*, vol. 9, no. 2–3, pp. 111–119, 2021, doi: 10.1680/jsuin.20.00024.

[23] M. S. Hasan and M. Nosonovsky, “Triboinformatics: Machine learning algorithms and data topology methods for tribology,” *Surf. Innov.*, vol. 10, no. 4–5, pp. 229–242, 2022, doi: 10.1680/jsuin.22.00027.

[24] M. S. Hasan, A. Kordijazi, P. K. Rohatgi, and M. Nosonovsky, “Triboinformatic modeling of dry friction and wear of aluminum base alloys using machine learning algorithms,” *Tribol. Int.*, vol. 161, no. March, p. 107065, 2021, doi: 10.1016/j.triboint.2021.107065.

[25] K. Velten, R. Reinicke, and K. Friedrich, “Wear volume prediction with artificial neural networks,” *Tribol. Int.*, vol. 33, no. 10, pp. 731–736, 2000, doi: 10.1016/S0301-679X(00)00115-8.

[26] I. Kopal, M. Harničárová, J. Valíček, and M. Kušnerová, “Modeling the temperature dependence of dynamic mechanical properties and visco-elastic behavior of thermoplastic polyurethane using artificial neural network,” *Polymers (Basel).*, vol. 9, no. 10, 2017, doi: 10.3390/polym9100519.

[27] N. S. Sigamani, “Characterization of Polyurethane at multiple scales for erosion mechanisms under sand particle impact,” Texas A&M University, 2010. [Online]. Available: http://landing.adobe.com/en/sea/products/acrobat/69210-may-prospects.html?trackingid=KTKAA

[28] G. Arena *et al.*, “Solid particle erosion and viscoelastic properties of thermoplastic polyurethanes,” *Express Polym. Lett.*, vol. 9, no. 3, pp. 166–176, 2015, doi: 10.3144/expresspolymlett.2015.18.

[29] 1 L. Torre1 E. Fortunati , 1 F. Luzi, 1 A. Janke, 2 L. H€außler, 2 J. Pionteck, 2 J.M. Kenny, “Reinforcement Effect of Cellulose Nanocrystals in Thermoplastic Polyurethane Matrices Characterized by Different Soft/Hard Segment Ratio,” *Polym. Eng. Sci.*, vol. 51, no. 7, pp. 1–10, 2017, doi: 10.1002/pen.

[30] Y. Kahraman, B. Özdemir, V. Kılıç, Y. A. Goksu, and M. Nofar, “Super toughened and highly ductile PLA/TPU blend systems by in situ reactive interfacial compatibilization using multifunctional epoxy-based chain extender,” *J. Appl. Polym. Sci.*, vol. 138, no. 20, pp. 1–16, 2021, doi: 10.1002/app.50457.

[31] S. Kore, M. Theodore, and U. Vaidya, “Effect of the Segmental Structure of Thermoplastic Polyurethane (Hardness) on the Interfacial Adhesion of Textile-Grade Carbon Fiber Composites,” *Appl. Polym. Mater.*, vol. 3, no. 12, pp. 6138–6146, 2021, doi: 10.1021/acsapm.1c01001.

[32] F. N. Cogswell, *Thermoplastic Aromatic Polymer Composites A Study of the Structure, Processing and Properties of Carbon Fibre Reinforced Polyetheretherketone and Related Materials*, 1st ed. Elsevier, 2013.

[33] C. Lozano-Pérez, J. V. Cauich-Rodríguez, and F. Avilés, “Influence of rigid segment and carbon nanotube concentration on the cyclic piezoresistive and hysteretic behavior of multiwall carbon nanotube/segmented polyurethane composites,” *Compos. Sci. Technol.*, vol. 128, pp. 25–32, 2016, doi: 10.1016/j.compscitech.2016.03.010.

[34] K. N. Raftopoulos *et al.*, “Effects of Segment Length and Crosslinking via POSS on the Calorimetric and Dynamic Glass Transition of Polyurethanes with Aliphatic Hard Segments,” *Int. J. Mol. Sci.*, vol. 24, no. 22, 2023, doi: 10.3390/ijms242216540.

[35] Y. Wang *et al.*, “Polyurethane as smart biocoatings: Effects of hard segments on phase structures and properties,” *Prog. Org. Coatings*, vol. 150, no. October 2020, p. 106000, 2021, doi: 10.1016/j.porgcoat.2020.106000.

[36] M. Nofar, M. Mohammadi, and P. J. Carreau, “Effect of TPU hard segment content on the rheological and mechanical properties of PLA/TPU blends,” *J. Appl. Polym. Sci.*, vol. 137, no. 45, 2020, doi: 10.1002/app.49387.

[37] Y. Sharma, P. Ferreira, and L. Justham, “Hardness Classification Using Cost-Effective Off-the-Shelf Tactile Sensors Inspired by Mechanoreceptors,” *Electron.*, vol. 13, no. 13, 2024, doi: 10.3390/electronics13132450.

[38] A. Jaisingh, M. W. Halloran, B. S. Rajput, and M. D. Burkart, “Tailoring High Hardness and Rigidity in Biodegradable Thermoplastic Polyurethanes,” *ACS Appl. Polym. Mater.*, vol. 6, no. 16, pp. 9724–9734, 2024, doi: 10.1021/acsapm.4c01579.

[39] Q. Sun, S. Wang, and X. Lv, “Research on Tribological Properties and Viscoelasticity of EPDM Rubber in the Main Drive Sealing System of Shield Machine,” *J. Tribol.*, vol. 144, no. 5, pp. 1–9, 2022, doi: 10.1115/1.4051977.

[40] D. Banoriya, R. Purohit, and R. K. Dwivedi, “Tribological behaviour of biocompatible TPU composites with reinforced titanium,” *Adv. Mater. Process. Technol.*, vol. 8, no. sup2, pp. 802–813, 2022, doi: 10.1080/2374068X.2021.1946759.

[41] Y. Roh, G. Heo, and S. E. Whang, “A Survey on Data Collection for Machine Learning: A Big Data-AI Integration Perspective,” *IEEE Trans. Knowl. Data Eng.*, vol. 33, no. 4, pp. 1328–1347, 2021, doi: 10.1109/TKDE.2019.2946162.

[42] “CAMPUS ® (Computer Aided Material Preselection by Uniform Standards),” *CAMPUS Plastics*, 2024. https://www.campusplastics.com/

[43] ISO-527-1, "527-1: Plastics—Determination of tensile properties—Part 1: General principles," *ISO Stand.*, vol. 2012, 1997, [Online]. Available: http://scholar.google.com/scholar?hl=en&btnG=Search&q=intitle:Plastics+-+Determination+of+tensile+properties+-+Part1:+General+principles#1

[44] T. S. Preview, "ISO 34-1:2015(E) ii COPYRIGHT PROTECTED DOCUMENT," vol. 2015, 2015, [Online]. Available: www.iso.orgiTehSTANDARDPREVIEW

[45] F. S. Association, "Plastics. Methods for determining the density of non-cellular plastics.," *Sfs-En Iso 1183-12019*, vol. 2019, 2019.

[46] T. S. Preview, "INTERNATIONAL STANDARD method (Shore hardness) iTeh STANDARD PREVIEW iTeh STANDARD PREVIEW," vol. 2018, 2018.

[47] M. C. Barbieri, B. I. Grisci, and M. Dorn, "Analysis and comparison of feature selection methods towards performance and stability," *Expert Syst. Appl.*, vol. 249, no. PB, p. 123667, 2024, doi: 10.1016/j.eswa.2024.123667.

[48] M. Ehsani, M. Ostovari, S. Mansouri, H. Naseri, H. Jahanbakhsh, and F. Moghadas Nejad, "Machine learning for predicting concrete carbonation depth: A comparative analysis and a novel feature selection," *Constr. Build. Mater.*, vol. 417, no. February, p. 135331, 2024, doi: 10.1016/j.conbuildmat.2024.135331.

[49] X. Cheng, "A Comprehensive Study of Feature Selection Techniques in Machine Learning Models," vol. 1, pp. 1–14, 2024.

[50] A. Ahmad, S. N. Mjeat, D. A. Q. Shakir, and M. A. Alfwair, "Credit Card Fraud Detection Model Based on Correlation Feature Selection," *J. Cybersecurity Inf. Manag.*, vol. 14, no. 2, pp. 334–342, 2024, doi: 10.54216/jcim.140224.

[51] I. H. Sarker, "Machine Learning: Algorithms, Real-World Applications and Research Directions," *SN Comput. Sci.*, vol. 2, no. 3, pp. 1–21, 2021, doi: 10.1007/s42979-021-00592-x.

[52] P. Chen, F. Li, and C. Wu, "Research on Intrusion Detection Method Based on Pearson Correlation Coefficient Feature Selection Algorithm," *J. Phys. Conf. Ser.*, vol. 1757, no. 1, 2021, doi: 10.1088/1742-6596/1757/1/012054.

[53] M. Chandra, K. E. K. Vimal, and S. Rajak, "A comparative study of machine learning algorithms in the prediction of bead geometry in wire-arc additive manufacturing," *Int. J. Interact. Des. Manuf.*, vol. 18, no. 9, pp. 6625–6638, 2023, doi: 10.1007/s12008-023-01326-4.

[54] A. F. Ahmad, S. Sayeed, K. Alshammari, and I. Ahmed, "Impact of Missing Values in Machine Learning," pp. 1–13, 2024, doi: 10.32604/cmc.202x.0xxxxx.

[55] S. S. Tripathy, "Comparison of Statistical Methods for Outlier Detection in Proficiency Testing Data on Analysis of Lead in Aqueous Solution," *Am. J. Theor. Appl. Stat.*, vol. 2, no. 6, p. 233, 2013, doi: 10.11648/j.ajtas.20130206.21.

[56] Y.-S. Kim, M. K. Kim, N. Fu, J. Liu, J. Wang, and J. Srebric, "Investigating the Impact of Data Normalization Methods on Predicting Electricity Consumption in a Building Using different Artificial Neural Network Models.," *Sustain. Cities Soc.*, p. 105570, 2024, doi: 10.1016/j.scs.2024.105570.

[57] P. J. Muhammad Ali, "Investigating the Impact of Min-Max Data Normalization on the Regression Performance of K-Nearest Neighbor with Different Similarity Measurements," *Aro-the Sci. J. Koya Univ.*, vol. 10, no. 1, pp. 85–91, 2022, doi: 10.14500/aro.10955.

[58] S. Hiremath, Y. Zhang, L. Zhang, and T. W. Kim, "Machine learning approach to evaluating impact behavior in fabric-laminated composite materials," *Results Eng.*, vol. 23, no. May, p. 102576, 2024, doi: 10.1016/j.rineng.2024.102576.

[59] K. Shah, K. K. Talamadupula, P. Acar, and G. D. Seidel, "Reduced-order model for multiphysics simulations of CNT/Polymer Composites via principal component regression and artificial neural networks," *Comput.*

Mater. Sci., vol. 244, no. September 2023, p. 113200, 2024, doi: 10.1016/j.commatsci.2024.113200.

[60] J. Wang, S. Karimi, P. Zeinalzad, J. Zhang, and Z. Gong, "Using machine learning and experimental study to correlate and predict accelerated aging with natural aging of GFRP composites in hygrothermal conditions," *Constr. Build. Mater.*, vol. 438, no. March, p. 137264, 2024, doi: 10.1016/j.conbuildmat.2024.137264.

[61] M. Novita *et al.*, "Exploring deep learning and machine learning for novel red phosphor materials," *J. Lumin.*, vol. 269, no. February, 2024, doi: 10.1016/j.jlumin.2024.120476.

[62] V. G. Costa and C. E. Pedreira, *Recent advances in decision trees: an updated survey*, vol. 56, no. 5. Springer Netherlands, 2023. doi: 10.1007/s10462-022-10275-5.

[63] J. B. Deb, J. Gou, H. Song, and C. Maiti, "Machine Learning Approaches for Predicting the Ablation Performance of Ceramic Matrix Composites," *J. Compos. Sci.*, vol. 8, no. 3, 2024, doi: 10.3390/jcs8030096.

[64] R. Gupta, A. K. Yadav, S. K. Jha, and P. K. Pathak, "Predicting global horizontal irradiance of north central region of India via machine learning regressor algorithms," *Eng. Appl. Artif. Intell.*, vol. 133, no. PE, p. 108426, 2024, doi: 10.1016/j.engappai.2024.108426.

[65] N. M. Shahani, M. Kamran, X. Zheng, C. Liu, and X. Guo, "Application of gradient boosting machine learning algorithms to predict uniaxial compressive strength of soft sedimentary rocks at Thar coalfield," *Adv. Civ. Eng.*, vol. 2021, 2021, doi: 10.1155/2021/2565488.

[66] R. Sibindi, R. W. Mwangi, and A. G. Waititu, "A boosting ensemble learning based hybrid light gradient boosting machine and extreme gradient boosting model for predicting house prices," *Eng. Reports*, vol. 5, no. 4, pp. 1–19, 2023, doi: 10.1002/eng2.12599.

[67] V. K. Mahakur, S. Bhowmik, and P. K. Patowari, "Tribo-informatics evaluation of dry sliding friction of silanized jute filler reinforced epoxy composites using machine learning techniques," *Tribol. Int.*, vol. 183, no. November 2022, p. 108388, 2023, doi: 10.1016/j.triboint.2023.108388.

[68] M. Sabzekar, S. Mohammad, and H. Hasheminejad, "Robust regression using support vector regressions," *Chaos, Solitons Fractals Nonlinear Sci. Nonequilibrium Complex Phenom.*, vol. 144, p. 110738, 2021, doi: 10.1016/j.chaos.2021.110738.

[69] R. R. Esmaeili Hamed, Avateffazeli Maryam, Haghshenas Meysam, "Fatigue Fract Eng Mat Struct - 2024 - Esmaeili - A Hybrid Framework for Characterizing and Benchmarking Fatigue S-N Curves.pdf." 2024.

[70] V. K. Mahakur, S. Bhowmik, and P. K. Patowari, "Experimental evaluation and prediction on drilling of Corchorus olitorius filler-based composite," *Mater. Manuf. Process.*, vol. 39, no. 9, pp. 1203–1212, 2024, doi: 10.1080/10426914.2024.2311384.

[71] P. Xu, X. Ji, and M. Li, "Small data machine learning in materials science," pp. 1–15, 2023, doi: 10.1038/s41524-023-01000-z.

[72] B. Panigrahi, K. Chaitanya, R. Kathala, and M. Sujatha, "A Machine Learning-Based Comparative Approach to Predict the A Machine Learning-Based Comparative Approach to Predict the Crop Yield Using Supervised Learning With Regression Models Crop Yield Using Supervised Learning With Regression Models," *Procedia Comput. Sci.*, vol. 218, no. 2022, pp. 2684–2693, 2023, doi: 10.1016/j.procs.2023.01.241.

[73] V. K. Mahakur, R. Paul, S. Bhowmik, and P. K. Patowari, "Influence of surface modification on mechanical and tribology performance of jute filler polymer composites and prediction of the performance using artificial neural network," *Polym. Bull.*, vol. 80, no. 11, pp. 11953–11974, 2023, doi: 10.1007/s00289-022-04636-x.

[74] G. M. Raja, A. Vasanthanathan, and K. Jeyasubramanian, "Novel Ternary Epoxy Resin Composites Obtained by Blending Graphene Oxide and Polypropylene Fillers: An Avenue for the Enhancement of Mechanical Characteristics," *J. Inorg. Organomet. Polym. Mater.*, vol. 33, no. 2, pp. 383–397, 2023, doi: 10.1007/s10904-022-02494-8.

Chapter 6:
Case Study [Industrial Contribution] Machine Learning-Aided Accelerated Design and Characterization of Automotive Composites

6-1- Chapter Preface

This chapter presents an industrial case study based on a long-term collaborative project conducted during the PhD program with a Tier-1 automotive company in Canada. The project focused on the accelerated design, characterization, and performance evaluation of polymer-based automotive composite materials using experimental and data-driven approaches.

Due to confidentiality agreements with the industrial partner, proprietary material formulations, processing details, component-level information, experimental datasets, performance targets, and quantitative results are not disclosed in this dissertation. Instead, this chapter provides a non-confidential overview of the technical motivation, industrial relevance, general workflow, and scholarly contribution of the project. The chapter is included as an additional contribution completed during the PhD period and demonstrates the broader application of machine learning-aided materials design and characterization in an industrial automotive context.

Although the main body of this dissertation focuses on elastomeric composites for ice traction and abrasion resistance, the industrial project is relevant to the broader theme of data-driven materials development. In particular, it highlights how machine learning can support faster material screening, reduce experimental burden, and assist engineering decision-making in complex polymer composite systems.

6-2- Background: Automotive Composite Materials

The automotive sector is undergoing a significant transformation driven by sustainability requirements, vehicle electrification, energy efficiency targets, and the need for improved structural performance [1]. Within this transition, lightweighting has become one of the most

important engineering strategies for reducing vehicle mass while maintaining safety, functionality, durability, and passenger comfort. Reducing vehicle weight is especially important because it can contribute to improved fuel economy, reduced greenhouse gas emissions, increased driving range in electric vehicles, and improved overall vehicle performance [2]–[4].

Lightweighting can be achieved through several complementary strategies. One approach is design optimization, in which existing materials are used more efficiently through improved geometry, topology optimization, and component integration. Advances in computer-aided engineering and simulation tools have enabled the design of structures that reduce unnecessary material use while preserving mechanical integrity [1]. Another strategy is the use of alternative manufacturing methods, such as hydroforming, tailor-welded blanks, additive manufacturing, and advanced forming processes, which allow material to be distributed more efficiently in load-bearing regions. A third strategy is the adoption of alternative lightweight materials, including high-strength steels, aluminum alloys, magnesium alloys, plastics, and fiber-reinforced polymer composites [1], [4]. Figure 6-1 illustrates the Ashby plot of strength vs. density for engineering materials [5].

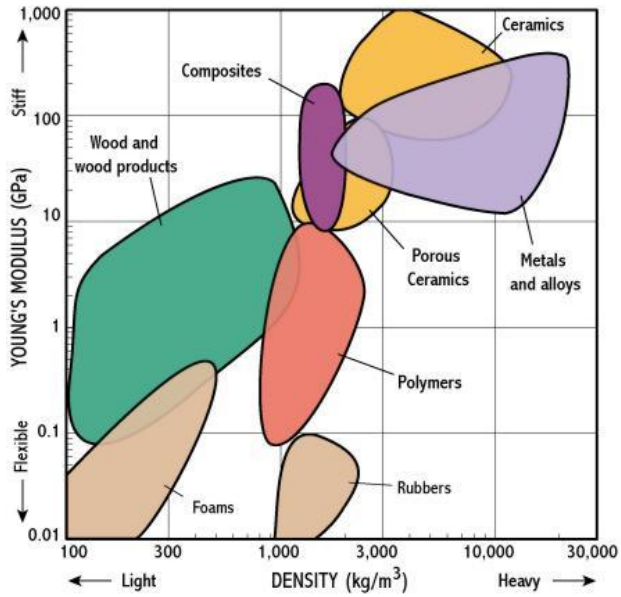


Fig. 6- 1- Strength versus density of engineering materials. Composites demonstrate strength comparable to metals while exhibiting lower density [5].

Among these material classes, composites have attracted increasing attention in automotive applications because they provide high specific strength, high specific stiffness, and strong design flexibility [5]. Composite materials can be tailored by changing the matrix, reinforcement type, fiber architecture, filler content, interface quality, and processing conditions. This tunability

enables engineers to design material systems for specific mechanical, thermal, environmental, and durability requirements. Compared with conventional metallic materials, composites can provide substantial weight savings while maintaining or improving performance in selected applications [6].

The importance of composite materials has further increased with the development of hybrid and electric vehicles. In electric vehicles, weight reduction directly influences battery efficiency and driving range. Therefore, composite materials are increasingly considered for structural, semi-structural, and functional automotive components. Applications include energy-absorbing structures, underbody shields, interior panels, storage systems, brackets, housings, and other components where lightweight design, corrosion resistance, and functional integration are beneficial [3], [6]. Figure 6-2 depicts potential applications for composite components in automobile manufacturing.

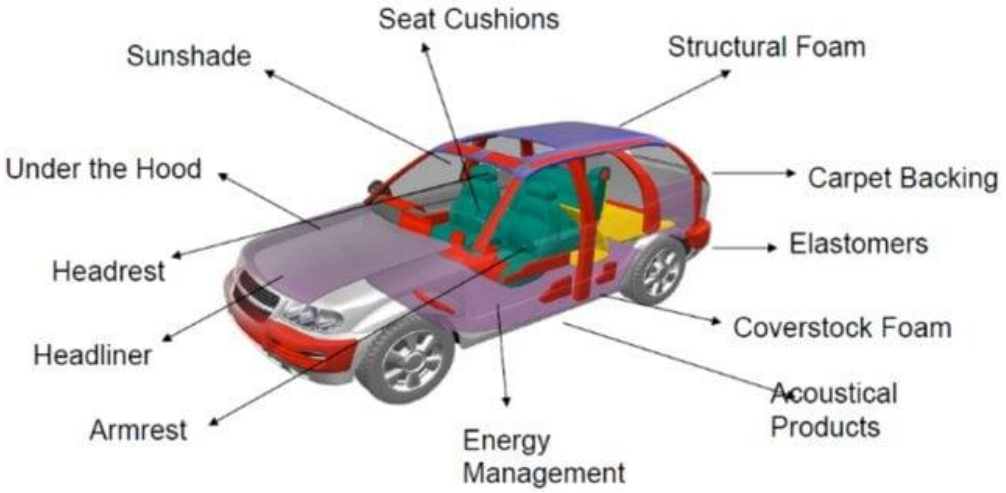


Fig. 6- 2- Diverse applications of polymer composites in the automotive industry [7].

Despite their advantages, automotive composites also present significant design and characterization challenges. Unlike metals, which are often treated as relatively homogeneous and isotropic in engineering design, many composite materials are heterogeneous and anisotropic. Their properties depend not only on the intrinsic behavior of the matrix and reinforcement, but also on fiber orientation, filler distribution, interfacial adhesion, void content, processing history, and environmental exposure. As a result, their mechanical response can vary with loading direction, strain rate, temperature, humidity, and component geometry [8]. This complexity makes the characterization of automotive composites time-consuming and resource intensive. Full

material qualification may require tensile, compressive, flexural, shear, fatigue, creep, impact, and environmental tests. In addition, polymer composites may show strong sensitivity to processing and testing conditions. Therefore, experimental characterization must be carefully designed to capture performance-relevant properties while avoiding unnecessary testing. These challenges provide a strong motivation for using data-driven and machine learning-based approaches to support faster and more efficient composite materials development.

6-3- Project Motivation and Industrial Relevance

The industrial motivation for this project was the need to accelerate the evaluation and development of automotive composite materials while reducing reliance on repeated experimental trial-and-error. In an industrial setting, material selection and formulation development are often constrained by cost, timeline, testing capacity, manufacturing feasibility, and confidentiality requirements. These constraints are especially important for composite materials because small changes in formulation, processing, or reinforcement structure can significantly influence mechanical behavior and component-level performance.

Traditional materials development workflows typically involve selecting candidate formulations, manufacturing test specimens, performing mechanical characterization, analyzing performance, and comparing results against target requirements or baseline materials. Although this process is necessary for final validation, it can become slow and expensive when the design space is large. Automotive composites may involve many variables, including matrix chemistry, reinforcement type, filler content, filler orientations, processing conditions, and environmental conditioning. Exploring all possible combinations experimentally is often impractical.

Machine learning provides a useful framework for addressing this challenge. By learning relationships between material descriptors, processing variables, and performance outputs, ML models can assist in identifying promising candidates, predicting mechanical properties, and guiding experimental prioritization. ML approaches have also been used to predict the mechanical performance of polymer composites [9]. For example, regression-based ML models have been used to predict the density, tensile strength, elongation, and wear intensity of thermoplastic-matrix composites containing different fibrous, dispersed, and nano-dispersed fillers. These models demonstrated strong predictive capability and supported the rational selection of filler type and content to improve wear resistance while reducing the need for extensive experimental testing

[10]. Similarly, artificial neural network models have been applied to cotton fiber/polypropylene composites to predict load-displacement behavior within the experimental filler-content range, supporting smart manufacturing and industry-oriented composite design [11]. These studies collectively demonstrate the potential of ML to capture complex structure-property relationships in polymer and composite systems and to support faster materials design and characterization when experimental testing is costly, time-consuming, or limited by available resources.

In this industrial project, the broader objective was to support accelerated composite materials development through a combined experimental and data-driven workflow. The project aimed to improve the efficiency of material screening, extract useful trends from experimental data, and support technical decision-making in the context of automotive composite design. Due to confidentiality restrictions, the specific materials, formulations, testing conditions, performance targets, and model outputs are not disclosed.

6-4- Materials and Methods: Industrial Contribution Workflow

The methodology followed in this project involved a general workflow for machine learning-aided design and characterization of automotive composite materials. The workflow consisted of material selection and formulation review, experimental characterization, data organization and analysis, model development or data-driven interpretation, and comparison against baseline materials.

6-4-1- Materials Selection and Formulation Review

The first stage of the workflow involved reviewing candidate composite material systems relevant to the industrial partner's application. This step included evaluating the general material class, reinforcement strategy, expected mechanical response, processing feasibility, and compatibility with automotive performance requirements. The material selection process considered the role of polymer matrix, reinforcement phase, filler morphology and orientation, and formulation variables in controlling mechanical and functional behavior.

6-4-2- Mechanical Testing and Characterization

The next stage involved mechanical testing and characterization of selected material candidates. In automotive composite development, mechanical characterization is essential because material properties must be validated under conditions relevant to service performance including service

temperature, range of humidity, applied loads and so forth. Depending on the intended application, material characterization may include tensile, flexural, creep, impact, fatigue, and other mechanical tests. For polymer composites, the testing framework should also account for factors such as temperature sensitivity, loading direction, strain rate, and environmental exposure, as these parameters can significantly influence the measured response. In addition to mechanical testing, complementary characterization techniques, including morphological analysis and thermal evaluation, are often required to obtain a more comprehensive understanding of material structure, stability, and performance.

In this project, the experimental data were used to evaluate candidate materials and compare their performance against baseline or reference materials. The specific test methods, specimen geometries, testing parameters, and quantitative results are not disclosed due to confidentiality. However, the generated data provided the technical basis for subsequent analysis and data-driven interpretation.

6-4-3- Data Organization and Preprocessing

After experimental characterization, the data were organized into a structured format suitable for analysis. Data organization is an important step in any machine learning or data-driven workflow because inconsistencies in format, missing values, and uncontrolled variability can reduce the reliability of conclusions. In general, preprocessing may include checking data consistency, identifying outliers, normalizing variables, aligning test conditions, and converting experimental information into numerical descriptors.

In the context of automotive composites, relevant descriptors may include formulation variables, processing-related information, mechanical property values, filler content, filler orientation, reinforcement characteristics, or environmental conditioning parameters. The target outputs may include measured mechanical properties, or comparison metrics relative to a baseline material. The specific descriptors and outputs used in this project are not disclosed.

6-4-4- Data Analysis and Model Development

The data analysis stage focused on identifying trends and relationships between material variables and performance outputs. Depending on the size and structure of the dataset, this stage may involve statistical analysis, feature correlation, regression modeling, or machine learning model

development. Supervised learning is particularly relevant when measured properties are available as output labels and the objective is to predict performance metrics.

In a general ML-based workflow, the dataset is divided into input descriptors and target outputs. The model is then trained to map the input variables to the measured material response. Common regression algorithms used in materials property prediction include linear regression, polynomial regression, support vector regression, decision tree regression, random forest regression, gradient boosting regression, and artificial neural networks. Model selection depends on dataset size, feature complexity, expected nonlinearity, interpretability requirements, and generalization performance.

For this industrial contribution, the data-driven analysis was used to support interpretation of material behavior and assist comparison among candidate materials. Due to confidentiality, the specific algorithms, hyperparameters, model performance metrics, and prediction results are not reported.

6-4-5- Comparison Against Baseline Materials

A key component of the workflow was comparing candidate materials against baseline or reference systems. Baseline comparison is essential in industrial materials development because new formulations must demonstrate measurable advantages or meet predefined performance requirements before further development. Such comparisons may involve mechanical performance, weight reduction potential, processability, cost, durability, or multifunctional performance.

In this project, candidate materials were assessed relative to relevant baseline materials using available experimental and analytical data. This comparison supported technical decision-making by identifying promising material directions and clarifying the trade-offs among performance, manufacturability, and application requirements.

6-5- Results and Technical Contribution [Non-Confidential Results and Technical Contributions]

Due to confidentiality agreements, detailed material information, formulations, test parameters, numerical results, and performance targets cannot be disclosed. Therefore, the contribution of this

project is presented at a non-confidential level, focusing on the overall technical workflow and its industrial value.

The project supported the evaluation of candidate automotive composite materials through a structured process involving material review, characterization, data organization, and comparison against baseline systems. This approach helped identify relative performance trends and provided technical insight into material behavior under application-relevant conditions.

The project also demonstrated how experimental characterization and data-driven analysis can be integrated to support faster material screening and more efficient decision-making. This is particularly valuable for composite systems, where the design space is large and conventional experimental screening can be time-consuming and costly.

Overall, this work provided an applied example of how materials science, mechanical characterization, and machine learning-aided analysis can be combined to address practical industrial challenges in automotive composite development.

6-6- Relevance to Dissertation Theme

Although this chapter is presented as an industrial case study, it is connected to the broader theme of this dissertation through the use of polymer composites, mechanical characterization, and machine learning-assisted materials design. The main chapters of this dissertation focus on the development of durable elastomeric composites for ice traction and abrasion resistance, while Chapter 5 applies machine learning to predict TPU abrasion resistance from mechanical and viscoelastic properties. The present industrial case study extends this data-driven materials design concept to automotive composites.

The relevance of this chapter can be understood in three ways. First, it highlights the importance of mechanical performance and durability in polymer-based composite systems. Whether the target application is ice-traction elastomers or automotive components, material performance depends on the interaction between composition, structure, processing, and mechanical response. Second, this chapter demonstrates the practical value of data-driven methods in accelerating materials development. In both academic and industrial settings, experimental testing remains essential, but ML can support early-stage screening, guide material selection, and reduce unnecessary trial-and-error. Third, the industrial project shows that machine learning-aided materials design is not

limited to a single application area. The same general principles used to predict abrasion resistance in TPU systems can also be applied to broader composite design challenges, including automotive lightweighting and mechanical property characterization.

Therefore, this chapter is included as an additional contribution completed during the PhD period. It demonstrates the broader impact of the research training and shows how the knowledge developed throughout the dissertation can be translated into an industrial materials engineering context.

6-7- References

[1] F. Czerwinski, "Current trends in automotive lightweighting strategies and materials," *Materials (Basel).*, vol. 14, no. 21, 2021, doi: 10.3390/ma14216631.

[2] D. Mann, *Automotive Plastics and Composites: Worldwide Markets and Trends to 2007*. Elsevier, 1999.

[3] N. T. K. Lindsey, *An Introduction to Automotive Composites*. iSmithers Rapra Publishing, 2002.

[4] L. Yan and H. Xu, "Lightweight composite materials in automotive engineering: State-of-the-art and future trends," *Alexandria Eng. J.*, vol. 118, no. November 2024, pp. 1–10, 2025, doi: 10.1016/j.aej.2024.12.002.

[5] M. F. Ashby, "Materials Property Charts," in *Materials Selection and Design*, G. E. Dieter, Ed. ASM International, 1997, pp. 266–280.

[6] F. Khan *et al.*, "Advances of composite materials in automobile applications – A review," *J. Eng. Res.*, vol. 13, no. 2, pp. 1001–1023, 2025, doi: 10.1016/j.jer.2024.02.017.

[7] R. A. Ilyas, S. M. Sapuan, M. L. Sanyang, M. R. Ishak, and E. S. Zainudin, "Nanocrystalline cellulose as reinforcement for polymeric matrix nanocomposites and its potential applications: A review," *Curr. Anal. Chem.*, vol. 14, no. 3, pp. 203–225, 2018, doi: 10.2174/1573411013666171003155624.

[8] F. C. Campbell, *Structural Composites Materials*. ASM International, 2010.

[9] M. K. Kazi, F. Eljack, and E. Mahdi, "Optimal filler content for cotton fiber/PP composite based on mechanical properties using artificial neural network," *Compos. Struct.*, vol. 251, p. 112654, 2020, doi: 10.1016/j.compstruct.2020.112654.

[10] K. Berladir, K. Antosz, V. Ivanov, and Z. Mitaľová, "Machine Learning-Driven Prediction of Composite Materials Properties Based on Experimental Testing Data," *Polymers (Basel).*, vol. 17, no. 5, 2025, doi: 10.3390/polym17050694.

[11] M. K. Kazi, F. Eljack, and E. Mahdi, "Data-driven modeling to predict the load vs. displacement curves of targeted composite materials for industry 4.0 and smart manufacturing," *Compos. Struct.*, vol. 258, no. August 2020, p. 113207, 2021, doi: 10.1016/j.compstruct.2020.113207.

Chapter 7: Conclusions and Future Work

7-1- Summary of Key Findings

This dissertation investigated the design, evaluation, and prediction of elastomeric composite surfaces for improved ice traction and abrasion resistance. The work combined lab-scale ice tribology, surface texturing, TPU/graphene nanoplatelet nanocomposite design, filler functionalization, wear-activated surface engineering, and machine learning-based abrasion prediction.

First, a lab-scale high-velocity ice friction testing method was developed using the Bruker UMT Tribolab. Custom sample holders, ice trays, and testing scripts were designed to enable controlled evaluation of small rubber and composite specimens on ice. Key testing parameters, including normal load, dwell time, data sampling rate, and sliding mode, were systematically optimized. The results showed that a 5 N normal load, short dwell time, and high-frequency data acquisition were necessary to capture the transient static friction peak and stick-slip response. Comparison of reciprocating and rotational configurations demonstrated that rotational motion provided a more reliable sliding response, while reciprocating motion introduced ploughing effects and artificially high kinetic friction values. Using this testing method, the effect of surface texturing on ice friction was evaluated for TPU-glass fiber composites and commercial slip-resistant outsole materials. The results confirmed that textured surfaces significantly enhanced ice traction by increasing localized shear resistance and mechanical interlocking at the rubber-ice interface. Hard protruding phases, such as glass fibers and SiC particles, contributed to increased static and kinetic friction responses. These findings demonstrated that the developed tribotest can serve as a high-throughput screening method for comparing ice-traction materials at the laboratory scale.

Second, TPU/GNP nanocomposites were developed to address the coupled requirements of ice traction and abrasion durability. Pristine and acid-functionalized graphene nanoplatelets were incorporated into TPU at different filler loadings. FTIR and TGA results confirmed successful GNP functionalization through the introduction of oxygen-containing surface groups. SEM analysis showed that functionalized GNPs improved filler dispersion and filler-matrix adhesion compared with pristine GNPs, which exhibited larger agglomerates and interfacial gaps. Tensile testing showed that GNP incorporation increased composite stiffness, while functionalized GNPs

provided stronger early-stage reinforcement due to improved interfacial load transfer. Ice-traction testing of TPU/GNP nanocomposites showed that surface condition strongly influenced frictional performance. Wire-brushed surfaces consistently increased the static coefficient of friction compared with molded surfaces by generating microscale asperities and exposed rigid features. Post-abrasion surfaces also retained traction in graphene-reinforced systems, indicating that abrasion-induced surface evolution can contribute to wear-activated friction control. The formation of post-abrasion asperities and microchannels supported mechanical interlocking and liquid-layer disruption at the ice interface. Abrasion testing identified TPU-20 f/GNP as the most balanced formulation. This composition showed the lowest abrasion volume loss and the highest abrasion resistance index, indicating improved durability due to enhanced filler-matrix anchoring and reduced filler pull-out. In contrast, excessive functionalized GNP loading reduced wear resistance due to restricted polymer chain mobility, reduced matrix compliance, and brittle wear behavior. These findings showed that optimal tribological performance requires a balance between filler reinforcement, interfacial adhesion, and elastomeric deformability.

Third, machine learning models were developed to predict TPU abrasion resistance from mechanical and viscoelastic property descriptors. Nonlinear regression models outperformed simple linear approaches, confirming that TPU abrasion behavior is governed by complex property interactions. Support vector regression and gradient boosting regression showed the strongest predictive performance among the evaluated models. Feature analysis indicated that mechanical and viscoelastic descriptors related to stiffness, strength, hardness, and energy dissipation play important roles in controlling abrasion resistance. The results demonstrated that machine learning can support early-stage TPU material screening and reduce reliance on extensive abrasion testing.

Finally, the industrial case study demonstrated the broader applicability of data-driven materials design in automotive composite development. Although proprietary details could not be disclosed, the case study showed how materials selection, mechanical characterization, data organization, model development, and comparison against baseline materials can be integrated into an industrial composite design workflow.

Overall, the findings demonstrate that durable ice-traction materials require an integrated design strategy involving controlled surface morphology, optimized filler dispersion, strong but balanced interfacial adhesion, and wear-activated surface functionality. The combined experimental and

machine learning approaches developed in this dissertation provide a framework for designing TPU-based elastomeric composites with improved ice traction, abrasion resistance, and predictive material-selection capability.

7-2- Main Contributions

This dissertation makes several original contributions to the fields of ice tribology, elastomeric composite design, wear-activated surface engineering, and machine learning-assisted materials development.

The first contribution is the development of a novel lab-scale high-velocity ice tribotesting method for evaluating the frictional response of rubber and elastomeric composite materials on ice at high kinetic motion. This method was developed using a modified Bruker UMT Tribolab equipped with custom-designed sample holders, ice trays, and testing scripts. Unlike conventional footwear slip-resistance tests that require full-size shoes or large specimens, the developed method enables high-throughput evaluation of small laboratory-prepared composite samples. This provides an important research and development tool for screening new rubber composite formulations and surface texturing technologies for ice-traction applications. The method enables controlled evaluation under high-speed sliding conditions relevant to walking, which represents a novel contribution to lab-scale ice tribology testing.

The second contribution is the development of a TPU/graphene nanoplatelet nanocomposite design strategy that integrates interfacial engineering with bioinspired wear-activated surface functionality. Inspired by natural traction mechanisms, this work demonstrated that surface features generated during abrasion can be used beneficially rather than being treated only as material damage. Acid functionalization of GNPs improved filler-matrix interfacial bonding, enhanced dispersion, and reduced filler pull-out during wear. As abrasion progressed, the composites generated new micro-asperities and microchannels that supported mechanical interlocking and liquid-layer disruption at the ice interface. Therefore, the material design converted wear into a functional surface-renewal mechanism, helping preserve ice traction after abrasion and reducing the concern of traction loss due to surface wear.

The third contribution is the identification of an optimized composite formulation capable of balancing ice traction and abrasion resistance. The results showed that TPU-20 *f*/GNP provided

the most favorable combination of low abrasion volume loss, high abrasion resistance index, and retained post-abrasion ice-traction performance. This finding demonstrates that the trade-off between durability and ice traction can be addressed through controlled filler loading, improved interfacial adhesion, and preservation of elastomeric deformability. The work provides a structure-interface-tribology framework for designing durable anti-slip elastomeric composites.

The fourth contribution is the development of machine learning models for predicting TPU abrasion resistance using mechanical and viscoelastic material descriptors. The novelty of this approach is that abrasion resistance was predicted from existing material property patterns without introducing filler-specific variables or requiring new composite formulations. Instead, the model used the relationship between material chemistry, mechanical behavior, viscoelastic response, and abrasion performance to extract predictive information from the available data. This contribution demonstrates that machine learning can be used to obtain abrasion-performance insight from measurable material-property data and can support early-stage screening of TPU grades before extensive experimental wear testing.

The fifth contribution is the industrial application of machine learning-assisted polymer composite development through a large-scale experimental and data-driven project conducted with a Tier-1 automotive company. This project involved building a composite materials dataset from the ground up, conducting experimental characterization, developing AI-based predictive models, and translating the trained models into a graphical user interface for polymer composite behavior prediction under service-relevant conditions. Although proprietary details cannot be disclosed, this industrial contribution demonstrates the practical implementation of data-driven materials engineering for accelerated polymer composite design and performance prediction.

In addition to the technical contributions described above, the outcomes of this dissertation have been disseminated through peer-reviewed journal publications, conference presentations, and industry-facing research activities. The high-velocity ice tribotesting and surface-textured rubber composite work was published in *Tribology International* and presented at national and international conferences. The TPU/GNP nanocomposite study further extended the concept of wear-activated surface engineering for durable anti-slip materials and is currently under review. The machine-learning framework for TPU abrasion prediction was published in the *Journal of*

Applied Polymer Science, demonstrating the applicability of data-driven methods to polymer durability assessment. The related dissemination outputs are listed below.

- S. Zahmatkesh and R. Rizvi, "Evaluating Surface Texturing Technologies of Rubber Composites on Ice Using a Novel High-Velocity Tribotest Method," *Tribology International*, vol. 206, p. 110538, June 2025. Available online: https://www.sciencedirect.com/science/article/pii/S0301679X25000337
- S. Zahmatkesh and R. Rizvi, "Effect of Sliding Speed on Tribological Responses of Ice Traction in Surface-Damaged Elastomeric Composites," *Progress in Canadian Mechanical Engineering*, CSME Conference, Université de Sherbrooke, May 2023. Available online: https://usherbrooke.scholaris.ca/items/60ee8aee-ace2-49f8-b56a-5aa5aa2c621f
- S. Zahmatkesh and R. Rizvi, "Bioinspired Rubber Composites for Superior Ice Traction: Enhancing Winter Safety through Innovative Laboratory Testing in Tribology," *SPIE Smart Structures + Non-Destructive Evaluation, Biologically Inspired Materials, Processes, and Systems*, Proceedings Volume 13430, Vancouver, March 2025. Available online: https://www.spiedigitallibrary.org/conference-proceedings-of-spie/13430/1343009/Bioinspired-rubber-composites-for-superior-ice-traction--enhancing-winter/10.1117/12.3051455.short
- S. Zahmatkesh, S.-N. Leung, and R. Rizvi, "Wear-Activated Surface Engineering of TPU/Graphene Nanoplatelet Nanocomposites for Ice Friction Control," *Polymer Composites*, under review.
- S. Zahmatkesh, H. Esmaeili, A. T. Valerio, and R. Rizvi, "Predicting Abrasion Resistance in Thermoplastic Polyurethanes Using Machine Learning," *Journal of Applied Polymer Science*, vol. 142, no. 42, e57619, July 2025. Available online: https://onlinelibrary.wiley.com/doi/full/10.1002/app.57619
- S. Zahmatkesh and R. Rizvi, "Data-Driven Prediction of Abrasion Resistance in Thermoplastic Polyurethane Elastomers Using Machine Learning Approach," *25th International Conference on Wear of Materials (WOM)*, Sitges, Spain, April 2025.

Beyond academic dissemination, the industrial component of this dissertation was conducted through a Mitacs-supported collaboration with Magna International®, where experimental characterization, data generation, predictive modeling, and graphical user-interface development were used to translate machine-learning-assisted composite design into an applied engineering context. Together, these dissemination activities demonstrate that the knowledge generated through this dissertation extends beyond academic publication and contributes to both fundamental materials research and practical polymer composite development.

Overall, the dissertation contributes an integrated experimental and computational framework for durable elastomeric material development. The work advances lab-scale ice tribology testing, demonstrates bioinspired and wear-activated composite surface design, establishes interfacial functionalization as a strategy for improving TPU/GNP durability, and applies machine learning to support predictive abrasion analysis and industrial composite materials development.

7-3- Future Research Directions

The findings of this dissertation provide several directions for future research in ice tribology, durable elastomeric composites, environmentally responsible material design, and machine learning-assisted abrasion prediction.

One important future direction is the further development of the lab-scale ice tribotesting method through the integration of a cryogenic or environmental chamber. In the current work, the testing method enabled high-velocity ice friction evaluation under controlled load and sliding conditions. However, ice friction is strongly influenced by temperature because the thickness and stability of the quasi-liquid layer at the ice surface vary with thermal conditions. Incorporating a temperature-controlled chamber would allow systematic investigation of rubber-ice friction over a wider range of subzero temperatures. This improvement would provide a more complete understanding of the temperature-dependent frictional behavior of elastomeric and composite surfaces on ice and would increase the applicability of the testing method for real winter environments.

Future research should also address the environmental impact of outsole wear and microplastic generation. Although this dissertation focused on improving abrasion resistance to reduce material loss, further work is needed to develop greener anti-slip materials that can minimize or eliminate microplastic release. One promising direction is the use of bio-based or natural rubber alternatives,

biodegradable elastomers, or environmentally friendly fillers that provide sufficient ice traction and durability while reducing the long-term ecological impact of worn outsole particles. Such work could connect ice-traction material design with sustainability-driven polymer engineering.

Another important direction is the scale-up and manufacturability of TPU/*f*-GNP composites. The present work demonstrated that low-loading functionalized GNPs can improve abrasion resistance while maintaining ice-traction performance through wear-activated surface evolution. However, further optimization is required to translate this concept toward practical manufacturing. Future studies should focus on optimizing GNP functionalization chemistry, filler loading, dispersion methods, processing conditions, and surface-texturing procedures at larger scales. In particular, lower GNP contents should be systematically investigated to determine the minimum filler loading required to achieve the best balance between ice traction, abrasion resistance, processability, cost, and mechanical performance.

Future work should also examine the long-term durability of the developed composites under more realistic service conditions. Repeated abrasion, cyclic loading, wet-dry exposure, salt contamination, freeze-thaw cycling, and mixed walking surfaces should be considered to better simulate footwear service environments. Such studies would help determine whether the wear-activated surface-texturing mechanism remains effective over extended use and whether the composites can retain traction after repeated exposure to both icy and abrasive non-ice surfaces.

For the machine learning component, future research should focus on improving both the quantity and quality of the training data. The present work demonstrated the feasibility of predicting TPU abrasion resistance from mechanical and viscoelastic property descriptors. However, the predictive capability of machine learning models is strongly dependent on the size, consistency, and diversity of the available dataset. Future studies should generate additional experimental data using systematically selected TPU grades and controlled abrasion testing conditions. Increasing the dataset size and including more balanced property ranges would improve model generalization, reduce uncertainty, and enhance performance metrics. In addition, future machine learning studies could incorporate broader material descriptors, including chemical structure, hard- and soft-segment composition, phase morphology, processing conditions, and surface characteristics. Combining experimentally measured properties with microstructural and molecular descriptors would allow more detailed interpretation of structure-property-wear relationships in TPU systems.

Such an expanded framework could support inverse materials design, where desired abrasion resistance or traction performance is used to guide the selection or formulation of TPU-based materials.

Overall, future research should build on the integrated approach developed in this dissertation by combining temperature-controlled ice tribology, sustainable material design, scalable TPU/GNP composite manufacturing, long-term durability assessment, and expanded machine learning datasets. These directions would further advance the development of durable, environmentally responsible, and predictive anti-slip elastomeric materials for real-world winter safety applications.

7-4- Closing Remarks

This dissertation advanced the development of durable elastomeric composite surfaces for ice-traction applications by integrating lab-scale tribological testing, surface texturing, interfacial engineering, wear-activated surface design, and machine learning-based abrasion prediction. The findings demonstrate that ice traction and abrasion resistance can be improved simultaneously when material composition, filler-matrix interaction, surface morphology, and wear evolution are considered as interconnected design parameters.

The developed high-velocity ice tribotesting method provides a practical platform for laboratory-scale evaluation of new anti-slip materials, while the TPU/f-GNP composite system demonstrates a promising pathway toward durable, self-texturing surfaces that retain traction after wear. In parallel, the machine learning framework shows the potential of data-driven tools to accelerate TPU material selection and reduce experimental burden.

Overall, this work contributes to the broader goal of designing safer, more durable, and more predictive polymer composite systems for winter safety and wear-resistant applications.